A METHOD OF COMPUTING THE POTENTIAL FLOW ON THICK WING TIPS

A THESIS

Presented to

The Faculty of the Division

of Graduate Studies

By

Pradeep Raj

In Partial Fulfillment

of the Requirements for the Degree

Doctor of Philosophy

in the School of Aerospace Engineering

Georgia Institute of Technology

October 1976

A METHOD OF COMPUTING THE POTENTIAL

FLOW ON THICK WING TIPS

Approved:

Robin B. Gray, Chairman

J. Alvin Pierce

James C. Wu

Date Approved by Chairman: 10/5/76

ACKNOWLEDGMENTS

It gives me great pleasure to record my deep gratitude to my teacher and advisor Dr. Robin B. Gray for suggesting the problem and for his constant guidance and encouragement. I am indebted to him for many enlightening discussions and suggestions which significantly contributed to my research work.

My thanks are due to Dr. James C. Wu and Dr. G. Alvin Pierce for being on my Thesis Reading Committee and for their valuable advice and criticism. My appreciation goes to Dr. Howard M. McMahon and Dr. Charles S. Martin who, as members of the Final Oral Examination Committee, offered useful suggestions.

I wish to extend my very special thanks and sincere appreciation to my mother and to both of my sisters for their moral support, patience and understanding. I am especially indebted to Mr. Jai K. Hakhu and Mr. Vimal K. Dubey for everything they did for me prior to and during the period when this work was undertaken.

I owe my thanks to many friends and acquaintances for their help in making my stay at Georgia Tech a very pleasant one.

My appreciation goes to Mrs. Pat Gunnells for an excellent job done in typing the Thesis.

The financial support of the Georgia Institute of Technology and the services of the Rich Computing Center are gratefully acknowledged.

TABLE OF CONTENTS

LIST OF ILLUSTRATIONS

LIST OF SYMBOLS

A_{ij}	induced velocity influence coefficient for the two-dimensional problem
[A]	induced velocity influence coefficient matrix for the two-dimensional problem
{b}	the right-hand-side column vector in the system of linear algebraic equations
c	chord length
C_ℓ	section lift coefficient
C_p	pressure coefficient
c_1, c_2, c_3	direction cosines of a tangential vector at any control point on the surface
$\vec{e}$	unit vector denoting the direction of the induced velocity due to a vortex filament
F	prescribed normal velocity on the boundary surface
g	surface vorticity strength distribution function for an Elementary Vortex Distribution
$\vec{i}, \vec{j}, \vec{k}$	unit vectors along X,Y,Z axes respectively
k	a station on the body surface at a selected value of x
K	total number of k-stations
ℓ	a station inboard of the tip at a selected value of y on the body surface
L	total number of ℓ-stations
m	a station on the tip body of revolution at selected value of ψ
M	total number of m-stations

$\vec{n}$	unit vector normal to the surface
N	total number of surface elements on two-dimensional body
p	static pressure
P	a control point on the surface
$\vec{r}$	a vector drawn from any point on the surface to the control point
R	flow region exterior (or interior) to the boundary surface
s	arc length along the profile of the body
S	boundary surface of a body
t	maximum thickness of the airfoil
t/c	thickness ratio
$\vec{t}$	unit vector tangent to the surface
v	disturbance velocity field
Δv_{ij}	normal component of induced velocity at i-th control point due to j-th Elementary Vortex Distribution
V	total fluid velocity
$\Delta V_{k\ell}$	tangential component of induced velocity at i-th control point due to surface vorticity distribution on k-ℓ element
ΔV_{km}	tangential component of induced velocity at i-th control point due to surface vorticity distribution on k-m element
x,y,z	Cartesian coordinates of a point in space
X,Y,Z	Cartesian coordinate system
α	one of the two orthogonal components of the local surface vorticity
α_o	angle of attack

β	one of the two orthogonal components of the local surface vorticity
γ	surface vorticity strength
$\gamma(x)$	chordwise distribution of surface vorticity
Γ	total circulation
δ	total surface vorticity strength
θ	inclination of the surface tangential vector with respect to X-axis for two-dimensional flows; also, for semi-infinite circular cylinder, an angle between a radial plane and the X-Y plane
ρ	fluid density
Σ	summation
ϕ	disturbance velocity potential
Φ	total velocity potential
ψ	angular location of m-th station on the tip
∇	del operator ($= \vec{i}\,\frac{\partial}{\partial x} + \vec{j}\,\frac{\partial}{\partial y} + \vec{k}\,\frac{\partial}{\partial z}$ in Cartesian)
∇^2	Laplacian operator ($= \frac{\partial^2}{\partial x^2} + \frac{\partial^2}{\partial y^2} + \frac{\partial^2}{\partial z^2}$ in Cartesian)

Subscripts:

a	noncirculatory flow in two-dimensional problem
c	cross-flow in two-dimensional problem
i,I	quantities associated with i-th control point
j	EVD station; also, surface element
k	quantities associated with k-th station
ℓ	quantities associated with ℓ-th station
L	contribution of lower surface
m	quantities associated with m-th station

M	mean value
n	quantities normal to the surface
P	control point
T	contribution of the tip
U	contribution of the upper surface
α	contribution of α-type surface vorticity; also quantities associated with α-type vorticity
β	contribution of β-type surface vorticity

Superscripts

$( )'$	surface element
$(\vec{\ })$	vector quantity

Abbreviations

AR	Aspect Ratio of wing
EVD	Elementary Vortex Distribution

SUMMARY

An iterative procedure to compute detailed velocity and pressure distributions on the surface of thick wing tips is developed using potential flow theory. The method uses a two-dimensional surface vorticity distribution as an initial approximation. Therefore, the two-dimensional problem is first formulated in the form of an integral equation using vorticity as the surface singularity. This is solved by the Elementary Vortex Distribution technique. The continuous, piecewise linear surface vorticity distribution so obtained is directly equivalent to the velocity distribution. A comparison of the flow computed on a circular cylinder with the exact analytical results provides a measure of accuracy. The two-dimensional noncirculatory and circulatory flow is computed for NACA basic thickness form airfoils.

The iterative procedure is mathematically formulated for the semi-infinite circular cylinder with a hemispherical tip. The numerical results for this case exhibit good convergence in three iterations to give the three-dimensional velocity distribution on the tip region which merges smoothly with the two-dimensional distribution further inboard from the tip.

A modified iterative procedure is used to compute the

nonlifting potential flow for the semi-infinite NACA 0012 wing with half-body-of-revolution tip and the NACA 0012 wing of aspect ratio three. The chordwise surface velocity and pressure distributions are presented for representative spanwise locations.

CHAPTER I

INTRODUCTION

Potential flow solutions have been used successfully for many years to predict the real flow situations for a surprisingly large range of aerodynamic problems. Inviscid, incompressible fluid flow theory agrees very well with the low speed real flow except in wakes and for problems involving regions of separated flow. Moreover, the potential flow solutions are almost always essential for viscous flow calculations and the accuracy of the latter depends to a large extent on that of the former. These are some of the primary reasons which account for the continued interest in attempts to develop new computational methods for potential flow problems. The aim of the present investigation is to develop a numerical method to compute detailed velocity and pressure distribution on the tip region of thick wings using potential flow theory.

The wake downstream of a lifting wing is a surface of tangential velocity discontinuity in potential flow and may therefore be considered as a surface distribution of vortices. It has long been known that self-induced distortions cause the edges of the wake to rollup into a pair of counter-rotating tip vortices. However, the exact

mechanism of the rollup and the structure of the tip vortex are not completely understood. This knowledge is required for a more accurate computation of the chordwise velocity and pressure distributions on the lifting wing and the wing loading. An improved analysis of the blade/vortex interaction for a helicopter also depends to some extent on a better understanding of the various aspects of the tip vortex. The knowledge of the precise flow field in the tip region of the wing is in turn essential for a proper study of the tip vortex and related problems. The present work describes a procedure to compute the detailed flow field on the surface of nonlifting wings. Therefore, this study takes only a first step towards solving the more complex problems of lifting wings. It should also be noted that the potential flow approach to the problem affords considerable simplicity in the mathematical formulation and the numerical computation.

The governing equations of the potential flow problems which are considered in the present work are briefly described in the following section. A review of the methods for solving the equations is presented in Section 1.2. The integral equation formulation of the two-dimensional problems using a surface vorticity distribution is given in Chapter II. An Elementary Vortex Distribution technique is utilized to approximate the integral equation by a set

of linear algebraic equations. The solution of this system of equations directly gives the surface velocity distribution. The two-dimensional flow solutions are obtained for a circular cylinder and for NACA basic thickness form airfoils.

The general outline and development of an iterative procedure utilizing surface vorticity distribution to compute the three-dimensional flow field on the tip region of a semi-infinite body is presented in Chapter III. The mathematical formulation is illustrated for a semi-infinite circular cylinder with a hemispherical tip. The application of the basic iterative scheme to this case and the application of a modified iterative procedure to a semi-infinite symmetrical wing with half-body-of-revolution tip is presented in Chapter IV. The modified scheme is extended to compute the flow field on a finite, nonlifting, symmetrical wing and this case is discussed in Chapter V. The concluding remarks and some suggestions for possible extension of the present work are given in the last chapter.

1.1. The Statement of the Problem of Potential Flow

The steady flow of an incompressible and inviscid fluid in the region, R, exterior to (or interior to) a given boundary surface, S, is adequately described by the

equation of continuity

$$\nabla \cdot \vec{V} = 0, \tag{1}$$

and the Eulerian equation of motion

$$(\vec{V} \cdot \nabla)\vec{V} = -\frac{1}{\rho}\nabla p \ . \tag{2}$$

It has been assumed that all body forces are conservative and their potentials have been absorbed in the pressure. In addition, it is assumed that the locations of all boundary surfaces are known and the normal component of fluid velocity is prescribed on the boundaries. Mathematically speaking

$$\vec{V} \cdot \vec{n}\Big|_S = F \ . \tag{3}$$

For the exterior problem (body immersed in fluid), a regularity condition at infinity must also be imposed.

The velocity field is also irrotational for all flows that can be generated from rest by the action of conservative body forces or by the motion of the boundaries. Then the velocity field, $\vec{V}$, can be represented as the gradient of a scalar potential function, Φ. However, it is more convenient to express $\vec{V}$ at any point of the region R as

$$\vec{V} = \vec{V}_\infty + \vec{v} \ . \tag{4}$$

The velocity field, $\vec{V}_\infty$, would exist in R in the absence of the boundary surface. The vector $\vec{v}$, the disturbance velocity field due to the boundaries, is assumed to be irrotational so that $\vec{v}$ may be expressed as

$$\vec{v} = \nabla\phi \ . \tag{5}$$

Since $\vec{V}_\infty$ satisfies Eq. (1), Eqs. (4) and (1) give

$$\nabla\cdot\vec{v} = 0 \ . \tag{6}$$

Combining Equations (5) and (6), it is found that the potential, ϕ, satisfies the Laplace's equation

$$\nabla^2\phi = 0 \tag{7}$$

in region R. The associated boundary condition on ϕ from Eqs. (3), (4), and (5) is

$$\nabla\phi\cdot\vec{n}\Big|_S = \frac{\partial\phi}{\partial n}\Big|_S = -\vec{V}_\infty\cdot\vec{n} + F \ . \tag{8}$$

The regularity condition at infinity is

$$|\nabla\phi| \to 0 \ . \tag{9}$$

The equations (7), (8), and (9) completely describe the potential flow problems considered in the course of the present investigation except that all the boundary surfaces will also be assumed to be impermeable. Consequently F is set equal to zero.

The onset flow, $\vec{V}_\infty$, must be such that $\vec{v}$ is a potential flow. In the usual case of potential onset flow, the condition is obviously satisfied. In principle, however, there is no other restriction on $\vec{V}_\infty$.

The essential simplicity of the potential flow formulation is that the velocity field is determined by Eqs. (4), (5), and (7)-(9), completely independent of the equation of motion. The latter, Eq. (2), is used to calculate the pressure field once the velocity field is known. The special case of a steady uniform onset stream offers additional simplification. Then, Eq. (2) can be integrated to give the pressure coefficient in terms of the velocity field as

$$C_p = \frac{p-p_\infty}{\frac{1}{2}\rho V_\infty^2} = 1 - \frac{|\vec{V}|^2}{|\vec{V}_\infty|^2} . \qquad (10)$$

The problem defined by Eqs. (7)-(9) is the well-known Neumann problem of potential theory. The fluid-dynamic problems under consideration here have, in addition, certain special features. For the exterior flow, the major interest lies in the solution on the boundaries though the extent of ϕ is infinite. Also, the boundary conditions for a variety of boundary surfaces remain unchanged. The significance of these features will be apparent in the following sections of the thesis.

1.2. Review of the Methods of Solution

Laplace's equation is one of the simplest and best known of all the partial differential equations. The exact analytical solutions of the direct problem as defined by Eqs. (7)-(9) can be obtained only by the technique of the separation of variables in axisymmetric and three-dimensional cases. However, separability conditions[1,2] restrict the solutions to an extremely limited class of boundary surfaces. This technique, though applicable to two-dimensional problems, is not commonly used. The primary difficulty lies in satisfying the boundary conditions. For two-dimensional problems, conformal transformations[3,4] of the boundary offer a simple and more useful alternative. For instance, Theodorsen's method[5] maps an airfoil into a pseudo-circle by an inverse Joukowski transformation and then into an exact circle by a second transformation. The procedure can be generalized by using one or more inverse Kármán-Trefftz[3] transformations. A large number of two-dimensional and axisymmetric solutions have been obtained from indirect methods[3,4] also. They involve the superposition of the stream functions of a set of singularities (point sources, line sources, doublets, and vortices) and the onset flow to calculate streamlines, any one of which may form a boundary surface. These methods are not useful when the boundary is prescribed. The number of exact

analytical solutions thus available is far too small to suit wide practical applications. The chief value of these solutions is to evaluate the accuracy of other methods of solution.

The approximate solutions of the direct potential flow problem received most of the attention of a majority of investigators before the advent of high-speed digital computers. Linear Theory[6] spans a large class of approximate solutions which is based on one or both of the following assumptions: (1) the body is slender, with small local surface slope; (2) the velocity components due to the body are small perturbations on the onset flow. This obviously excludes a variety of problems of practical interest. In some instances, the results behave in a fictitious manner e.g., the pressure distribution at the nose of an airfoil approaches infinity. Moreover, the validity of the theory for a given body is not always predictable. Another type of approximate solution, first introduced by Kármán,[7] uses a distribution of various types of singularities interior to the body surface. In some cases, the general solution can be written in closed form while in others considerable computation is required to obtain the solution. All of these techniques place restrictions on the type of body about which flow can be computed. Also, the approximate solutions introduce analytical approximation into the formulation itself, imposing a limit on

the accuracy that can be obtained.

The exact numerical methods have been steadily gaining importance in the last decade or so. They now constitute an important aspect of the relatively new but rapidly expanding discipline of Computational Fluid Dynamics. One of the striking features of these methods is that the analytical formulation, including all equations, is exact. The errors resulting from the numerical approximations introduced for purposes of calculation can, in principle, be made as small as desired by sufficiently refining the numerical procedures. These methods are also best suited for solving the potential flow problems for arbitrary boundaries. The most straightforward way of solving the problem defined by Eqs. (7)-(9) is by finite difference approximations of the Laplacian. But, this is not a very efficient procedure, even more so if the solution is desired only on the boundary surface as is the case in a large variety of fluid dynamic problems.

An especially efficient procedure for two- and three-dimensional bodies has been formulated using Green's Theorem. Lamb[8] shows that any solution of the Laplace's equation can be expressed in integral form over the bounding surfaces where the surfaces are replaced by distributions of singularities (sources, doublets, and vortices). The elementary potentials of these singularities satisfy the regularity condition at infinity and the linearity of the Laplace's

equation suggests that any linear combination of the singularities is a valid solution. The integral equation (usually a Fredholm integral equation of the second kind for source distribution, and a Fredholm integral equation of the first kind for doublet and vorticity distributions) so derived is mostly replaced by a set of linear algebraic equations which are numerically solved. Once the surface singularity distribution is known, the velocity and pressure fields can be readily computed. One of the most important advantages of this procedure lies in the fact that the potential flow solution can be computed on the body surface without considering the remainder of the flow field.

The surface source distribution method, first stated by Lotz[9] and later developed and extended by Vandrey[10] has been extensively used in the recent past with considerable success to solve the direct potential flow problems for a large variety of boundary surfaces. Giesing[11] describes in detail the problem of two-dimensional airfoils. The pioneering work of Hess and Smith for extension to three-dimensional surfaces of arbitrary shape is documented in detail in Reference 12. In their basic approach, the body surface is approximated by plane rectangular surface elements, over each of which the source density is assumed to be constant. Hess[13,14,15,16,17] presents the improvements to the basic approach and the applications to different types of bodies. The emphasis is on the surface

source method and the vorticity distribution is superimposed only to provide the circulation for the cases of lifting bodies. Geissler[18] computes the potential flow about the bodies of revolution by a combination of source, sink, and vorticity distributions on the surface. The two-dimensional integral equation is reduced to one dimension by means of Fourier series expansions for velocity, source, and vorticity strengths. Pien[19] points out the disadvantage of the surface source methods, namely, the difficulties in computing the velocity potential, velocity, and pressure on the surface even after the source densities are determined. This is overcome by using the doublet distributions. Summa[20] developed a numerical method based on a "step" doublet distribution over each element of a discrete set of approximate quadrilateral elements on the surface. This method is applied to the exact calculation of three-dimensional lifting potential flows.

The alternate approach based on surface vorticity distribution, first suggested by Prager[21], has attracted only limited attention. In Germany, Martensen[22], Jacob, and Riegels[23] have developed a procedure for two-dimensions, based on the stream function. The boundary condition is that the total tangential velocity be zero on the inside of the profile curve. This results in a Fredholm integral equation of the second kind. Computationally, the procedure

is equivalent to a distribution of a set of concentrated line vortices at the control points. Mavriplis[24,25] considers the problems of a single airfoil and a two-element airfoil. It is indicated that the surface vorticity methods may be more accurate than the surface source methods. A surface vorticity method for axisymmetric flows has been developed by Klein and Mathew[26]. A three-dimensional formulation based solely on surface vorticity was put forward by Kress[27], but this explicitly deals with the case of a nonsimply connected body such as a torus.

The surface vorticity formulation has certain advantages over other methods which deserve careful attention. This is the only procedure which directly gives the surface velocity - the important quantity - as the solution of the integral equation. This follows from the fact that the discontinuity in the tangential velocity is proportional to the local vorticity strength and, if the interior velocity is zero, the surface vorticity distribution is equivalent to the surface velocity field. Also, the vorticity represents the physically observed phenomenon most closely. In contrast, sources and doublets are rather fictitious as surface singularities. For lifting bodies, some vorticity is unavoidably required to provide the necessary circulation. The author finds it more natural to formulate the entire problem of incompressible, inviscid

flow, in terms of vorticity. In the following chapter, the integral equation formulation for two-dimensional nonlifting and lifting bodies is presented. The integral equation is solved by utilizing an Elementary Vortex Distribution technique for a right circular cylinder and for the NACA basic thickness form airfoils.

CHAPTER II

TWO-DIMENSIONAL FLOWS

2.1. Integral Equation Formulation

The basic problem of determining the potential flow on a two-dimensional body placed in infinite fluid medium is approached by replacing the body surface by a sheet of unknown vorticity strength distribution. The velocity associated with the vorticity sheet can be computed at any point in the flow field by the application of the Biot-Savart law[3]. On the sheet itself, the induced velocity at any point P (see Figure 1) is given by

$$\vec{v}_p = \oint \frac{\gamma(s)\ ds}{2\pi|\vec{r}|}\ \vec{e}, \tag{11}$$

where

$$\vec{r} = (x_p - x)\vec{i} + (z_p - z)\vec{k},$$

$$\vec{e} = [(z_p - z)\vec{i} - (x_p - x)\vec{k}]/|\vec{r}|,$$

and

$$ds = [(dz)^2 + (dx)^2]^{1/2}.$$

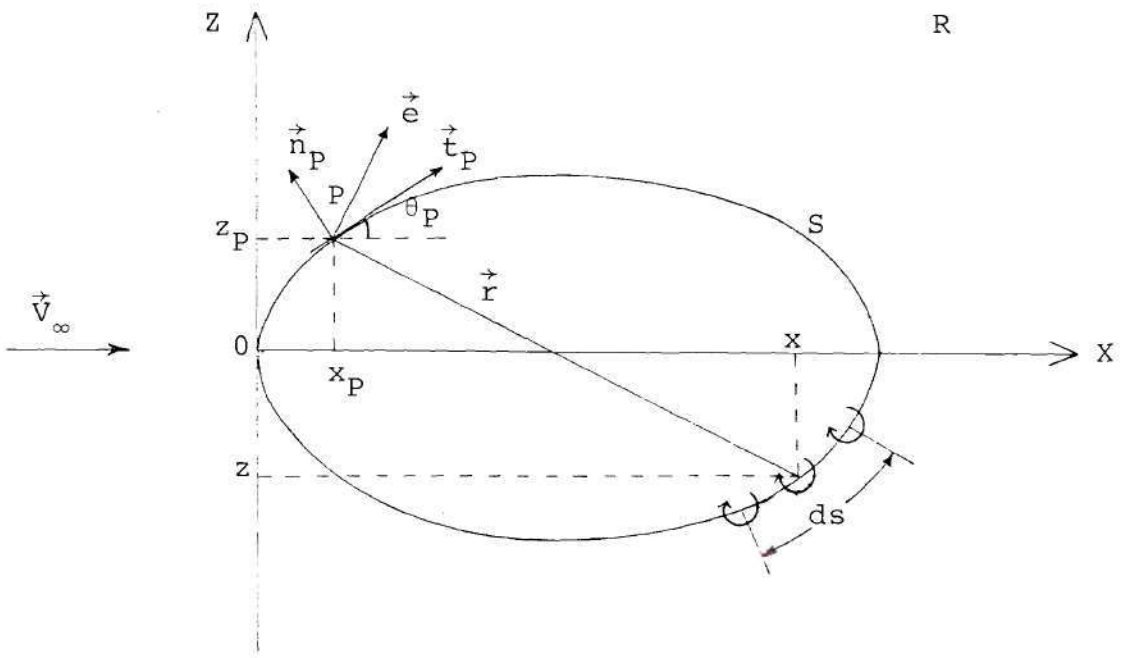

Figure 1. Induced Velocity at a Control Point, P, due to Surface Vorticity Distribution

The zero normal velocity boundary condition gives

$$\vec{v}_P \cdot \vec{n}_P = -\vec{V}_\infty \cdot \vec{n}_P, \tag{12}$$

where

$$\vec{n}_P = -\sin\theta_P \vec{i} + \cos\theta_P \vec{k},$$

and

$$\tan\theta_P = \left(\frac{dz}{dx}\right)_P .$$

Combining Eqs. (11) and (12) a Fredholm integral equation of the first kind for the unknown vorticity strength, γ, is obtained as,

$$\oint \frac{\gamma(x)}{2\pi}\left[\frac{(z_P-z)\sin\theta_P + (x_P-x)\cos\theta_P}{(x_P-x)^2 + (z_P-z)^2}\right]\left[1+\left(\frac{dz}{dx}\right)^2\right]^{\frac{1}{2}} dx$$

$$= -V_\infty \sin\theta_P . \tag{13}$$

Since the region exterior to the body is not simply connected, an auxiliary condition must be specified for uniqueness of the solution.[8] The total circulation around a closed path enclosing the body is defined as

$$\Gamma = \oint \vec{V} \cdot \vec{d\ell} . \tag{14}$$

For the specific case of uniform onset flow,

$$\Gamma = \oint \gamma(s)ds \ . \qquad (15)$$

The problem reduces essentially to solving Eq. (13) subject to Eq. (15) with specified total circulation Γ. Nonlifting flows are noncirculatory and Γ is set equal to zero. Nonzero circulations are associated with lifting flows and there, Γ is arbitrary except when the body has a sharp edge. In the latter case, the Kutta-Joukowski condition fixes, once and for all, the value of the total circulation. For an airfoil with a sharp trailing edge, this condition requires that the circulation be of just sufficient strength to make the flow leave the airfoil smoothly at the trailing edge.[4] This can be more explicitly expressed as follows. If the trailing edge angle is finite, the velocity at the trailing edge must be zero; otherwise a velocity discontinuity which cannot be permitted will result. For a cusped trailing edge, the velocity must be finite and have the same magnitude on either side of the airfoil as the flow leaves the trailing edge.

2.2. Method of Solution using EVD

A careful examination of the integral equation, Eq. (13), reveals that the kernel of the equation has a singularity at $x = x_p$. This indicates that a direct analytical solution will be extremely difficult, if not impossible, to

obtain; even more so if the profile curve of the body is not expressible in simple functional form. The possibility of an appropriate iterative numerical procedure suggests itself but a singular integral equation of the first kind may not be easy to handle. Alternatively, the integral equation may be approximated by a set of linear algebraic equations which may be solved by any one of the usual numerical techniques. This approach is adopted here largely because of its conceptual simplicity. The integral equation is reduced to a set of linear algebraic equations by the following finite element method.

The boundary region, that is, the vorticity sheet is divided into a finite number of small surface elements. Each of the surface elements contains an unknown vorticity distribution. A control point is selected on each of the elements, and the procedure requires that the zero normal flow boundary condition be satisfied at each of the control points, i.e.,

$$v_i + \vec{V}_\infty \cdot \vec{n}_i = 0, \quad i = 1,2,\ldots,N \ . \tag{16}$$

Using the set of Eqs. (12), the Eq. (16) can be rewritten as

$$v_i = V_\infty \sin \theta_i, \quad i = 1,2,\ldots,N \ . \tag{17}$$

The normal component of the induced velocity at the i-th control point, (x_i, z_i), due to the vorticity distribution on the j-th element (see Figure 2) may be expressed as

$$\Delta v'_{ij} = -\int_{x_j}^{x_{j+1}} \frac{\gamma'_j(x)}{2\pi}\left\{\frac{(x_i-x)\cos\theta_i + (z_i-z)\sin\theta_i}{(x_i-x)^2 + (z_i-z)^2}\right\}\left\{1+\left(\frac{dz}{dx}\right)^2\right\}^{\frac{1}{2}} dx, \tag{18}$$

using the Biot-Savart law. Therefore, the total normal induced velocity at the i-th control point due to the entire vorticity sheet is

$$v_i = \sum_{j=1}^{N} \Delta v'_{ij} \quad . \tag{19}$$

Next, it is necessary to find a model, preferably a simple one, to represent the unknown vorticity distribution, $\gamma'_j(x)$, over each of the elements. If $\gamma'_j(x)$ can be expressed as

$$\gamma'_j(x) = \gamma'_j \cdot g'_j(x) \quad , \tag{20}$$

then from Eq. (18)

$$\Delta v'_{ij} = \gamma'_j \cdot A'_{ij} \tag{21}$$

where

$$A'_{ij} = -\frac{1}{2\pi}\int_{x_j}^{x_{j+1}} g'_j(x)\left\{\frac{(x_i-x)\cos\theta_i + (z_i-z)\sin\theta_i}{(x_i-x)^2+(z_i-z)^2}\right\}\left\{1+\left(\frac{dz}{dx}\right)^2\right\}^{\frac{1}{2}} dx.$$

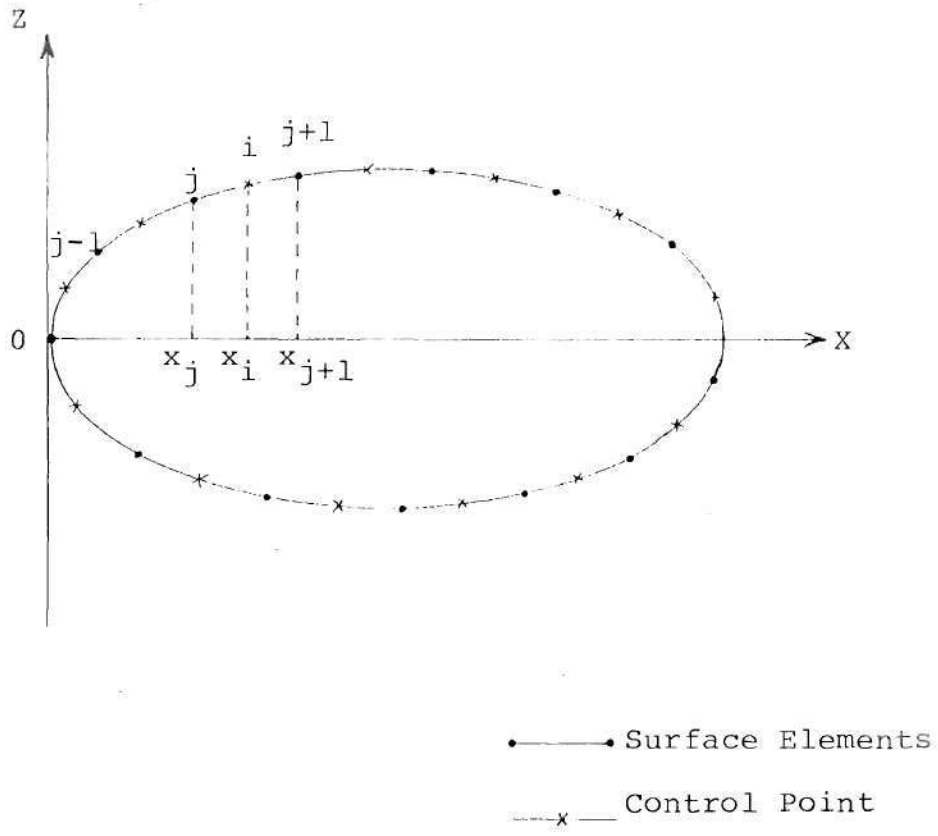

Figure 2. Surface Elements and Control Points for Two-dimensional Body

The term A'_{ij}, the induced velocity influence coefficient, is the induced velocity at the i-th control point due to the j-th elementary vorticity distribution of unit magnitude. The advantage of this formulation is that only one unknown, γ'_j, is associated with one element. It will be seen shortly that a set of linear algebraic equations can be easily constructed with the same number of unknowns as equations. Before that, a simple model for the distribution function, $g'_j(x)$, will be defined.

The representation for $g'_j(x)$ adopted here, consists of a continuous, piecewise linear vorticity distribution approximating the correct distribution as closely as possible yet not sacrificing simplicity. As shown in Figure 3, all linear elementary distributions are actually equivalent to a set of overlapping triangular distributions[28]. Each triangular distribution spanning two successive surface elements will be called an Elementary Vortex Distribution (EVD). Each EVD can be represented by only one unknown which is the vortex intensity value, γ_j, at the apex of the vorticity distribution over the j-th EVD station. The normal component of induced velocity at i-th control point due to the j-th EVD can be written as

$$\Delta v_{ij} = \gamma_j A_{ij} \ , \qquad (22)$$

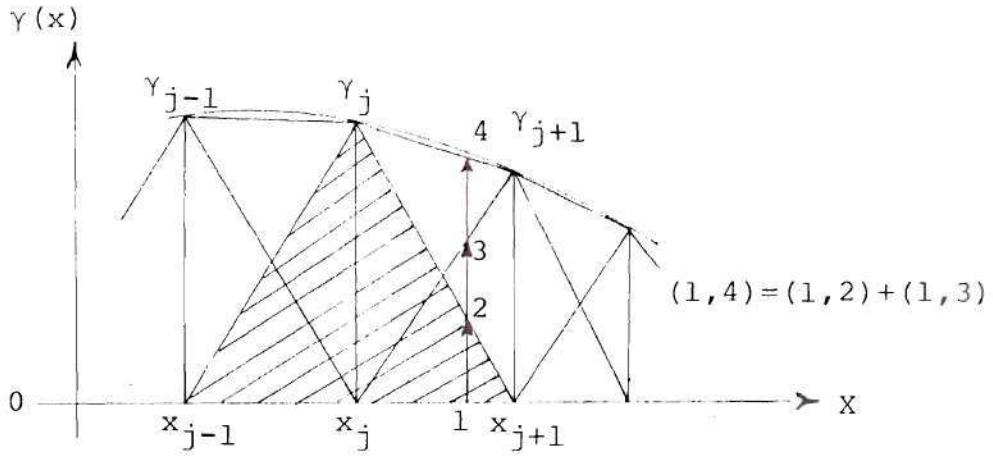

Figure 3. EVD Model for Surface Vorticity Distribution

where

$$A_{ij} = -\frac{1}{2\pi}\int_{x_{j-1}}^{x_{j+1}} g_j(x)\left[\frac{(x_i-x)\cos\theta_i+(z_i-z)\sin\theta_i}{(x_i-x)^2+(z_i-z)^2}\right]\left[1+\left(\frac{dz}{dx}\right)^2\right]^{\frac{1}{2}} dx.$$

The distribution function, $g_j(x)$, can be expressed as

$$g_j(x) = (x_{j+1}-x)/(x_{j+1}-x_j) \quad x_j \leq x \leq x_{j+1}$$

$$= (x-x_{j-1})/(x_j-x_{j-1}) \quad x_{j-1} \leq x \leq x_j \tag{23}$$

The total normal induced velocity at the i-th control point is

$$v_i = \sum_{j=1}^{N} \Delta v_{ij} \ . \tag{24}$$

Combining Eqs. (17), (22), and (24), one has

$$\sum_{j=1}^{N} A_{ij}\gamma_j = V_\infty \sin\theta_i, \quad i = 1,2,\ldots,N \ . \tag{25}$$

This is a system of N linear algebraic equations for N unknown γ_j's. In matrix notation, Eq. (25) can be rewritten as

$$[A]_{NxN}\{\gamma\}_{Nx1} = \{b\}_{Nx1} \ . \tag{26}$$

For the sake of uniqueness of the potential flow solution, the γ_j's must also satisfy the auxiliary condition that

$$\sum_{j=1}^{N} \gamma_j f_j = \Gamma \tag{27}$$

where

$$f_j = \int_{x_{j-1}}^{x_{j+1}} g_j(x)\{1+(\frac{dz}{dx})^2\}^{\frac{1}{2}} dx \ .$$

2.3. Application to Two-dimensional Bodies

2.3.1. Circular Cylinder

The circular cylinder is one of the simplest geometries for which an exact, theoretical potential flow solution is known. The problem under consideration here is one of a right circular cylinder of unit radius placed with its axis normal to a steady, uniform stream of unit magnitude as shown in Figure 4. The results, when compared with the exact solution, serve as a check on the accuracy of the present method.

The surface of the cylinder is divided into N small elements, not necessarily equal. Each of the surface elements is an arc of a circle of unit radius which is mathematically expressed as

$$(x-1)^2 + z^2 = 1 \ . \tag{28}$$

The surface elements need be chosen for only one quadrant owing to the symmetry of the bodv about any diametric plane.

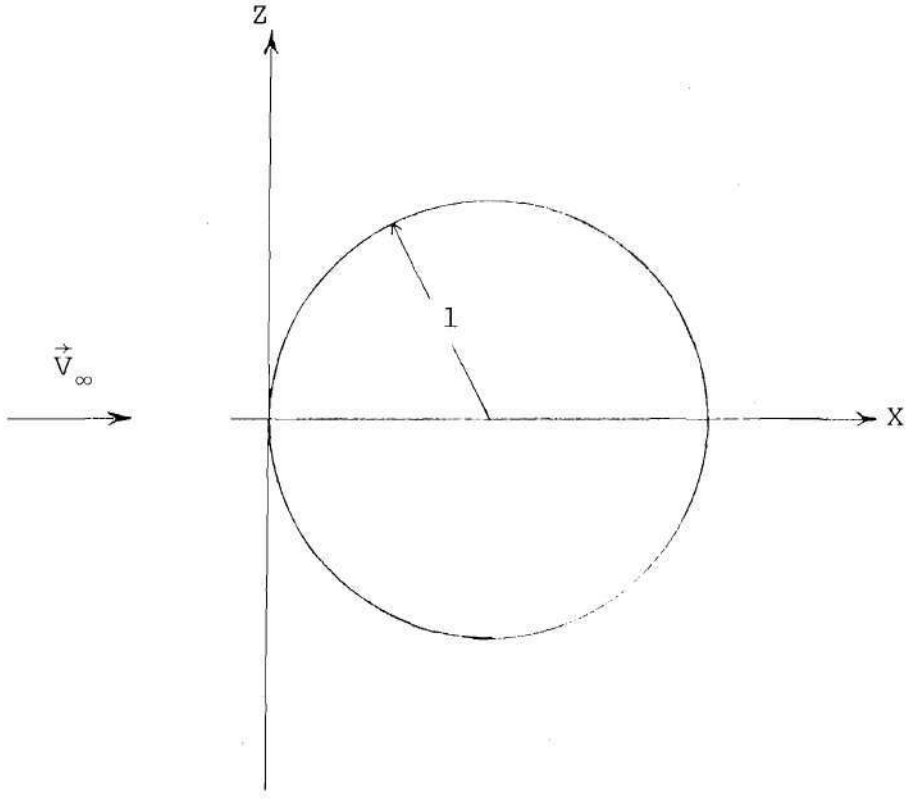

Figure 4. Circular Cylinder of Unit Radius in Steady, Uniform Stream

The end points of each element are the EVD stations where the γ_j's are to be determined. The ordinate for the j-th station at x_j is to be obtained from Eq. (28). On each element, a control point is selected at which the zero normal flow boundary condition is to be satisfied. The abscissa of the i-th control point is chosen to be the mid-point of the projection of the surface element containing the control point on the X-axis, that is

$$x_i = (x_j+x_{j+1})/2, \tag{29}$$

and the corresponding z_i is obtained from Eq. (28). This appears to be a reasonable choice and the results substantiate it further.

The accuracy of the computed velocity and pressure distributions depends on the number and the mode of distribution of the surface elements. A large number of elements results in a large order of the induced velocity influence coefficient matrix, [A]. However, the number of equations to be solved, and hence the order of the matrix is reduced to one-fourth its original value by making use of the symmetry of this problem. Also, the use of symmetry implicitly imposes the zero total circulation condition and thus ensures uniqueness of the solution. The proper distribution of surface elements is largely a matter of experience but it is intuitively clear that it is desirable to place

more EVD stations near the leading edge and the trailing edge where the velocity varies relatively rapidly. Better agreement with exact results is obtained in the leading edge and the trailing edge region when the distribution function, which is linear over successive elements, is replaced, only on the first element, by one proportional to the ordinate of the surface in that region. Specifically, for the circular cylinder, the distribution function for the first element is derived from Eq. (28) as

$$g_1(x) = \sqrt{\frac{x}{x_j}}\left[32 - \frac{8x}{x_j} - \left(\frac{x}{x_j}\right)^2\right]/23 \qquad 0 \leq x \leq x_j \ . \tag{30}$$

The induced velocity influence coefficient, A_{ij}, is computed numerically in order to be consistent with the airfoil problem where the use of an exact, analytical expression for the profile curve makes it almost impossible to obtain a closed form result for A_{ij} from Eq. (22). The integral on the right hand side in Eq. (22) is evaluated by using Simpson's rule[29], with 20 equally spaced divisions, for each control point and EVD station except when the control point lies on the element spanned by the EVD station. In the latter case, the integral is singular but the Cauchy Principal Value[29] exists. This is obtained by using a combination of Simpson's rule and the Trapezoidal rule[29]. The latter is employed to obtain the contribution of the intervals of length ε on either side of the control point

(see Figure 5). The slope of the integrand in Eq. (22) with respect to the X-axis tends to infinity near the control point and Simpson's rule is not likely to give very reliable results.

Having obtained the induced velocity influence coefficient matrix [A], the system of Eq. (26) in first reduced in size by the use of symmetry (see Appendix A). The resulting system is then solved for the unknown vorticity strengths, γ_j's, by applying Gauss-Jordan reduction using maximum pivot strategy[30]. The vorticity strength at each EVD station directly gives the local velocity. Thus, a piecewise linear but continuous velocity (and vorticity) distribution over the entire body is obtained. The pressure coefficient is readily computed from Eq. (10).

2.3.2. NACA Basic Thickness Form Airfoils

The NACA basic thickness form airfoil can be analytically expressed[31] as

$$\frac{z}{c} = \pm \frac{t}{c}\{q_1(\frac{x}{c})^{\frac{1}{2}} + q_2(\frac{x}{c}) + q_3(\frac{x}{c})^2 + q_4(\frac{x}{c})^3 + q_5(\frac{x}{c})^4\}. \quad (31)$$

The coefficients, q's, are constants determined by certain conditions on the airfoil geometry:

$$\begin{aligned} x &= 0.1c \quad & z &= 0.39t, \\ x &= 0.3c \quad & z &= 0.5t, \ \frac{dz}{dx} = 0, \\ x &= c \quad & z &= 0.01t, \ \frac{dz}{dx} = -1.17t\ . \end{aligned} \quad (32)$$

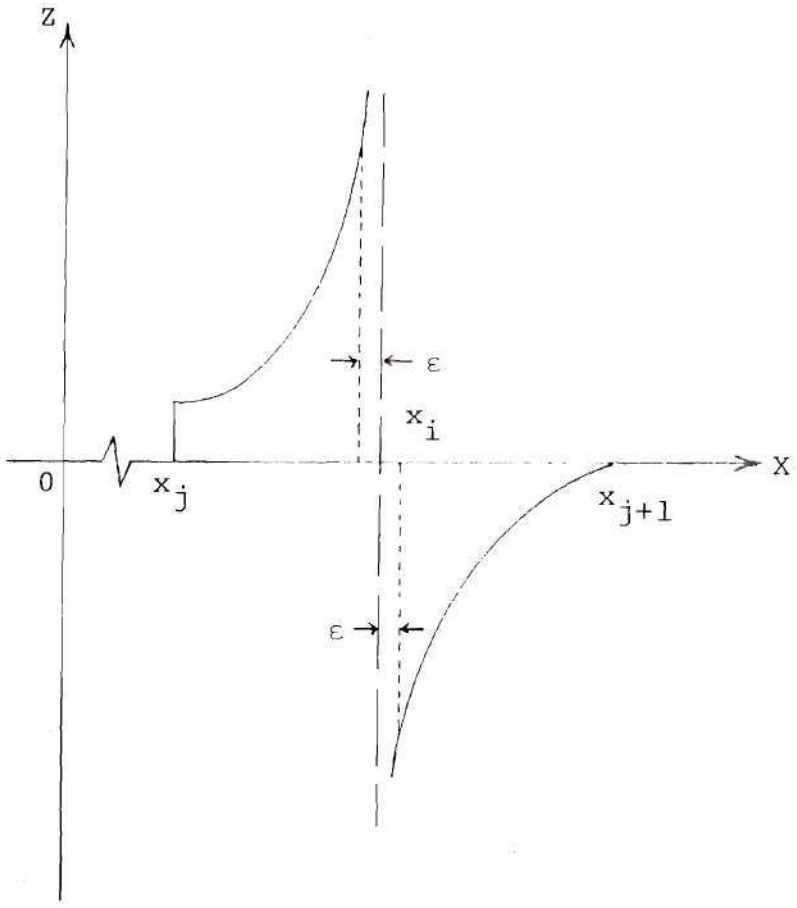

Figure 5. Cauchy Principal Value for a Singular Control Point

Since the airfoil has finite thickness at the trailing edge, the resulting corners are undesirable for the potential flow. An airfoil, with a sharp trailing edge, is obtained by extending the upper and lower surfaces along the tangent at x=c (see Figure 6). This appears reasonable because in real flow, viscous effects will smooth out any corner flow.

The procedure for dividing the airfoil surface into elements is based on reasoning similar to that for the circular cylinder. The airfoil, however, offers symmetry only about its chord. Therefore, the unknowns, γ_{j_a}'s, need to be obtained for either upper or lower surface EVD stations, i.e., for half the number of elements. The Kutta-Joukowski condition forces the vorticity strength at the sharp trailing edge to be zero. While computing the flow for zero angle of attack (see Figure 7), symmetry also demands that the peak value, γ_{j_a}, at the leading edge (x=0) EVD station be zero.

The steady state flow on the airfoil at an angle of attack, α_o, can be obtained by superimposing the non-circulatory flow solution (zero angle of attack, nonlifting case) and a cross-flow solution which is entirely circulatory (see Figure 8). The change in direction of the onset flow enters Eq. (12) and gets reflected as a different column vector {b} in Eq. (26) for the cross-flow. The A_{ij}'s

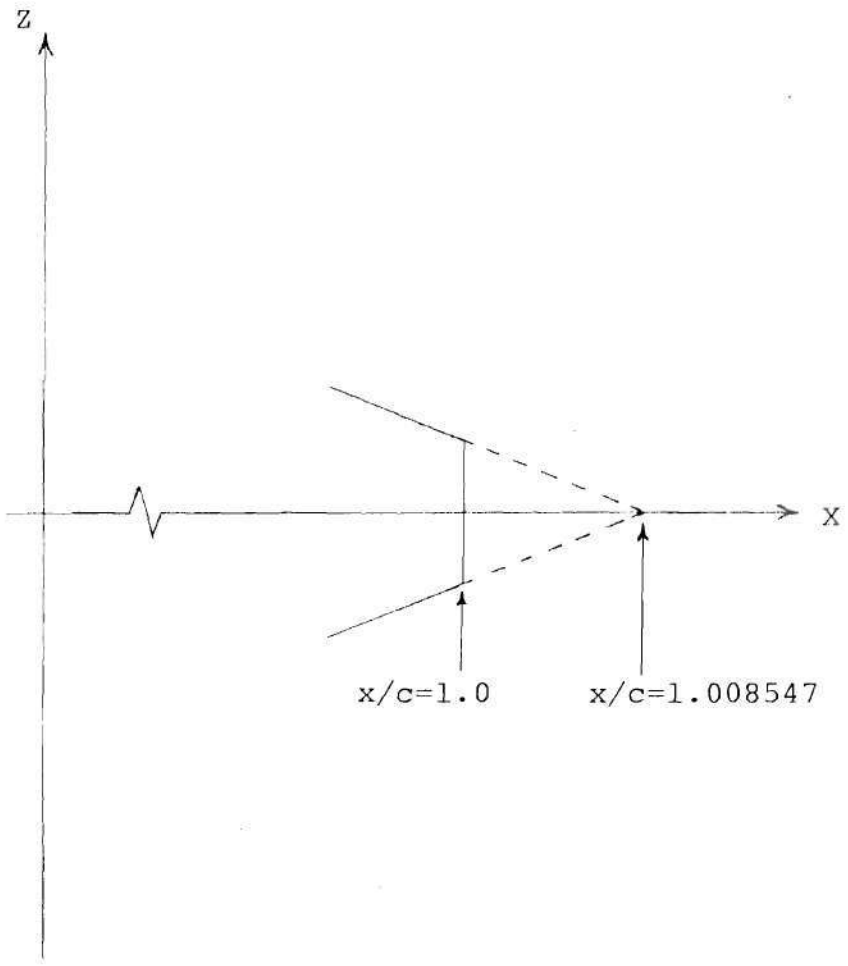

Figure 6. Sharp Trailing Edge for NACA Basic Thickness Form Airfoil

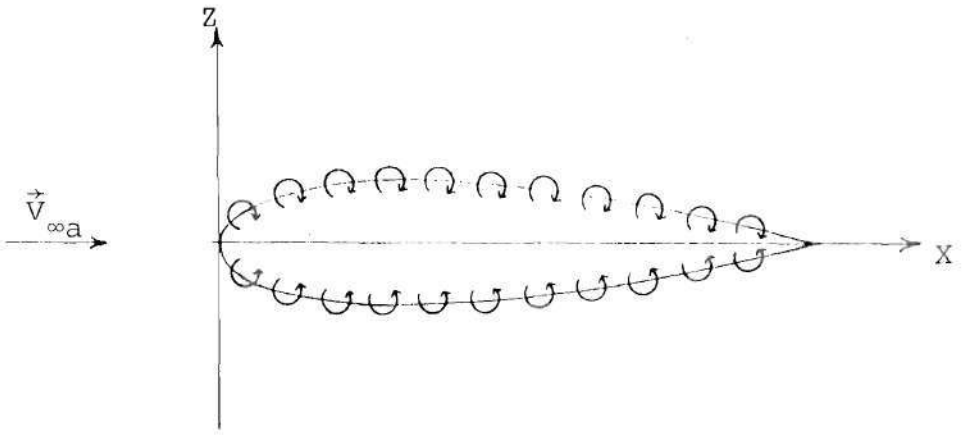

Figure 7. NACA Basic Thickness Form Airfoil in Noncirculatory Flow, $\alpha_o=0°$

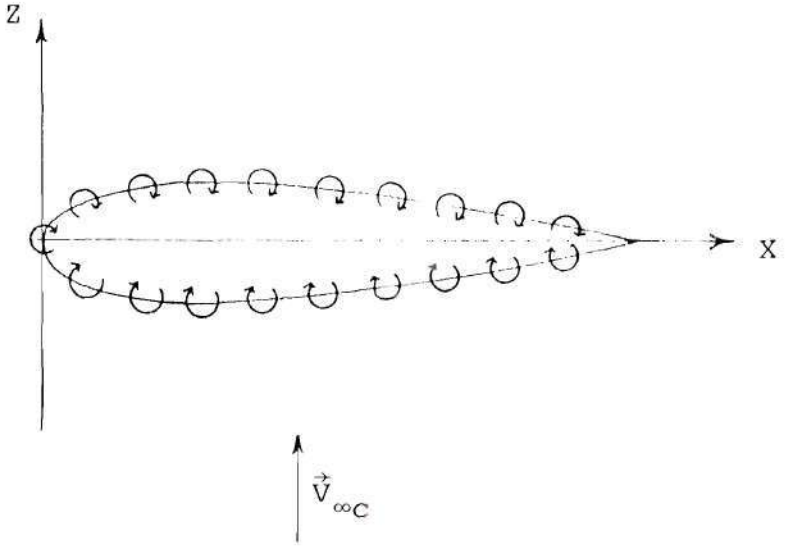

Figure 8. NACA Basic Thickness Form Airfoil in Cross-flow, $\alpha_o=90°$

remain unchanged for both the noncirculatory and the cross-flow cases except the one at the leading edge which is different from zero in the latter. For cross-flow also, the Kutta condition forces the vorticity strength at the trailing edge to be zero and the use of symmetry reduces the number of unknowns, γ_{j_c}'s, to be determined. Once the solutions are obtained, the vorticity (velocity) strength at a j-th station for an angle of attack, α_o, is given by

$$\gamma_{j_{\alpha_o}} = \gamma_{j_a} \cos\alpha_o + \gamma_{j_c} \sin\alpha_o \ . \tag{33}$$

The induced velocity influence coefficients have to be obtained numerically because of the complicated Eq. (31) for the airfoil profile curve to be used in Eq. (22). The numerical procedure is exactly the same as for the circular cylinder and described earlier. For the distribution function on the first element near the leading edge, the use of

$$g_1(x) = 1.225\sqrt{\frac{x}{x_j}} - 0.225\left(\frac{x}{x_j}\right), \quad 0 \leq x \leq x_j, \tag{34}$$

is made (in accordance with the results for the circular cylinder) for the case of noncirculatory flow; for the cross-flow, it is taken to be linear.

2.3.3. Results

The chordwise velocity distribution on the upper

surface (from the leading edge to the midchord) of a circular cylinder of unit radius placed with its axis normal to a steady, uniform, unit onset flow is presented in Table 1. For four sets of different numbers of surface elements and for different modes of chordwise distribution of these elements, the agreement with exact, theoretical results appears to be good and only marginal variations in local velocities are noticed. This is also reflected in rather insignificant changes in the total circulation around a path enclosing the vorticity on the upper surface from the leading edge to the midchord. The effect on the vorticity distribution of a change in the mode of distribution of the surface elements is found to be confined to rather localized regions. Based on the uniform free stream value of unity, the errors in the magnitudes of the local velocities are less than one percent when compared with the theoretical values. The chordwise variation of the nondimensional local velocity on the upper surface of the circular cylinder is plotted in Figure 9.

Four thickness ratios, 6%, 12%, 18%, and 24%, were selected for NACA basic thickness form airfoils. For each case, the chordwise velocity distribution on the upper surface of the airfoil placed at zero angle of attack in a steady, uniform stream of unit magnitude is documented in

Table 1. Chordwise Surface Velocity Distribution on a Circular Cylinder of Unit Radius using Elementary Vortex Distribution Technique

Vel / x/c	Exact Analytical	N = 72	N = 88	N = 108	N = 128
.0	.0	.0	.0	.0	.0
.00025	.0632	.0654	.0642	.0654	.0645
.0005	.0894	.0915	.0901	.0914	.0904
.001	.1264	.1296	.1266	.1295	.1275
.005	.2821	.2860	.2837	.2858	.2838
.01	.3980	.4056	.3973	.4054	.3983
.025	.6245	.6322	.6248	.6318	.6312
.05	.8718	.8814	.8810	.8765	.8766
.1	1.2000	1.2072	1.2074	1.2017	1.2018
.15	1.4283	1.4324	1.4325	1.4292	1.4293
.2	1.6000	1.6029	1.6030	1.6006	1.6007
.25	1.7320	1.7343	1.7344	1.7325	1.7326
.3	1.8330	1.8349	1.8350	1.8334	1.8335
.35	1.9079	1.9095	1.9096	1.9082	1.9083
.4	1.9596	1.9611	1.9612	1.9599	1.9600
.45	1.99	1.9914	1.9915	1.9903	1.9903
.5	2.0	2.0014	2.0015	2.0003	2.0004
Circu-lation	2.0	1.9994	1.99975	1.99971	1.99999

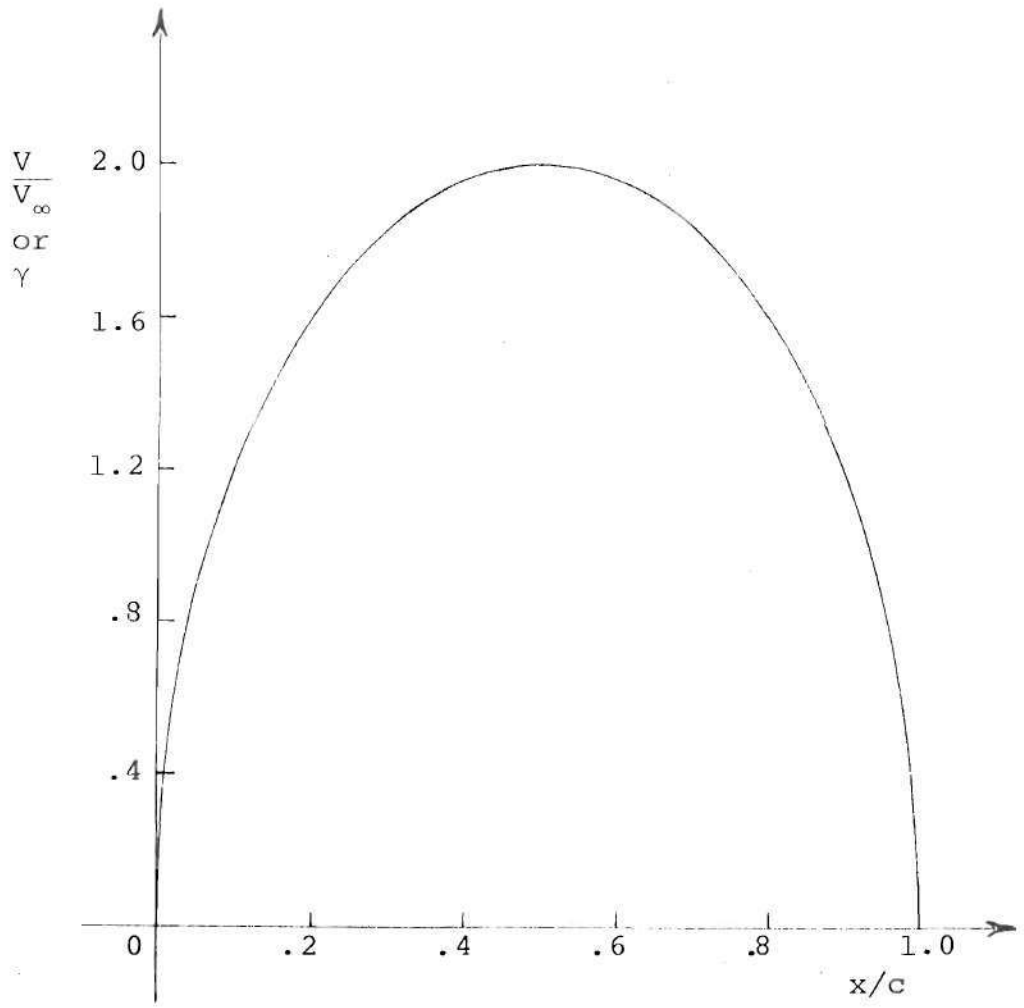

Figure 9. Velocity/Vorticity Distribution on the Upper Surface of a Unit Circular Cylinder Placed in Unit Free Stream

Tables 2 and 3. The velocity distributions as reported by Abbott, von Doenhoff, and Stivers[32] and computed from Theodorsen's[5] procedure, are also given for the purpose of comparison. The corresponding plots are given in Figures 10-13. The chordwise velocity distribution on the upper surface of the 12% thick airfoil in cross-flow (α_o=90°), and the values of the local surface velocity and the pressure coefficient at α_o=6° are presented in Table 4. The C_p distributions at zero angle of attack and at 6° angle of attack for 12% thick airfoil are plotted in Figure 14 and Figure 15 respectively. The section lift coefficient and its variation with angle of attack is shown in Figure 16, for 6%, 12%, and 18% thick airfoils. The values of C_ℓ from linearized thin airfoil theory ($= 2\pi \sin\alpha_o$) are also plotted in the same figure. The corresponding numerical values are given in Table 5. The effect of the thickness of an airfoil on the sectional lift coefficient is quite clear from these results. It is further substantiated by the potential flow theory for Joukowski profiles[4] where

$$C_\ell \simeq 2\pi(1 + 0.77 \frac{t}{c})\sin \alpha_o \ . \qquad (35)$$

The computational time required to complete a typical case of a two-dimensional airfoil in noncirculatory or circulatory flow is approximately one minute on the

Table 2. The Chordwise Velocity Distribution on the Upper Surface of NACA 0006 and 0012 Airfoils

V/V_∞ / x/c	t/c = 0.06		t/c = 0.12	
	Ref. 32	EVD N = 60	Ref. 32	EVD N = 60
.0	.0	.0	.0	.0
.005	.938	.9718	.8	.8084
.025	1.089	1.0842	1.114	1.1106
.05	1.103	1.0959	1.174	1.1653
.075	1.107	1.0978	1.184	1.1807*
.1	1.101	1.0975	1.188	1.1866
.12		1.0964		1.1873
.15	1.098	1.0941	1.188	1.1856
.2	1.091	1.0892	1.183	1.1781
.25	1.086	1.0833*	1.174	1.1669*
.3	1.078	1.0775	1.162	1.1558
.4	1.066	1.0649*	1.135	1.13*
.5	1.053	1.0523	1.108	1.1041
.6	1.042	1.0395*	1.08	1.078*
.7	1.028	1.0267	1.053	1.052
.8	1.013	1.0117	1.022	1.0218
.9	.99	.9901	.978	.9791
.95	.974	.9705	.952	.9417
1.0	.0	.9026	.0	.8232
1.008547		.0		.0

* Linearly interpolated.

Table 3. The Chordwise Velocity Distribution on the Upper Surface of NACA 0018 and 0024 Airfoils

V/V_∞ / x/c	t/c = 0.18		t/c = 0.24	
	Ref. 32	EVD N = 60	Ref. 32	EVD N = 60
.0	.0	.0	.0	.0
.005	.682	.6739	.579	.5813
.025	1.103	1.095	1.063	1.0577
.05	1.228	1.2085	1.244	1.2295
.075	1.264	1.2475*	1.322	1.2984*
.1	1.276	1.266	1.354	1.3348
.12		1.2717		1.3488
.15	1.278	1.2737	1.374	1.358
.2	1.275	1.2665	1.368	1.354
.25	1.262	1.2506*	1.35	1.3341*
.3	1.247	1.2347	1.333	1.3141
.4	1.205	1.1949*	1.277	1.2597*
.5	1.154	1.1552	1.204	1.2052
.6	1.116	1.1152*	1.151	1.1508*
.7	1.074	1.0753	1.097	1.0964
.8	1.025	1.0298	1.032	1.0355
.9	.966	.9666	.944	.9524
.95	.914	.9127	.879	.8833
1.0	.0	.7548	.0	.6938
1.008547		.0		.0

* Linearly interpolated.

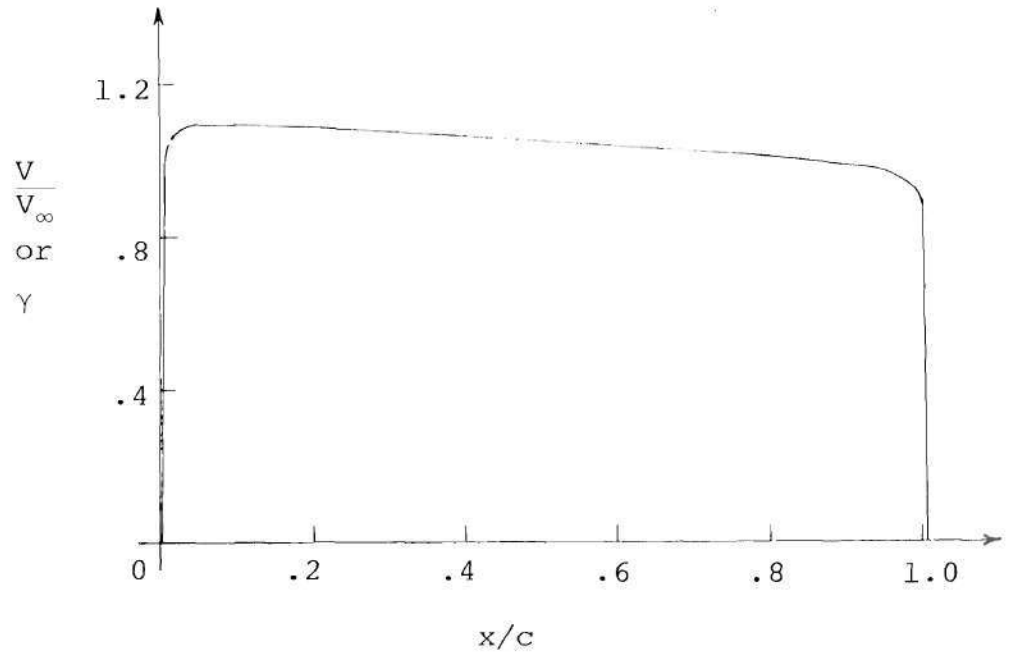

Figure 10. Chordwise Surface Velocity/Vorticity Distribution on NACA 0006 Airfoil at α_o=0°

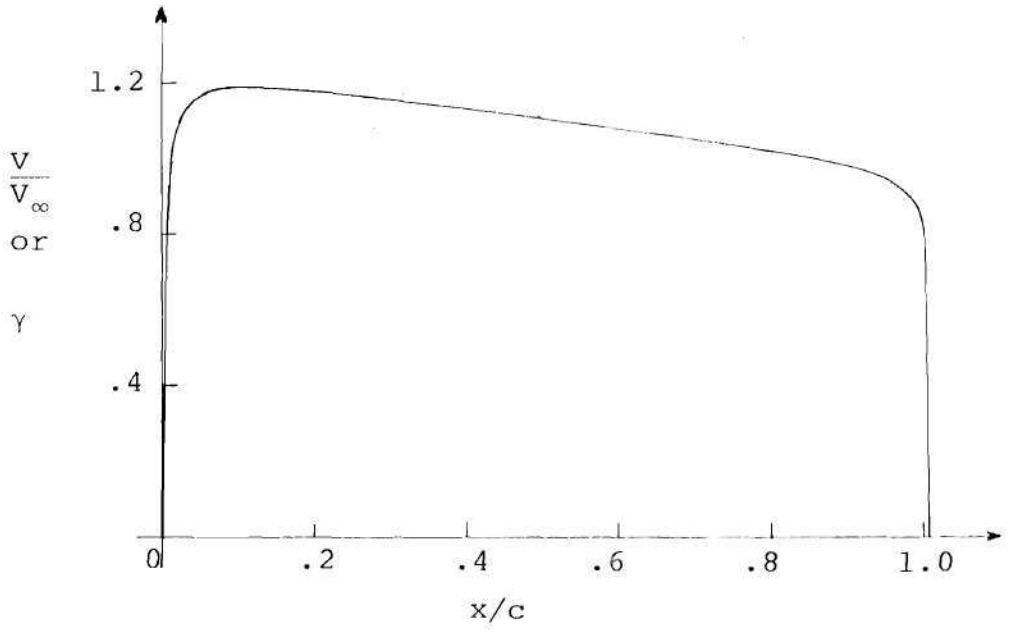

Figure 11. Chordwise Surface Velocity/Vorticity Distribution on NACA 0012 Airfoil at α_o=0°

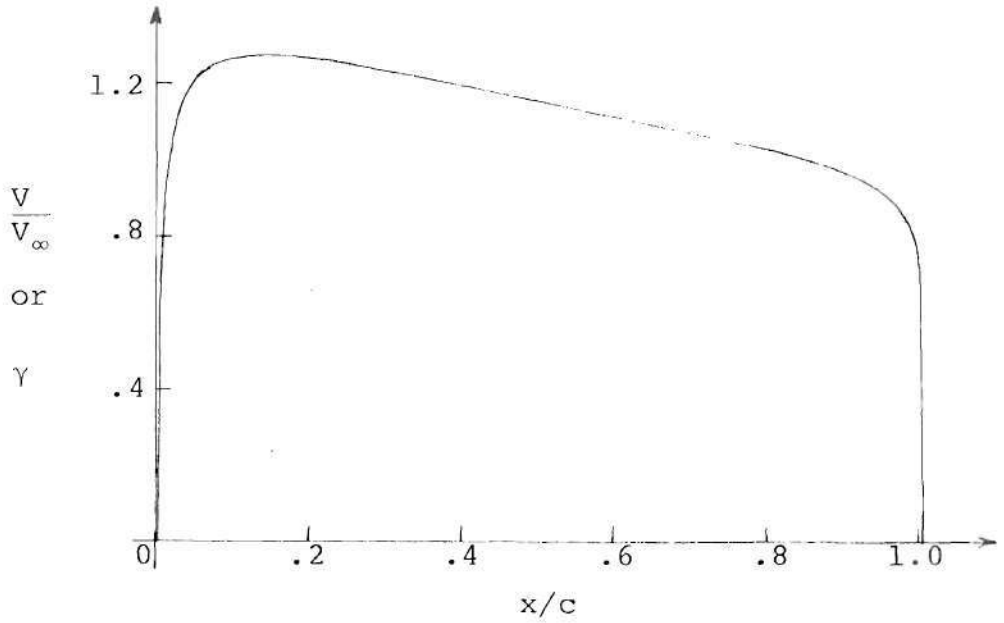

Figure 12. Chordwise Surface Velocity/Vorticity Distribution on NACA 0018 Airfoil at $\alpha_o=0°$

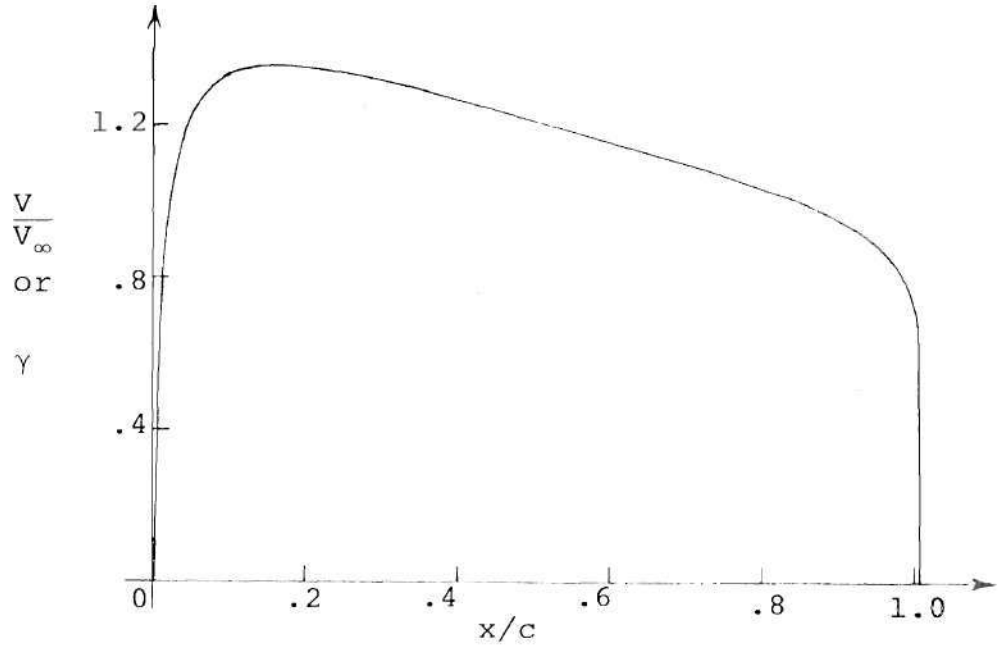

Figure 13. Chordwise Surface Velocity/Vorticity Distribution on NACA 0024 Airfoil at $\alpha_o=0°$

Table 4. The Cross-flow Velocity Distribution on the Upper Surface, and the Chordwise Velocity and C_p Distributions at $\alpha_o=6°$, for NACA 0012 Airfoil

	$\alpha_o=90°$	$\alpha_o=6°$		$\alpha_o=6°$	
		Upper Surface		Lower Surface	
x/c	VEL N = 62	VEL	C_p	VEL	C_p
.0	13.506	1.412	-0.993	1.412	-0.993
.0015	12.505	1.737	-2.016	0.807	+0.348
.003	11.623	1.893	-2.582	0.527	+0.711
.005	10.670	1.919	-2.684	0.311	+0.903
.01	8.992	1.9	-2.611	0.020	+0.9996
.025	6.483	1.783	-2.176	0.427	+0.818
.05	4.785	1.659	-1.752	0.659	+0.566
.1	3.367	1.532	-1.347	0.828	+0.314
.12	3.043	1.499	-1.247	0.863	+0.256
.15	2.662	1.457	-1.124	0.901	+0.189
.2	2.211	1.403	-0.968	0.940	+0.115
.3	1.642	1.321	-0.745	0.978	+0.044
.5	1.027	1.205	-0.453	0.9907	+0.018
.7	0.647	1.114	-0.241	0.978	+0.042
.8	0.484	1.067	-0.138	0.966	+0.067
.9	0.312	1.006	-0.013	0.941	+0.114
.95	0.212	0.959	+0.081	0.914	+0.164
.98	0.136	0.907	+0.177	0.879	+0.228
1.0	0.067	0.826	+0.318	0.812	+0.341
1.008547	0.0	0.0	+1.0	0.0	+1.0

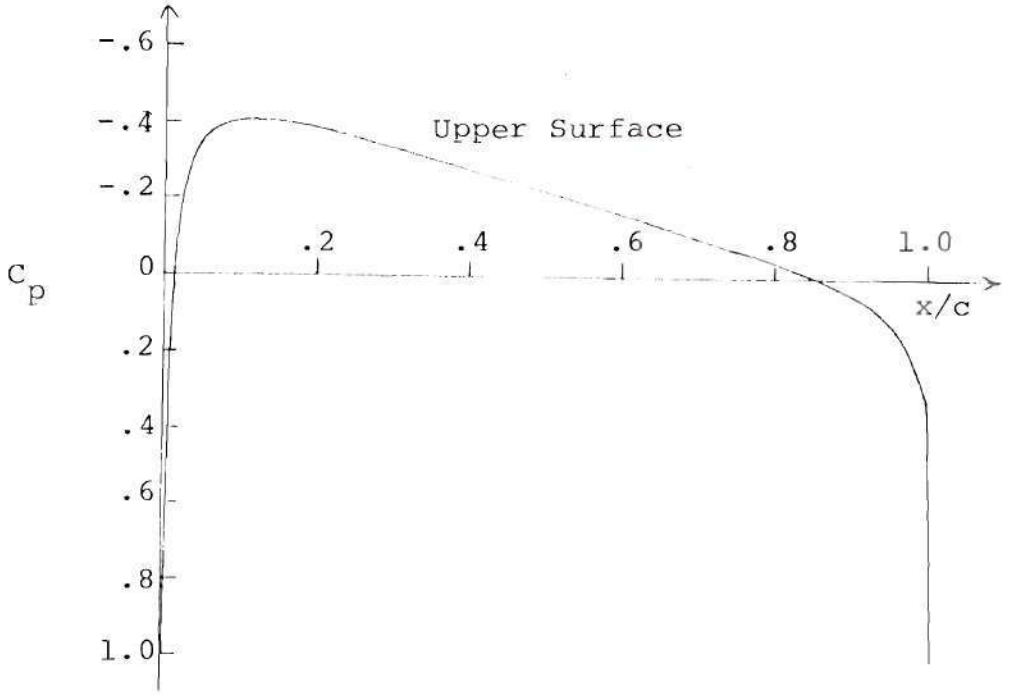

Figure 14. Chordwise Pressure Coefficient Distribution on NACA 0012 Airfoil at α_o=0°

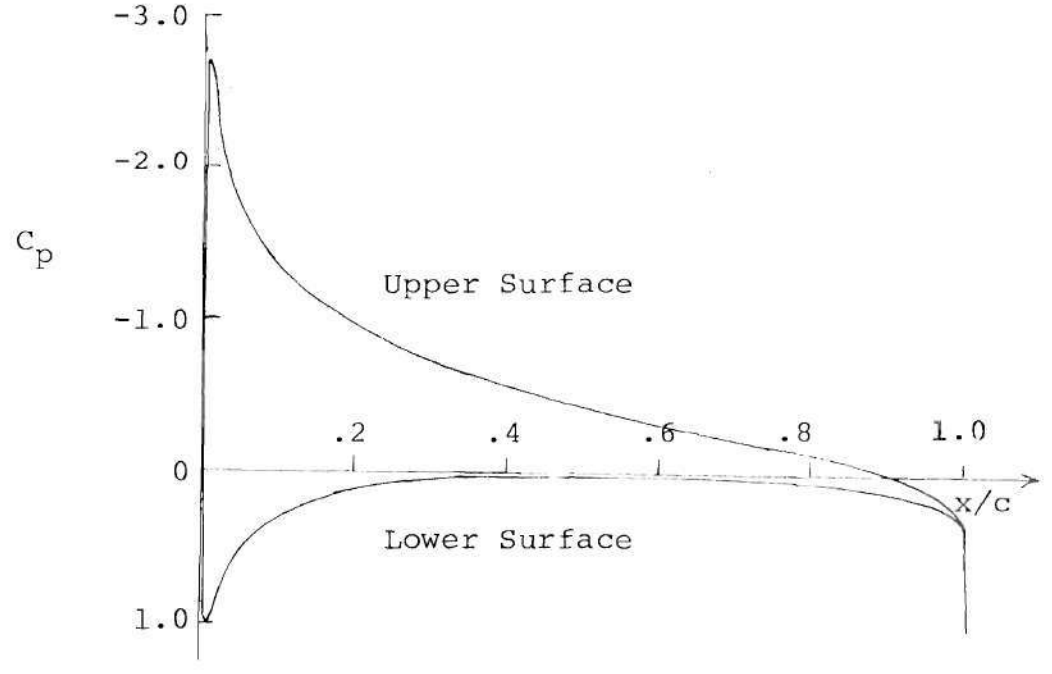

Figure 15. Chordwise Pressure Coefficient Distribution on NACA 0012 Airfoil at α_o=6°

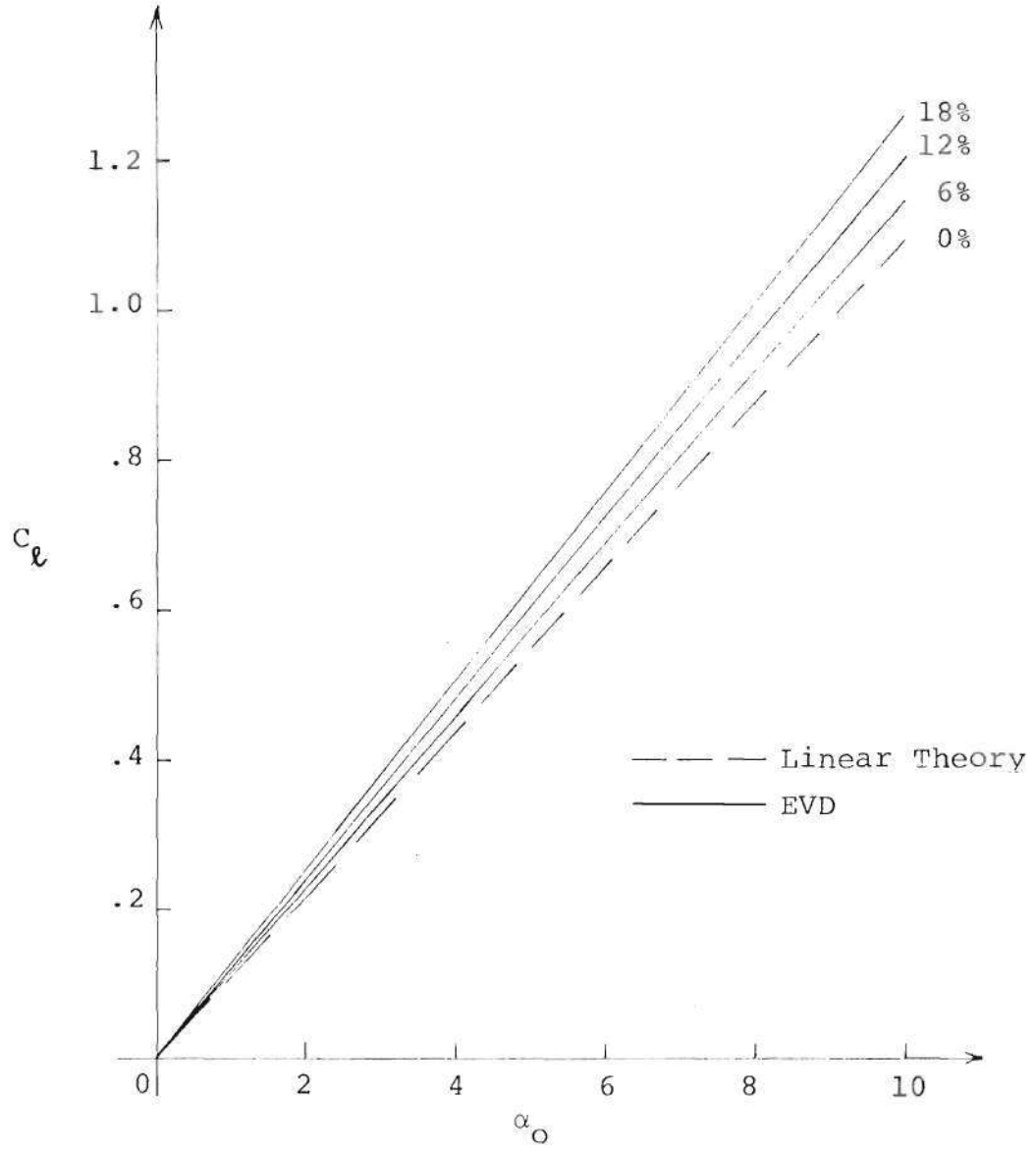

Figure 16. Variation of the Sectional Lift Coefficient, C_ℓ, with Angle of Attack, α_o

Table 5. Section Lift Coefficient Variation with Angle of Attack for NACA Basic Thickness Form Airfoils

α_o \ t/c	0.0 (Thin airfoil theory)	0.06	0.12	0.18
.0	.0	.0	.0	.0
2.0	.21928	.22998	.24103	.25219
4.0	.4383	.45969	.48177	.50406
6.0	.65677	.68884	.72192	.75533
8.0	.87445	.91714	.96119	1.00567
10.0	1.09106	1.14433	1.19929	1.25479

CDC Cyber 70/74 NOS 1.1 - 419/420 when the total number of elements is 60. Most of this is used in solving the system of algebraic equations. Depending on the number of elements, the computer time required varies from a few seconds to a few minutes.

CHAPTER III

THREE-DIMENSIONAL FLOWS

3.1. Development of an Iterative Procedure

The problem of computation of the three-dimensional flow on the tip region of a thick wing can also be approached from the integral equation standpoint in a manner conceptually identical to that for the two-dimensional formulation. However, a sufficiently detailed and accurate determination of the flow field would require an enormously large number of surface elements resulting in a very large induced velocity influence coefficient matrix. Moreover, the use of vorticity as the surface singularity distribution yields a Fredholm integral equation of the first kind which is very likely to pose problems in the numerical solution when approximated by a large set of linear algebraic equations. In this chapter, an alternate approach based on a simple iterative procedure is presented for computing detailed three-dimensional flow on the wing tips. The procedure starts from a two-dimensional or other suitable vorticity distribution on the entire surface. The successive iterations readjust the initial vorticity strength distribution to yield an appropriate surface vorticity distribution for a given body. In the following

sections, a semi-infinite body is considered to illustrate the formulation of the iterative procedure. This facilitates the development of the method because the flow is essentially two-dimensional on the entire region inboard of a limited zone of three-dimensional flow near the tip. Therefore, the iterative scheme must converge to the three-dimensional flow on the tip region which merges smoothly with the two-dimensional flow further inboard. It should also be noted that the surface velocity distribution approaches the nearly two-dimensional distribution within a small distance inboard from the tip for a large class of wing planforms and flows governed by the Laplace's equation. The present method is successfully applied to compute the surface velocity and pressure distributions on two semi-infinite bodies namely a circular cylinder with a hemispherical tip and a symmetrical wing whose cross-section is NACA basic thickness form airfoil with a half body of revolution forming its tip. These cases are presented in the next chapter.

3.2. General Outline of the Iterative Procedure for a Semi-infinite Body

It is first assumed that on the surface of a semi-infinite body the local vorticity strength at any chordwise location on the entire body is the same as the corresponding two-dimensional value. Obviously, this does not conform to

the actual three-dimensional vorticity distribution in the neighborhood of the tip. The next step is to divide the surface into a finite number of small elements each containing a control point. For each of the control points, the local tangential velocity resulting from the initial surface vorticity distribution is calculated using the Biot-Savart law. It is to be noted that the local tangential vorticity strength is equivalent to this value of the local surface velocity and the local velocity vector is perpendicular to the local vorticity vector. The vorticity at any point on the surface is completely specified in magnitude and direction by a pair of orthogonal vectors which are designated α-type and β-type. The two-dimensional vorticity distribution is entirely α-type. The β-type component is needed near the tip to account for the three-dimensionality. The surface vorticity strength,

$$\delta = (\alpha^2+\beta^2)^{\frac{1}{2}}, \tag{36}$$

computed for each control point will not, in general, agree with the initial value in magnitude and/or direction. However, the calculated values provide a closer approximation to the final result than the original distribution. The existing surface vorticity distribution is, therefore, replaced by this new set of computed values. This completes what is termed the zeroth iteration. For the first

iteration, the α-type and the β-type components are computed at each of the control points for the new surface vorticity distribution. The results so obtained are compared with the previous set of values obtained from the zeroth iteration. They may still not agree well at a number of control points. The first iteration values then replace the surface vorticity distribution. In principle, the procedure can be carried out until the differences of the α-type and the β-type values for two successive iterations are not significant. The results show that good convergence is obtained by the third or fourth iteration. Some modifications to make this basic procedure more efficient are described later in Section 4.2.

3.3. Mathematical Formulation

The details of the mathematical formulation of the iterative method for a semi-infinite body are described in this section. The semi-infinite body considered here is a cylindrical body whose cross-section is a circle of unit radius. A hemispherical cap is joined to one end of the cylinder. The origin of the Cartesian coordinate system is situated at the intersection of the leading edge and the circle which joins the hemisphere and the cylinder. The axis of the body is parallel to the Y-axis and the X-axis intersects the body-axis at the center of the hemisphere as

shown in Figure 17. The procedure to divide the body surface into small elements needs to be described first. On the circular cylinder ($y \leq 0$), any plane parallel to the Y-Z plane intersects the surface along a semi-infinite straight line which defines a k-station. A plane parallel to the X-Z plane intersects the cylinder along a circle of unit radius which defines an ℓ-station. The k-stations, the ℓ-stations, and the body surface form the surface elements on the cylinder.

On the hemispherical tip, the origin of the coordinate system is treated as a north or south pole on a globe and mutually orthogonal "longitudes" and "latitudes" are drawn as follows. A plane parallel to the Y-Z plane intersects the hemisphere along a semi-circle which corresponds to a "latitude" and defines a k-station. A radial plane inclined at an angle ψ to the X-Z plane intersects the hemisphere along a semi-circle of unit radius which corresponds to a "longitude" and defines a m-station. The k-stations, the m-stations, and the surface form the surface elements on the hemisphere which is mathematically expressed as

$$(x-1)^2 + y^2 + z^2 = 1 \qquad (37)$$

The surface elements on the cylinder and on the tip are curved surfaces of different shapes and sizes. The

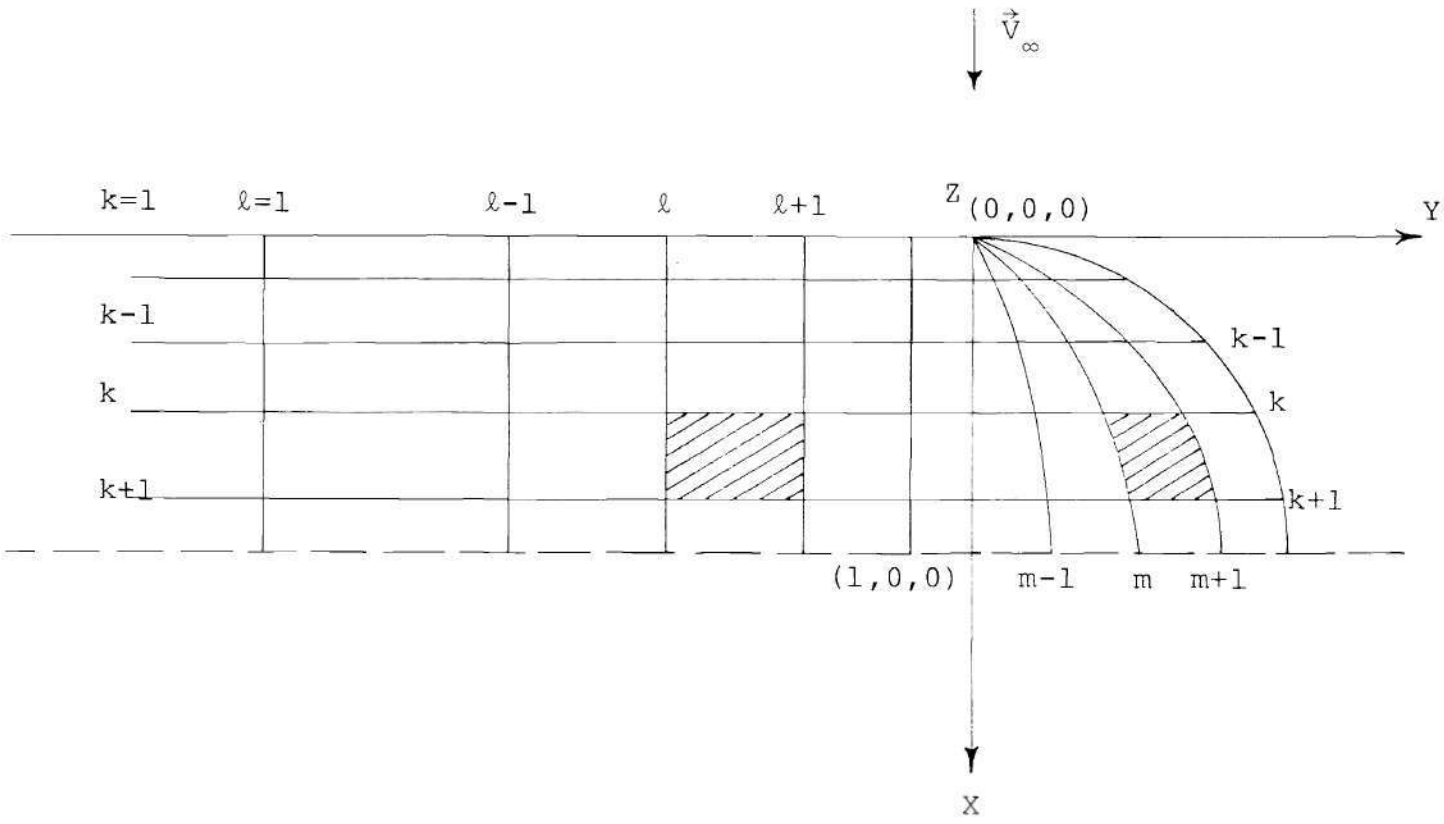

Figure 17. Semi-infinite Circular Cylindrical Body with a Hemispherical Tip

procedure offers enough flexibility for varying the number and the sizes of the surface elements.

As mentioned earlier, a control point is to be selected on each element. For lack of any previous experience for three-dimensional flows, the obvious choice is the geometric midpoint of each element. It is also to be noted that for this specific case, the control points need be selected in one quadrant only owing to symmetry about any diametric plane.

3.3.1. Zeroth Iteration

The body is first "wrapped" with a vorticity sheet whose chordwise strength distribution is the same as the two-dimensional chordwise distribution for a circular cylinder of unit radius as computed in Chapter II. Therefore, the chordwise vorticity distribution is identical at every ℓ- and m-station. The vorticity distribution on the cylinder ($y \leq 0$) is constituted of semi-infinite filaments and the tip vorticity is composed of semi-circular filaments for each value of x. The induced velocity due to this system of vorticity can be computed at the i-th control point (x_i, y_i, z_i) on the surface by the use of the Biot-Savart law. The direction cosines, (c_1, c_2, c_3) of a surface tangent vector, have definite constant values depending on the location of the control point and the direction of the tangential component of vorticity, α- or

β-type, to be computed. The total induced velocity is the sum of the contributions of the upper surface ($z>0$) and lower surface ($z<0$) of the cylinder and the contribution of the hemispherical tip. The induced velocity due to the former can be expressed as

$$V_{U,L} = \pm \sum_{k=1}^{K} \Delta V_{ik} \tag{38}$$

where

$$\Delta V_{ik} = \int_{x_k}^{x_{k+1}} \frac{\gamma(x)}{4\pi} \left[1 - \frac{y_i}{\{(x_i-x)^2+(z_i \mp z)\}^{1/2}}\right] \frac{(z_i \mp z)c_1 - (x_i-x)c_3}{(x_i-x)^2+(z_i \mp z)^2}$$

$$\cdot \{1 + (\frac{dz}{dx})^2\}^{1/2} \, dx,$$

with

$$\gamma(x) = \gamma(x_k) + [\{\gamma(x_{k+1})-\gamma(x_k)\}/(x_{k+1}-x_k)](x-x_k) \ .$$

Wherever two signs appear for a term, the upper sign corresponds to the upper surface and the lower one to the lower surface. The relation between z and x is given by

$$z = \{x(2-x)\}^{1/2} \tag{39}$$

The contribution of the tip may be written as

$$V_T = \sum_{k=1}^{K} \Delta V_{ik} \tag{40}$$

where

$$\Delta V_{ik} = \int_{x_k}^{x_{k+1}} \int_0^{\pi} \frac{\gamma(x)}{4\pi} \left[\frac{\{(z_i - z)\cos\varepsilon + (y_i - y)\sin\varepsilon\} c_1 - (x_i - x)(c_2 \sin\varepsilon + c_3 \cos\varepsilon)}{\{(x_i - x)^2 + (y_i - y)^2 + (z_i - z)^2\}^{3/2}} \right]$$

$$\cdot \lambda(x)(1+m^2)^{1/2} d\varepsilon dx,$$

with

$$\lambda(x) = \sqrt{x(2-x)} \ ,$$

$$m = \frac{d\lambda}{dx} \ ,$$

$$y = \lambda(x) \sin\varepsilon,$$

and

$$z = \lambda(x) \cos\varepsilon \ .$$

(For the definition of ε, see Figure 18).

The total induced velocity,

$$V_I = V_U + V_L + V_T \ , \tag{41}$$

at the i-th control point is added to the tangential component of the free stream velocity as appropriate for the computation of the α-type or the β-type vorticity. This sum gives the mean tangential velocity of the surface vorticity sheet and is therefore one-half of the local

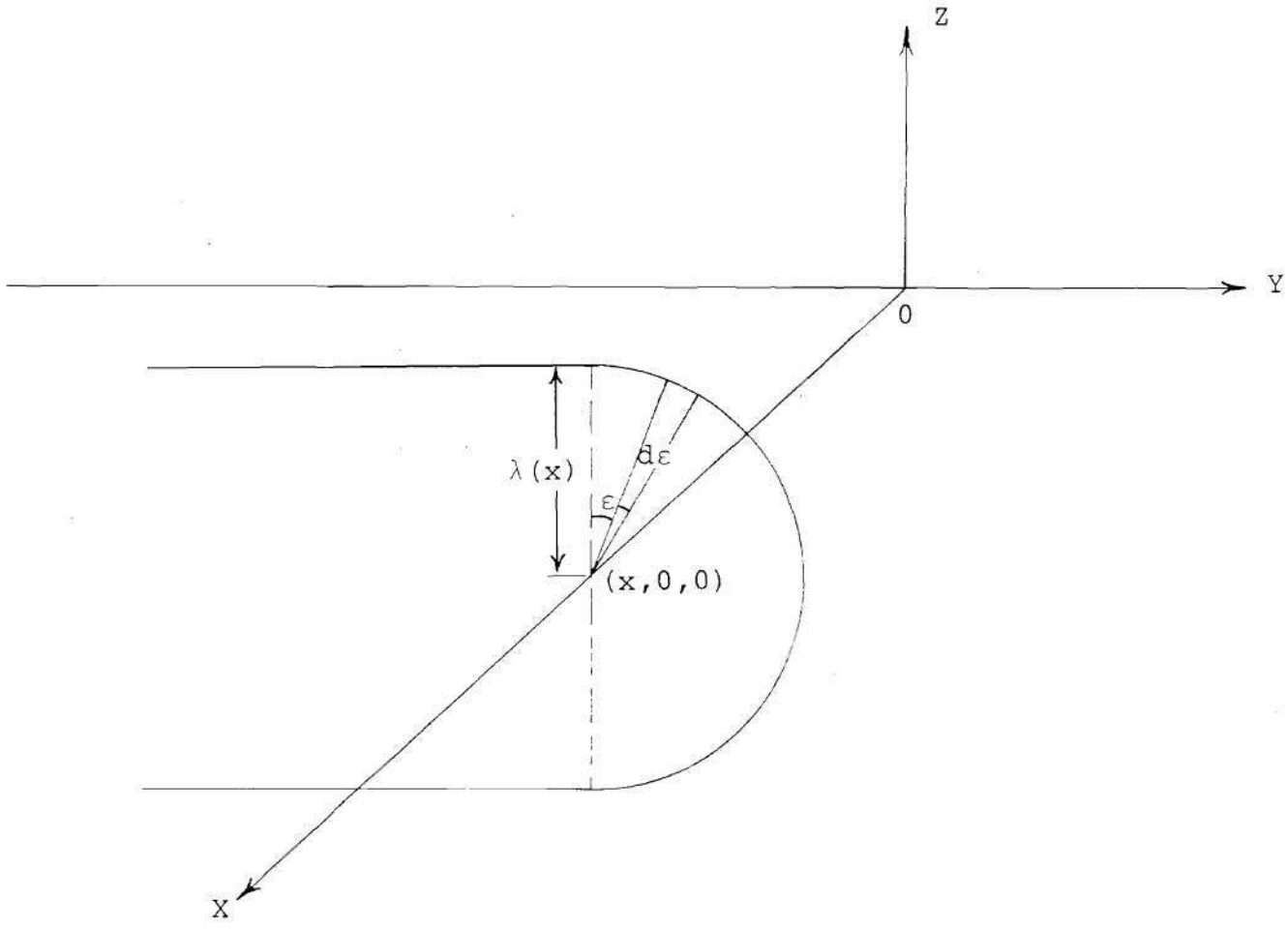

Figure 18. Definition of $\lambda(x)$ and ε

vorticity strength at the i-th control point.

It is expected and borne out by the results of the zeroth iteration that the α-type vorticity distribution at the ℓ-stations approaches the corresponding two-dimensional distribution at a few chords inboard from the tip. At the same time, the value of the β-type vorticity approaches zero. There is then, a cut-off station $\ell=1$, inboard of which, the flow can be assumed to be essentially two-dimensional. In the neighborhood of the tip, it is further assumed, for the sake of simplicity, that the values of the α- and the β-type vorticity vary linearly between any two adjacent control points. This is consistent with the assumption of a piecewise linear vorticity distribution in the x-direction for the two-dimensional case. There is, therefore, a new surface vorticity distribution which is entirely α-type inboard of the cut-off station, $\ell=1$, and is composed of both α- and β-type on and near the tip.

3.3.2. First Iteration

The results of the zeroth iteration provide the input surface vorticity distribution for the first iteration. The induced velocity due to this new system at any control point can once again be obtained by using the Biot-Savart law. It is convenient to consider the contributions of the α-type and the β-type distributions separately.

Contribution of the α-type Vorticity Distribution.

The total contribution of the α-type vorticity to the tangential components of induced velocity at the i-th control point is the sum of the individual contributions from the upper and lower surfaces of the cylinder ($y \leq 0$) and from the hemispherical tip. For the upper and the lower surface

$$V_{U_\alpha, L_\alpha} = \pm \sum_{k=1}^{K} \Delta V_k \pm \sum_{k=1}^{K} \sum_{\ell=1}^{L} \Delta V_{k\ell}, \tag{42}$$

where ΔV_k is the contribution of the entire strip, $x_k \leq x \leq x_{k+1}$, extending to infinity inboard of the cut-off station, $\ell=1$, and $\Delta V_{k\ell}$ is the contribution of the surface element lying between the stations ℓ and $\ell+1$ and the stations k and k+1 (see hatched area in Figure 17). Using the Biot-Savart law, ΔV_k is expressed as

$$\Delta V_k = \int_{x_k}^{x_{k+1}} \frac{\gamma(x)}{4\pi} \left[1 + \frac{(y_1 - y_i)}{\{(x_i - x)^2 + (y_i - y_1)^2 + (z_i \mp z)^2\}^{1/2}}\right] \cdot \frac{(z_i \mp z)c_1 - (x_i - x)c_3}{(z_i \mp z)^2 + (x_i - x)^2} \cdot$$

$$\cdot \left\{1 + \left(\frac{dz}{dx}\right)^2\right\} dx, \tag{43}$$

with

$$\gamma(x) = \gamma(x_k) + \frac{\gamma(x_{k+1}) - \gamma(x_k)}{x_{k+1} - x_k}(x - x_k).$$

The expression for the term $\Delta V_{k\ell}$ is a double integral which can be reduced to a one-dimensional integral by making

use of the fact that the vortex filaments are straight line segments with linear vorticity variation along the y-direction. Then

$$\Delta V_{k\ell} = \frac{1}{4\pi} \int_{x_k}^{x_{k+1}} [I_1+I_2]\cdot[(z_i-z)c_1-(x_i-x)c_3][1+(\frac{dz}{dx})^2]^{\frac{1}{2}}dx, \tag{44}$$

where

$$I_1 = 4\ \frac{A_1+A_2x}{q}\{\frac{y_{\ell+1}-y_i}{C} - \frac{y_\ell-y_i}{D}\},$$

$$I_2 = -4\ \frac{B_1+B_2x}{q}\{\frac{a-y_iy_{\ell+1}}{C} - \frac{a-y_iy_\ell}{D}\},$$

$$a = (x_i-x)^2+y_i^2+(z_i\mp z)^2,$$

$$q = 4\{(x_i-x)^2+(z_i\mp z)^2\},$$

$$C = \{a-2y_iy_{\ell+1}+y_{\ell+1}^2\}^{1/2},$$

$$D = \{a-2y_iy_\ell+y_\ell^2\}^{1/2},$$

$$A_1 = \frac{\gamma_2y_{\ell+1}-\gamma_4y_\ell}{y_{\ell+1}-y_\ell},$$

$$A_2 = \frac{\gamma_1y_{\ell+1}-\gamma_3y_\ell}{y_{\ell+1}-y_\ell},$$

$$B_1 = \frac{\gamma_4 - \gamma_2}{y_{\ell+1} - y_\ell} ,$$

$$B_2 = \frac{\gamma_3 - \gamma_1}{y_{\ell+1} - y_\ell} ,$$

$$\gamma_1 = \frac{\gamma_{k+1,\ell} - \gamma_{k,\ell}}{x_{k+1} - x_k}$$

$$\gamma_2 = \frac{\gamma_{k,\ell} x_{k+1} - \gamma_{k+1,\ell} x_k}{x_{k+1} - x_k} ,$$

$$\gamma_3 = \frac{\gamma_{k+1,\ell+1} - \gamma_{k,\ell+1}}{x_{k+1} - x_k} ,$$

$$\gamma_4 = \frac{\gamma_{k,\ell+1} x_{k+1} - \gamma_{k+1,\ell+1} x_k}{x_{k+1} - x_k}$$

In Eqs. (42)-(44), the upper sign corresponds to the upper surface and the lower one to the lower surface. The relationship between x and z is given by Eq. (39).

The contribution of the surface vorticity distribution on the hemispherical tip to the tangential induced velocity at the i-th control point can be written as

$$V_{T_\alpha} = \sum_{k=1}^{K} \sum_{m=1}^{M} \Delta V_{km} \qquad (45)$$

where

$$\Delta V_{km} = \int_{x_k}^{x_{k+1}} \int_{\psi_m}^{\psi_{m+1}} \frac{(\gamma_1 \cdot x + \gamma_2)}{4\pi} \lambda(x) \left[\frac{\{(z_i - z)\cos\varepsilon + (y_i - y)\sin\varepsilon\} c_1 - (x_i - x)(c_2 \sin\varepsilon + c_3 \cos\varepsilon)}{\{(x_i - x)^2 + (y_i - y)^2 + (z_i - z)^2\}^{3/2}} \right]$$

$$\cdot (1+m^2)^{1/2} \, dx d\varepsilon \, ,$$

with

$$\lambda(x) = \{x(2-x)\}^{1/2} \, ,$$

$$y = \lambda(x) \sin \varepsilon,$$

$$z = \lambda(x) \cos \varepsilon,$$

$$m = \frac{d\lambda}{dx} \, ,$$

$$\gamma_1 = \gamma_{11} \sin \varepsilon + \gamma_{12},$$

$$\gamma_2 = \gamma_{21} \sin \varepsilon + \gamma_{22} \, ,$$

$$\gamma_{11} = \frac{\gamma_5 \lambda_{k+1} - \gamma_3 \lambda_k}{x_{k+1} - x_k} \, ,$$

$$\gamma_{12} = \frac{\gamma_6 - \gamma_4}{x_{k+1} - x_k} \, ,$$

$$\gamma_{21} = \frac{\gamma_3 \lambda_k x_{k+1} - \gamma_5 \lambda_{k+1} x_k}{x_{k+1} - x_k} \, ,$$

$$\gamma_{22} = \frac{\gamma_4 x_{k+1} - \gamma_6 x_k}{x_{k+1} - x_k} \, ,$$

$$\gamma_3 = \frac{\gamma_{k,m+1} - \gamma_{k,m}}{y_{k,m+1} - y_{k,m}},$$

$$\gamma_4 = \frac{\gamma_{k,m} y_{k,m+1} - \gamma_{k,m+1} y_{k,m}}{y_{k,m+1} - y_{k,m}},$$

$$\gamma_5 = \frac{\gamma_{k+1,m+1} - \gamma_{k+1,m}}{y_{k+1,m+1} - y_{k+1,m}},$$

$$\gamma_6 = \frac{\gamma_{k+1,m} y_{k+1,m+1} - \gamma_{k+1,m+1} y_{k+1,m}}{y_{k+1,m+1} - y_{k+1,m}},$$

$$\lambda_k = \lambda(x_k),$$

$$\lambda_{k+1} = \lambda(x_{k+1}),$$

$$y_{k,m} = \lambda_k \sin \psi_m,$$

$$y_{k+1,m} = \lambda_{k+1} \sin \psi_m,$$

$$y_{k,m+1} = \lambda_k \sin \psi_{m+1},$$

$$y_{k+1,m+1} = \lambda_{k+1} \sin \psi_{m+1}.$$

Therefore, the total tangential induced velocity at the i-th control point due to the entire α-type vorticity is

$$V_{I_\alpha} = V_{U_\alpha} + V_{L_\alpha} + V_{T_\alpha} \quad . \tag{46}$$

Having obtained the contribution of the α-type, the next step is to compute the contribution of the β-type vorticity distribution.

Contribution of the β-type Vorticity Distribution. It was mentioned earlier that the β-type vorticity is confined to the hemispherical tip and a small neighborhood of the tip on the cylindrical portion, namely, the region between the cut-off station, $\ell=1$, and the station at $y=0$. The total contribution is composed of the individual contributions from the upper and the lower surfaces of the cylinder ($y\leq 0$) and from the hemispherical tip.

Using the Biot-Savart law, the tangential induced velocity at the i-th control point due to the vorticity distribution on the cylinder ($y\leq 0$) can be written as

$$V_{U_\beta, L_\beta} = \sum_{k=1}^{K} \sum_{\ell=1}^{L} \Delta V_{k\ell}, \tag{47}$$

where

$$\Delta V_{k\ell} = \int_{x_k}^{x_{k+1}} \int_{y_\ell}^{y_{\ell+1}} \frac{(\gamma_1 x+\gamma_2)}{4\pi} \cdot \left[\frac{c_2\{t_3(x_i-x)\mp t_1(z_i\mp z)\}-(y_i-y)\{t_3 c_1 \mp t_1 c_3\}}{\{(x_i-x)^2+(y_i-y)^2+(z_i\mp z)^2\}^{3/2}}\right]$$

$$\cdot \{1+(\frac{dz}{dx})^2\}^{1/2} \, dxdy \, ,$$

with

$$z = \{x(2-x)\}^{1/2} ,$$

$$t_1 = -\sin\theta ,$$

$$t_3 = -\cos\theta ,$$

$$\tan\theta = \left(\frac{dz}{dx}\right) ,$$

$$\gamma_1 = \gamma_{11}\cdot y + \gamma_{12} ,$$

$$\gamma_2 = \gamma_{21}\cdot y + \gamma_{22} ,$$

$$\gamma_{11} = \frac{\gamma_5-\gamma_3}{x_{k+1}-x_k} ,$$

$$\gamma_{12} = \frac{\gamma_6-\gamma_4}{x_{k+1}-x_k} ,$$

$$\gamma_{21} = \frac{\gamma_3 x_{k+1}-\gamma_5 x_k}{x_{k+1}-x_k} ,$$

$$\gamma_{22} = \frac{\gamma_4 x_{k+1}-\gamma_6 x_k}{x_{k+1}-x_k} ,$$

$$\gamma_3 = \frac{\gamma_{k,\ell+1}-\gamma_{k,\ell}}{y_{\ell+1}-y_\ell} ,$$

$$\gamma_4 = \frac{\gamma_{k,\ell} y_{\ell+1}-\gamma_{k,\ell+1} y_\ell}{y_{\ell+1}-y_\ell} ,$$

$$\gamma_5 = (\gamma_{k+1,\ell+1} - \gamma_{k+1,\ell}) / y_{\ell+1} - y_\ell) \ ,$$

$$\gamma_6 = (\gamma_{k+1,\ell} y_{\ell+1} - \gamma_{k+1,\ell+1} y_\ell) / (y_{\ell+1} - y_\ell) \ .$$

The induced velocity at the i-th control point due to the β-type surface vorticity distribution on the hemispherical tip can be written as

$$V_{T_\beta} = \sum_{k=1}^{K} \sum_{m=1}^{M} \Delta V_{km} \ , \tag{48}$$

where

$$\Delta V_{km} = \int_{x_k}^{x_{k+1}} \int_{\psi_m}^{\psi_{m+1}} \frac{\gamma_1 x + \gamma_2}{4\pi} \cdot \left[\frac{(x_i - x)(c_2 t_3 - c_3 t_2) + (y_i - y)(c_3 t_1 - c_1 t_3) + (z_i - z)(c_1 t_2 - c_2 t_1)}{\{(x_i - x)^2 + (y_i - y)^2 + (z_i - z)^2\}^{3/2}} \right]$$

$$\lambda(x)\{1 + m^2\} dx d\varepsilon \ ,$$

with

$$t_1 = -\sin \theta,$$

$$t_2 = -\cos \theta \sin \varepsilon,$$

$$t_3 = -\cos \theta \cos \varepsilon,$$

$$\tan \theta = \left(\frac{d\lambda}{dx}\right) = m,$$

and the other variables are defined in the Eq. (45). Of

course, the values of γ's to be used in numerical evaluation of Eqs. (47) and (48) are the ones for the β-type vorticity distribution. The total tangential induced velocity at the i-th control point due to β-type surface vorticity distribution is, then, given by

$$V_{I_\beta} = V_{U_\beta} + V_{L_\beta} + V_{T_\beta} \quad . \tag{49}$$

The net tangential induced velocity,

$$V_I = V_{I_\alpha} + V_{I_\beta} \quad , \tag{50}$$

at the i-th control point is added to the corresponding tangential component of the free stream velocity to obtain the α-type and the β-type vorticity at the control points as described earlier. This defines a new system of surface vorticity distribution to be used for the next iteration.

The procedure for all successive iterations is identical to the one for the first iteration except that the surface vorticity strength varies at each station for successive iterations.

In this chapter, the development of a basic iterative scheme has been outlined. The mathematical formulation for a semi-infinite body was exemplified by the specific case of a semi-infinite circular cylinder with a hemispherical tip.

The application of the procedure to semi-infinite bodies is presented in the next chapter.

CHAPTER IV

APPLICATION OF THE ITERATIVE PROCEDURE TO SEMI-INFINITE BODIES

The basic iterative procedure described in the last chapter is now applied to compute the velocity and pressure distribution on the tip region of two semi-infinite, non-lifting bodies. The successful results for these cases lead to an extension of the method to a finite, nonlifting wing which will be considered in the following chapter.

4.1. Circular Cylinder with a Hemispherical Tip

4.1.1. Numerical Procedure

First, the case of a semi-infinite cylindrical body whose cross-section is a circle of unit radius is considered. A hemispherical cap is joined to one end of this semi-infinite body. The axis of the body is parallel to the Y-axis (see Figure 17) and it is placed normal to a steady, uniform stream of unit magnitude which is parallel to the X-axis. The mathematical formulation of the iterative method, described in Section 3.3, is precisely for this body. The details of the numerical techniques used in each of the iterations which finally converges to give the three-dimensional flow on the tip region are now discussed.

Zeroth Iteration. Before starting the zeroth iteration, 31 k-stations are selected on the upper surface with the leading edge and the trailing edge representing the two extreme stations. There are 30 semi-infinite strips on the cylindrical portion and 30 semi-circular segments on the tip. The initial chordwise vorticity strength distribution at every spanwise location is the same as the two-dimensional distribution on the circular cylinder and, the one for 72 elements (see Table 1) is chosen as the input. Owing to the symmetry of this problem, the control points need be selected in one quadrant only and the induced velocity needs to be computed at these points only. For the rest of the body surface, the values can be directly assigned.

To compute the α- and β-type components of the surface vorticity at any control point on the cylinder ($y \leq 0$), Eq. (38) is used to obtain the desired components of the induced velocity due to the vorticity distribution on the upper and the lower surface of the cylinder ($y \leq 0$). In, general, the integral is evaluated using Simpson's rule with 20 equal intervals. However, when the control point lies on a strip whose contribution is being evaluated the integrand exhibits 0/0 form. The integral can still be evaluated numerically by a combination of Simpson's rule and the Trapezoidal rule. The latter is used very close to the control point where the slope of the integrand with respect to X-axis becomes large and

Simpson's rule is not likely to give reliable results. The contribution of the small interval on each side of the control point steadily reduces as this point is approached from both directions. Eq. (39) is used to obtain the components of the induced velocity due to the vorticity distribution on the hemispherical tip. The x interval is divided into 20 parts and the ε interval is divided into 60 parts. Simpson's rule is then used twice for Eq. (40).

For control points on the hemispherical tip, Eq. (38) is evaluated using Simpson's rule with 20 equal divisions, and Eq. (39) is evaluated by using Simpson's rule twice, with 20 divisions in the x-direction and 60 divisions for ε. However, when the control point lies on a segment such that $x=x_i$, the integrand exhibits the indeterminate form. It is handled in exactly the same way as described above.

The results indicate that the cut-off station, $\ell=1$, on the cylindrical surface can be taken to be at five chord lengths inboard from the y=0 plane. The intervening distance is divided into 10 parts. There are then 11 ℓ-stations on the cylinder including the station at y=0 and the cut-off station, $\ell=1$. On the hemispherical tip, 13 m-stations at 15° intervals are selected. On each element, the geometric midpoint is the control point at which the components of the induced velocity are calculated. These values are added to the appropriate components of the free stream velocity to

obtain the α- and β-type surface vorticity strengths at each of the control points on the surface. The α- and β-type vorticity is assumed to vary linearly between the control points. This concludes the zeroth iteration and furnishes input for the first iteration.

First Iteration. The control points on the surface for the zeroth iteration are taken to be the corners of the surface elements to be used for first iteration. Accordingly, the new locations of the control points are the geometric midpoints of the new surface elements. (It should be mentioned at this stage that a different procedure is followed for the semi-infinite wing where the surface elements and the control points are selected once and for all. This will be described in Section 4.2.) It should also be noted that the local vorticity strength at any point on the surface can be obtained by linear interpolation using the values at the corners of the surface elements.

The input vorticity distribution on the surface exhibits three-dimensionality (α- and β-type) on the tip region and is the same as the two-dimensional distribution (α-type only) inboard from the cut-off station, ℓ=1. Using this input vorticity distribution, the α- and β-type vorticity at each of the control points is computed. The appropriate components of the induced velocity are obtained from Eqs. (41)-(50). All the one-dimensional integrals are evaluated

using Simpson's rule with 20 equally spaced divisions and the double integrals are computed by using Simpson's rule twice with 20 divisions for each dimension. However, when the control point lies on an element whose contribution is being evaluated at that control point, the integrand exhibits an indeterminate form. The procedure for numerical evaluation is identical to the one described earlier for zeroth iteration. A combination of Simpson's rule and Trapezoidal rule is used for this case.

The numerical procedure remains unchanged for all successive iterations because the same mathematical formulae are to be used. Of course, the values of the surface vorticity distribution change from one iteration to the other. Also, the control points for the first iteration form the corners of the surface elements for the second iteration and so on; i.e., the control points for a certain iteration define the new surface elements for the next iteration. The locations of the control points which are situated at the midpoint of the elements change accordingly for each iteration. This procedure is used only for the case of the circular cylinder with hemispherical tip. It is more convenient to fix the locations of the surface elements once and for all and it will be followed for the cases considered later.

4.1.2. Results and Discussion

The iterative procedure applied to the semi-infinite circular cylinder with a hemispherical tip gives a three-dimensional vorticity distribution on the tip region which merges smoothly with the two-dimensional distribution at five chord lengths inboard from the station at y=0 (see Figure 17). The chordwise distribution of the α- and the β-type vorticity on the upper surface of the body is presented in tabulated form in Appendix B for two m-stations (at $\psi = 90°, 30°$), and three ℓ-stations (at $y/c = 0, -0.2, -0.5$). The results of the three complete iterations after the zeroth show that the values of the surface vorticity strength change by increasingly lesser amounts with each iteration. The maximum change is noticed between the values of the zeroth iteration and the initial two-dimensional distribution. The results of the first iteration differ from those of the third iteration by an amount which is less than five percent based on free stream value of unity. The difference in the results of the second and third iteration is less than two percent. A fourth iteration is carried out only for the α-type vorticity and the results differ from the values of the third iteration by an amount which is of the order of one percent or less. Another interesting feature of the results is a damped oscillatory pattern of convergence (see Figure 19 and Appendix B).

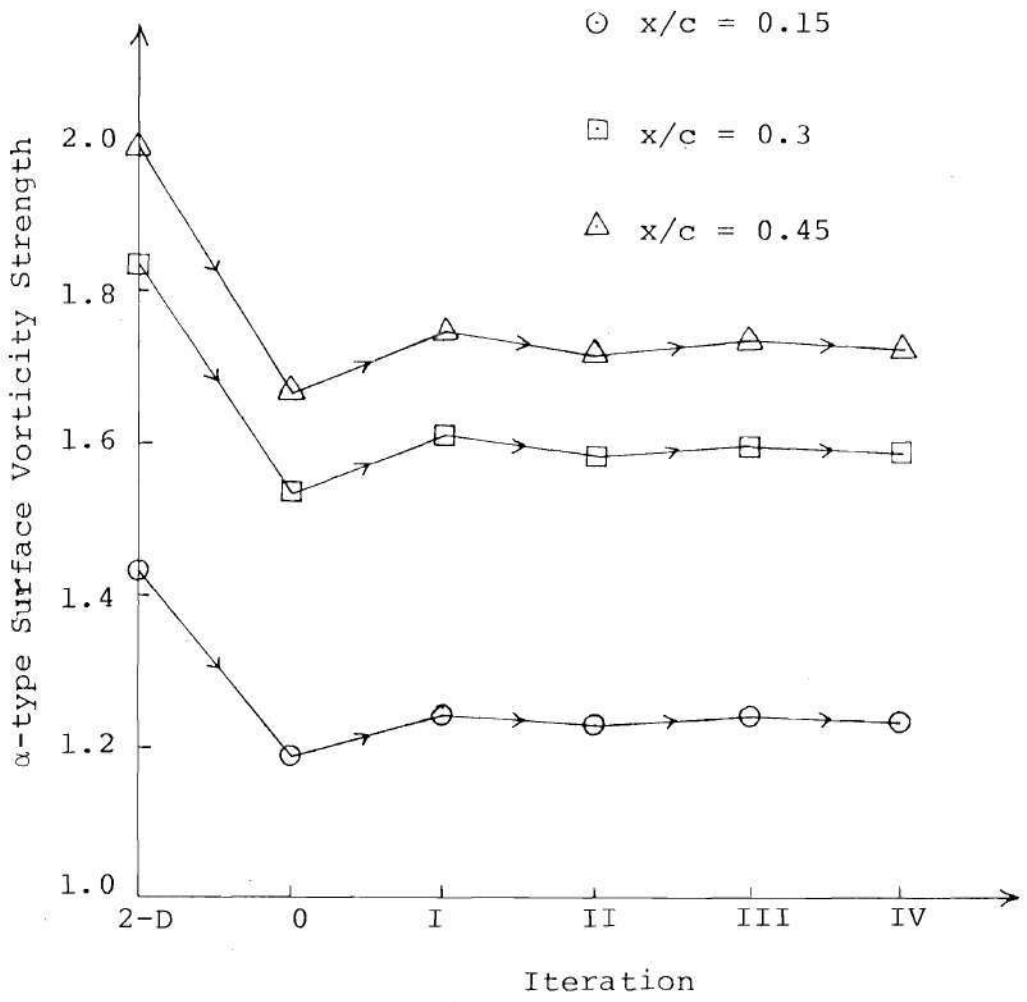

Figure 19. Typical Oscillatory Pattern of Convergence for α-type Vorticity on Semi-infinite Circular Cylinder with Hemispherical Tip; y/c = 0.0

The results of the third iteration are considered to be the converged solution. A verification of the conclusion is provided by the values of the normal component of the total velocity computed for a set of representative control points. Ideally, the normal component of velocity should be zero on the surface. In the present case, the values of these components are found to be less than one percent of the free stream value of unity. Moreover, the values of the velocity components normal to the surface steadily reduce with each successive iteration. It should also be noted that the distribution of surface elements is not necessarily the best possible, and that the vorticity strength is assumed to vary linearly on each element.

The circulation around a path which encloses the vorticity sheet crossing the m-station at $\psi=0°$ (see Figure 20(a)) is 1.731. The vorticity sheet strength distribution is the one obtained after third iteration. The value of the circulation around a path enclosing the vorticity sheet which crosses the m-station at $\psi=90°$ (see Figure 20(b)) is 1.7324. The agreement between the two values is good. This and other similar checks show that the conservation of vorticity is maintained during the execution of the iterative scheme.

An added measure of confidence in the results is provided by the following observation. The case under consideration is one of an axisymmetric body in a cross-flow.

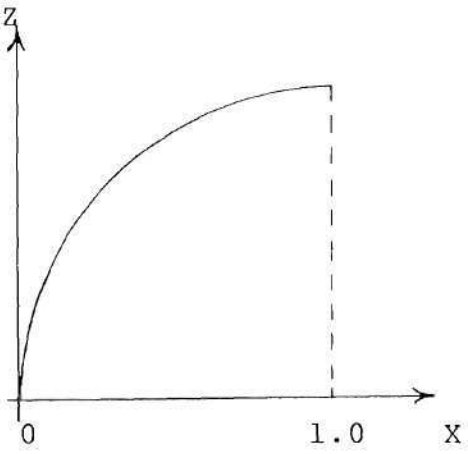

Figure 20(a). m-station at ψ=0.0

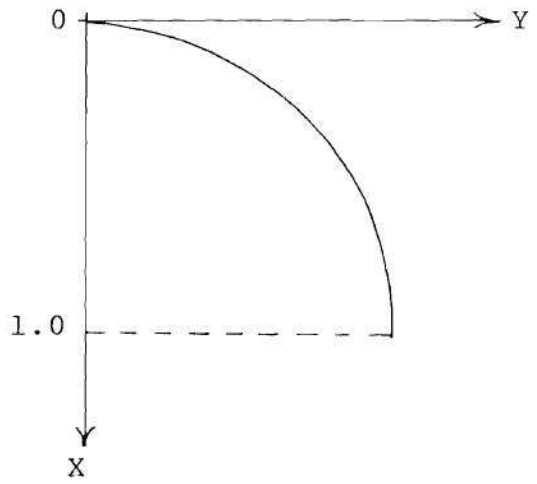

Figure 20(b). m-station at ψ=90°

Lotz[9] pointed out that the dependence of all quantities on a circumferential location is known in advance for an axisymmetric body immersed in a uniform flow which is directed normal to the body's axis of symmetry. In such a situation, the axial and the radial velocity components vary as cos θ, the quantity itself being characterized by its value at $\theta = 0$ (at a point in the X-Y plane). The circumferential velocity component varies as sin θ; the quantity is characterized by its value for $\theta = \pi/2$. In Tables 6 and 7, the variations of the circumferential velocity component and the axial velocity component as required by the above observation are compared with the corresponding values at the selected points as computed by the iterative scheme after three iterations. A good agreement is noted for almost all the points.

In Table 8, the values of the pressure coefficient, C_p, are tabulated for five stations on the surface of the circular cylindrical body having a hemispherical tip. The C_p values from exact analytical theory for the two-dimensional cylinder and for the sphere are also given for the purpose of comparison. The chordwise C_p distribution on the upper surface of a two-dimensional cylinder, at five stations on the cylindrical body, and on the sphere, between the leading edge and the midchord are plotted in Figure 21. The curves clearly show the so called three-

Table 6. Variation of the Circumferential Velocity Component on the Axi-symmetric Semi-infinite Circular Cylindrical Body in Cross-flow (see Figure 17) $V = V_\alpha\big|_{\theta=\pi/2} \cdot \sin\theta$; V_α Obtained from Appendix B

x/c	sin θ	y/c = -0.5		y/c = -0.2		y/c = 0.0	
		$\frac{V}{V_\alpha}$		$\frac{V}{V_\alpha}$		$\frac{V}{V_\alpha}$	
.025	.3122	.5894	.5896	.5681	.5685	.5431	.5426
.1	.6	1.1327	1.1328	1.0919	1.0922	1.0437	1.0418
.2	.8	1.5103	1.5104	1.4558	1.4558	1.3916	1.3888
.3	.9165	1.7303	1.7304	1.6678	1.6676	1.5942	1.5944
.4	.9798	1.8498	1.8498	1.7830	1.7826	1.7044	1.7052
.5	1.0	1.8879	1.8879	1.8198	1.8198	1.7395	1.7395

Table 7. Variation of the Axial Velocity Component on the Surface of the Axisymmetric Circular Cylindrical Body in Cross-flow (see Figure 17) $V = V_\beta\big|_{\theta=0.0} \cdot \cos\theta$; V_β Obtained from Appendix B

x/c	cos θ	y/c = -0.5		y/c = -0.2		y/c = 0.0	
		V	V_β	V	V_β	V	V_β
.025	.95	.07733	.0774	.1581	.1582	.3190	.3198
.1	.8	.06512	.06524	.1331	.1334	.2686	.2698
.2	.6	.04884	.0489	.09984	.1001	.2015	.2026
.3	.4	.03256	.0326	.06656	.0668	.1343	.1354
.4	.2	.01628	.01632	.03328	.0334	.0672	.0676
.5	.0	.0	.0	.0	.0	.0	.0

Table 8. Chordwise C_p Distribution on the Surface of the Circular Cylinder with a Hemispherical Tip

x/c	2-D Unit Cylinder	y/c=-0.5	y/c=-0.2	y/c=0.0	ψ=30°	ψ=90°	Unit Sphere
.0	1.0	.9937	.9737	.8931	.8931	.8931	1.0
.025	.61	.6466	.6530	.6087	.5603	.5429	.7806
.05	.24	.3175	.3492	.3396	.3073	.3111	.5725
.1	-.44	-.2873	-.2098	-.1543	-.1313	-.0887	.19
.15	-1.04	-.8213	-.7024	-.5905	-.5049	-.4304	-.1475
.2	-1.56	-1.2836	-1.1289	-.9677	-.8227	-.7229	-.44
.25	-2.0	-1.6755	-1.4904	-1.2873	-1.1052	-.9690	-.6875
.3	-2.36	-1.9953	-1.7851	-1.5595	-1.3261	-1.1697	-.89
.35	-2.64	-2.2442	-2.0147	-1.7647	-1.497	-1.325	-1.0475
.4	-2.84	-2.422	-2.179	-1.912	-1.6191	-1.4361	-1.16
.45	-2.96	-2.5292	-2.2771	-1.9995	-1.6917	-1.5027	-1.2275
.5	-3.0	-2.5736	-2.3182	-2.036	-1.7212	-1.5281	-1.25

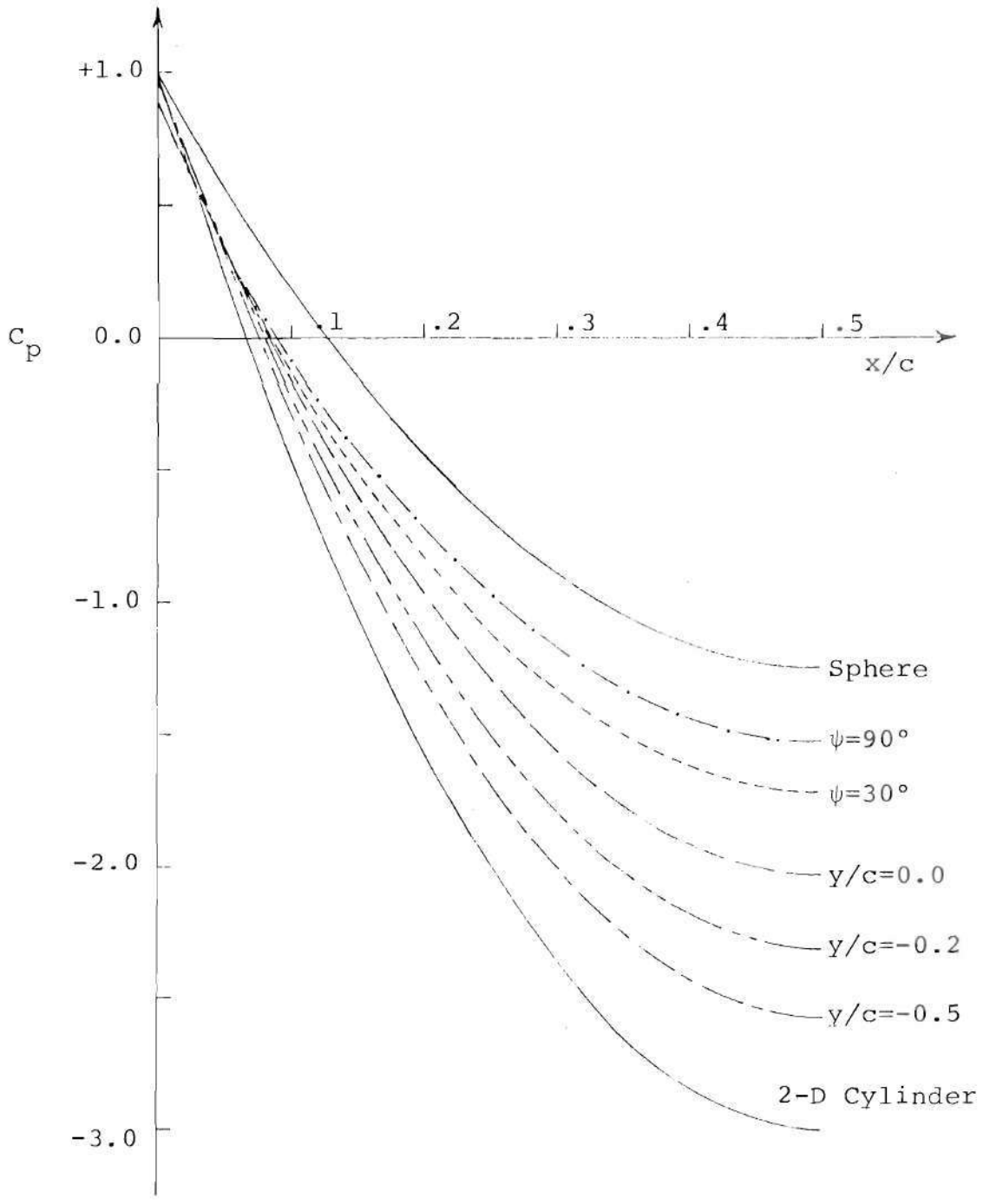

Figure 21. Chordwise Pressure Coefficient Distribution on the Semi-infinite Circular Cylindrical Body with a Hemispherical Tip

dimensional relief effect on the surface of the circular cylindrical body as the hemispherical tip is approached from further inboard where the flow is essentially two-dimensional.

4.2. Symmetrical Wing with Half-body-of-revolution Tip

4.2.1. Modified Iterative Procedure

The problem of computing the potential flow on the tip region of a semi-infinite wing whose cross-section is an NACA basic thickness form airfoil is conceptually identical to the case of a circular cylindrical body. All the equations required to compute the surface velocities are the same as given in Section 3.3 except that the profile curve of the wing is expressed in mathematical form by Eq. (31). The upper surface of the semi-infinite wing is divided into elements by selecting 16 k-stations including the leading edge and the trailing edge and nine ℓ-stations including the station at y=0 and the cut-off station, ℓ=1, which is found to be at y/c = -1.0 (see Figure 22). Inboard of the cut-off station, the 15 elemental strips extend to infinity. The k-stations are relatively closely spaced near the leading edge and the trailing edge. This follows from the observation of the two-dimensional results which show a relatively rapid variation of vorticity strengths in these regions. The locations of the ℓ-stations are also governed by the

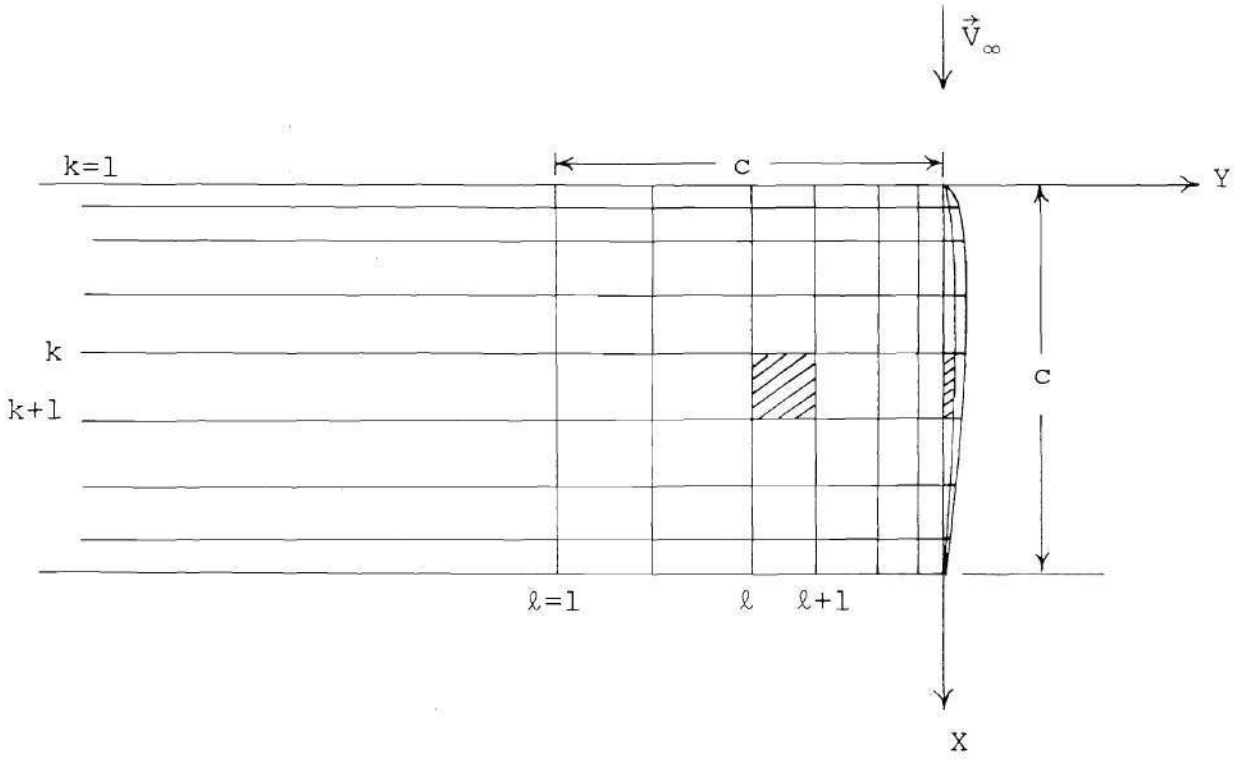

Figure 22. Semi-infinite Wing with Half-body-of-revolution Tip (Top View) Wing Airfoil Section NACA 0012

fact that the influence of the tip to render the flow three-dimensional reduces rapidly as the distance from the tip increases. The results show that the major changes in the surface vorticity strengths are confined to about 0.2 chord length inboard from the ℓ-station at y=0. The distribution of the surface elements is duplicated on the lower surface. On the half-body-of-revolution tip, 13 m-stations are selected at 15° intervals. Thus, there are a total of 420 surface elements plus 30 strips extending to infinity on the entire body. The geometric midpoint, as before, is chosen to be the control point on each of the elements. It must be noted that the control points need to be designated either on the upper or on the lower surface only, owing to the symmetry of the problem about the X-Y plane.

Initially, a vorticity sheet whose chordwise strength distribution corresponds to two-dimensional one is "wrapped" around the tip. Every ℓ-station inboard of the station at y=0 and every m-station on the tip is associated with a piecewise linear vorticity distribution in the X-direction. The zeroth iteration gives the α- and β- components of vorticity at each of the control points. It is to be noted that the distribution of the surface elements and the locations of the control points are fixed once and for all in the case under consideration. Using linear interpolation, the new values of the α- and β-type vorticity are obtained at the

corners of the surface elements. The vorticity strength is assumed to vary linearly on each of the elements. This defines a new surface vorticity distribution to start the next iteration. The numerical procedures involved in computing the surface velocities are the same as described in Section 4.1 since the equations are essentially the same.

The basic iterative procedure is carried out to four complete iterations after the zeroth one (and even a fifth iteration for the α-type) for a semi-infinite, NACA 0012 wing. The results do show a converging trend but at a rather slow rate. More interestingly, they exhibit an oscillatory pattern which is quite similar to that observed for the circular cylindrical body. The typical behavior of the α- and the β-components can be seen in Figure 23. A careful study of the results shows that on the major portion of the surface (between the k-stations at 5% and 80% of the chord) the zeroth iteration yields the surface vorticity strengths which are much less than the values to which the scheme is converging for α-type components, and much larger than the values for β-type components. The first iteration however, tends to correct the distribution but the α-type components become larger than the apparent final values, and the β-type become lesser. It should be noted that the difference of the values between the first and the zeroth iterations is less than the corresponding difference for

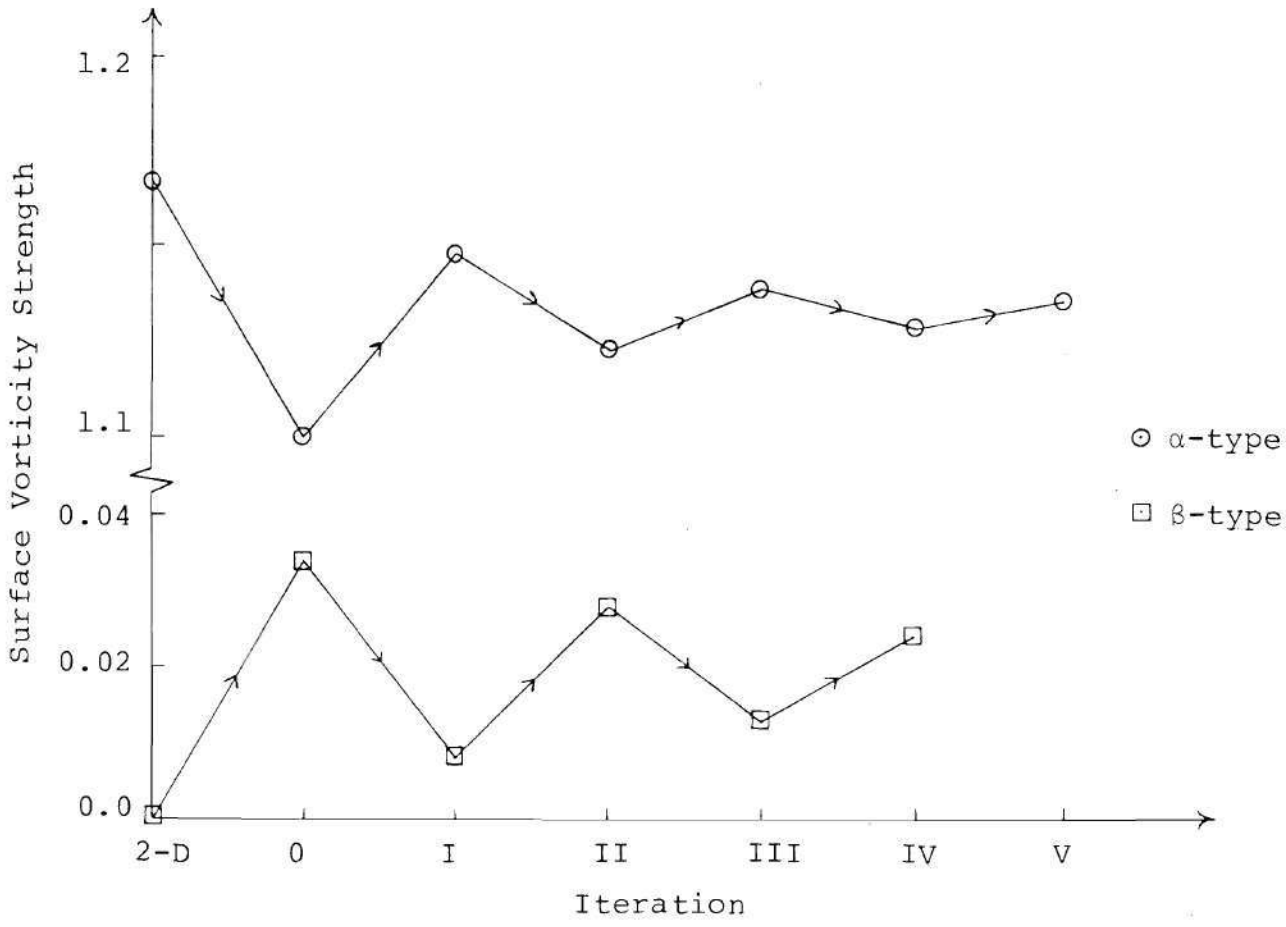

Figure 23. Typical Oscillatory Pattern of Convergence of α- and β-type Vorticity on Semi-infinite Wing at y/c=-0.1, x/c=0.25; Airfoil Section NACA 0012

the zeroth iteration and the initial two-dimensional values. Also, the behavior of the α- and the β-components is consistent with the requirement of the conservation of total vorticity. The second and fourth iterations result in surface vorticity strengths which are less than the apparent final values for α-type, and larger for the β-type. The trend is the opposite for the third (and the fifth for α-type) iteration. The difference in the values of the local vorticity strength for consecutive iterations gets increasingly smaller for successive iterations. It is therefore clear that the method exhibits a parallel of the damped oscillations for the surface vorticity strengths about a final converged distribution. A careful study of the results for the circular cylindrical body shows an exactly similar pattern of the vorticity distributions for successive *iterations (see Appendix B)*.

The above observations regarding the results obtained from the basic iterative method suggest the following modification to the procedure. Starting from the two-dimensional distribution, the zeroth and the first iterations are completed. At this stage, the input surface vorticity distribution for the second iteration should not be the result of the first iteration as in the basic scheme, but the arithmetic mean, I_M, of the results of the zeroth and the first iterations. In the light of the observations made

above, it is to be expected that I_M will be relatively closer to the final converged value than the I. Using I_M as the input, the second iteration is completed and the results, II, are compared with the I_M values to check for convergence. In case further computations are needed, two possibilities arise: (1) to choose the II as the input for the third iteration, or (2) to take the mean, II_M, of the II and the I_M and to use this as the input for the next iteration. A comparison of the results, III, obtained from the input vorticity distribution II, with the alternate results, III_A, obtained from the input vorticity distribution II_M is discussed in the next section. It is found that the II_M is the better choice for the input, and as might also be anticipated, results in accelerated convergence.

The modified iterative procedure can now be summarized as follows. After the zeroth and the first iterations, the surface vorticity distribution is replaced by the mean of the results of the zeroth and the first iterations. The second iteration results are compared with the input distribution for convergence. The criterion for convergence, of course, is the smallness of the difference of the results of two successive iterations. Every following iteration is started with the input surface vorticity distribution which is the mean of the two previous distributions.

The modified iterative method is used to compute the

potential flow on the semi-infinite wing whose cross-section is an NACA 0012 airfoil. In order to obtain a relatively more detailed and accurate surface vorticity strength distribution, the number of k-stations is increased to 20 and the number of ℓ-stations in increased to 10. There are then a total of 570 surface elements with 38 strips extending to infinity.

No approximations are made regarding the shape and/or size of any of the surface elements. The interval between any two adjacent k-stations is subdivided into 16 equal divisions when the integrals in the Eqs. (38)-(48) are evaluated by Simpson's rule. For the control points lying inboard of the ℓ-station at y=0, the interval between the adjacent ℓ-stations is subdivided into 16 equal divisions whereas the interval between two adjacent m-stations is divided into 10 equal divisions. When the control point lies on the half-body-of-revolution tip, the number of subdivisions for m-stations is increased to 16 and the number for ℓ-stations is decreased to 10. This offers saving in computational time without any appreciable loss of accuracy.

It must be mentioned at this stage that the numerical evaluation of the double integrals requires about three times as much time on the computer as is needed to evaluate the single integral other factors being the same. It should be recalled that Eq. (45), which gives the contribution of α-type

vorticity distribution on the tip to the induced velocity at a control point, involves a double integral. Eqs. (47) and (48) are used to evaluate the contribution of the β-type vorticity distribution on the surface to the induced velocity at a control point and these also involve double integrals. Moreover, the contribution of a surface element to the induced velocity at any control point is mainly dependent on the relative distance of the control point to the points on the surface element. Even though the contributions of the distant elements are small, none of the nearly 600 elements is ignored. These factors result in a total of approximately 85 minutes of execution time required for each complete iteration (after the zeroth one) on the CDC Cybler 70/74 NOS 1.1-419/420. This computational time is quite large. Nevertheless, an accurate and detailed solution once obtained provides a basis to check the accuracy of the results obtained for a procedure which involves approximations either for the mathematical formulation, for the numerical techniques, or both in order to achieve a saving on the computational time required. The execution time for each iteration can be reduced to approximately 30 minutes by making suitable approximations to the geometry of the surface elements. These are discussed in detail in the next chapter.

4.2.2. Results and Discussions

The results of the modified iterative procedure applied to a semi-infinite NACA 0012 wing with half-body-of-revolution tip illustrate the accelerated convergence pattern on the tip region as described in the last section. It was mentioned earlier that the cut-off station can be located at one chordlength inboard from the tip. The effect of the tip to render the flow three-dimensional is found to be confined to approximately 0.2 chordlength inboard from the tip. The typical results for the chordwise distribution of the α- and β-type surface vorticity are tabulated in Appendix C for two m-stations (ψ=90°, 30°) and three ℓ-stations (y/c = 0, -0.03, -.1).

In the modified scheme, the input for the second iteration is the mean of the resulting surface vorticity distributions for the zeroth and the first iterations. A comparison of the results of the second iteration with its input vorticity distribution, I_M, shows that their difference is less than one percent based on free stream of unit magnitude on a major portion of the wing (between the chordwise locations at 5% and 75% chordlength). Even on the remaining portion near the leading edge and the trailing edge, the differences are of the order of one to five percent.

The results for a third iteration, III, can be computed with the results of the second iteration, II, as the

input. A relatively large decrease in the values of the α-type vorticity and increase in the values of the β-type vorticity is observed when the results, II and III, are compared. This situation is similar to the case of the basic iterative procedure which shows that the surface vorticity components oscillate about the final values with ever decreasing amplitudes. Based on the insight provided by the results of the basic iterative procedure, it can be concluded that the values of the α-type vorticity resulting from the second iteration, II, are larger than the final values and those resulting from the third iteration, III, are smaller. For the β-type vorticity, the values resulting from the second iteration are smaller than the final values and those resulting from the third iteration are larger than the final values. A continuation from this third iteration, III, will involve several more iterations before the scheme converges to the actual surface vorticity distribution which lies between the values of the second, II, and the third, III, iterations.

An alternate third iteration, III_A, is carried out with an input surface vorticity distribution, II_M, which is the mean of the input, I_M, and the results, II, of the second iteration. The resulting values for the α- and the β-type vorticity are different from the values of the input distribution, II_M, by an amount which is less than half of one percent

on the entire wing except for a very small region of the tip near the leading edge. Even in this region, which lies between the leading edge and the chordwise location at five percent chordlength, the differences are less than (or at the most equal to) two percent. It is interesting to note that the results of the alternate third iteration are surprisingly close to the mean of the results of the second, II, and the third, III, iterations. These observations lead to the conclusion that the results of the alternate third iteration (i.e., III_A) are close to the final solution. It is naturally expected that a fourth iteration starting from the mean of the II_M and III_A will substantiate the conclusion. The results of an extension of this scheme to the finite aspect ratio wing, discussed in the next chapter, do indeed support it.

A check on the accuracy of the results is provided by the values of the normal component of the total velocity on the surface of the wing. The magnitudes of the normal components are less than one percent of the free stream value of unity. Also, the difference in the values of the circulations around contours which enclose the vorticity crossing the m-stations at $\psi=0°$ and at $\psi=90°$ is less than half of one percent. This indicates that the conservation of vorticity is maintained.

Three typical chordwise distributions of the α- and the

β-type surface vorticity are plotted in Figure 24. The chordwise distribution of the surface pressure coefficient is tabulated in Table 9 for six locations on the body. The corresponding plots are shown in Figure 25 for five locations. The three-dimensional relief effect can be clearly seen from these plots.

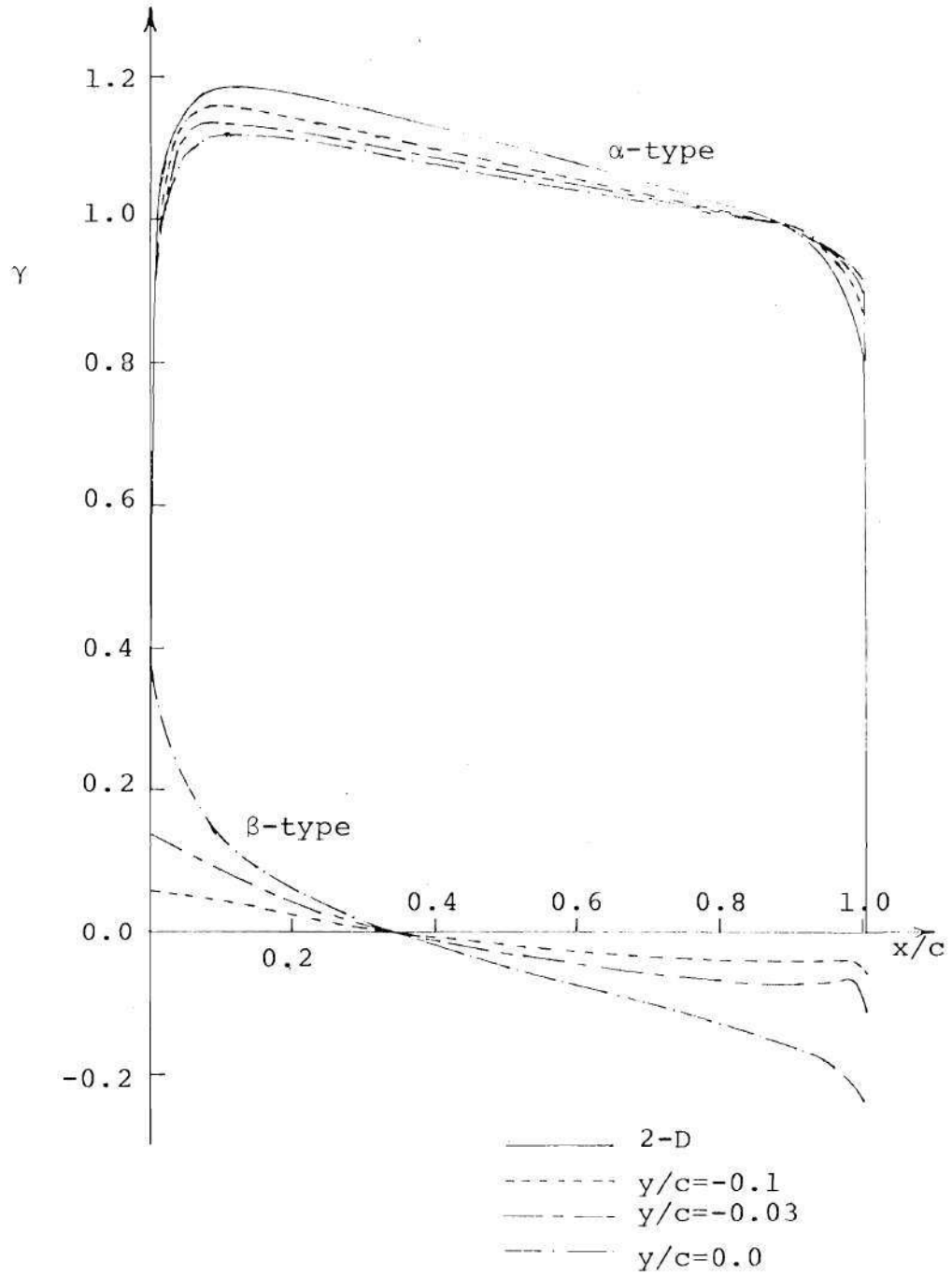

Figure 24. Chordwise Distribution of the α- and β-type Components of the Surface Vorticity Strengths on the Semi-infinite NACA 0012 Nonlifting Wing

Table 9. The C_p Distribution on the Surface of the Semi-infinite NACA 0012 Wing with Half-body-of-revolution Tip

x/c	2-D	y/c=-.325	y/c=0.1	y/c=-.03	ψ=0°	ψ=30°	ψ=90°
.0	1.0	.9997	.9964	.9803	.8292	.8292	.8292
.0055	.3215	.3347	.3426	.3389	.2642	.1766	.1122
.0125	-.0053	.0184	.0314	.0388	.0186	-.0361	-.0511
.025	-.2219	-.1965	-.1785	-.1573	-.1441	-.1638	-.1528
.055	-.3613	-.3427	-.3154	-.2766	-.2448	-.2359	-.2062
.105	-.4092	-.3824	-.3425	-.2965	-.2651	-.2485	-.2125
.17	-.3979	-.3665	-.3190	-.2759	-.2499	-.2330	-.2001
.25	-.3676	-.3273	-.2791	-.2415	-.2204	-.2083	-.1775
.4	-.2766	-.2435	-.2029	-.1751	-.1601	-.1592	-.1306
.6	-.1622	-.1389	-.1134	-.0958	-.0890	-.0995	-.0750
.775	-.0563	-.0488	-.0395	-.0308	-.033	-.0523	-.0300
.875	.0172	.0185	.0151	.0145	.0038	-.0228	.0013
.9575	.1299	.1145	.0995	.0812	.0535	.0196	.0463
1.00855	1.0	.9993	.9955	.9865	.9486	.9486	.9486

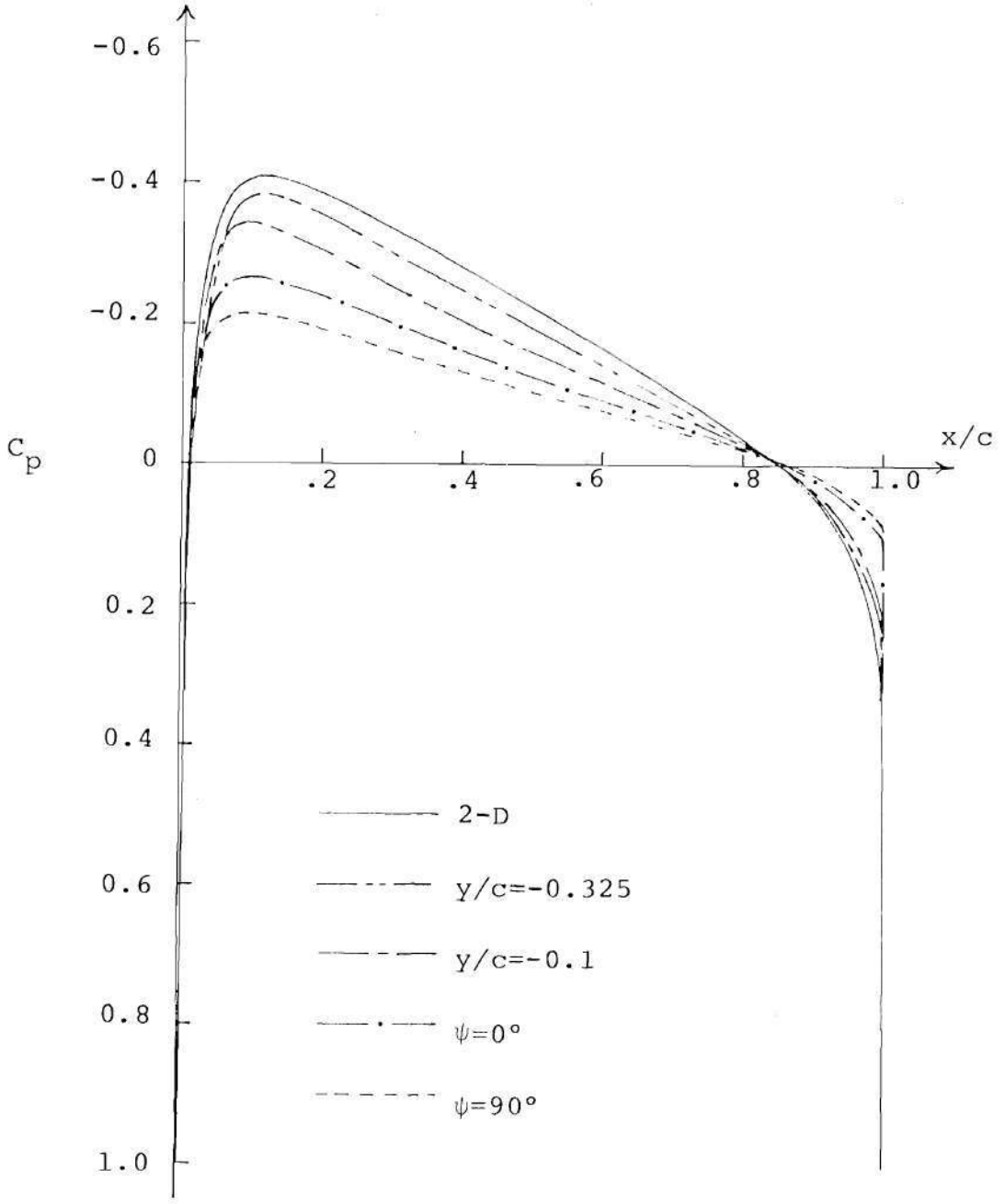

Figure 25. Pressure Distribution on the Surface of the Semi-infinite NACA 0012 Wing with Half-body-or-revolution Tip at Zero Angle of Attack

CHAPTER V

POTENTIAL FLOW ON A FINITE WING

5.1. Application of the Iterative Procedure

In the last two chapters, the development of an iterative procedure and its application to nonlifting, semi-infinite bodies was described and discussed. The apparent logical extension is to apply the iterative method to compute the potential flow on a conventional wing of finite aspect ratio. In this chapter, the case of a nonlifting, constant chord, rectangular wing is considered. One of the obvious ways the iterative procedure can be applied to this case is to start the procedure with an initial surface vorticity distribution which is the two-dimensional chordwise vorticity distribution for the cross-sectional airfoil of the wing at each of the spanwise stations. The steps described for a modified iterative scheme in Section 4.2 should lead to a converged solution. However, a more efficient procedure will be to start from an initial surface vorticity distribution which is closer to the final solution. This can be accomplished by choosing a surface vorticity distribution which, on the tip region of the finite wing, is the same as the distribution on the tip region of the corresponding semi-

infinite wing. It is expected, and is borne out by the results, that the number of iterations required for a reasonably good convergence is small even for a wing of small aspect ratio ($\sim$3).

The choice of the initial surface vorticity distribution mentioned above also affords another advantage which deserves mention. The number of surface elements on the finite wing will be of the order of twice the number of surface elements on the semi-infinite wing. A considerable saving of the computational time can be achieved by executing a few iterations for the semi-infinite wing, and then transferring to the finite wing. The specifics of the procedure are discussed in Section 5.3.

5.2. Approximations of the Surface Elements

It was mentioned earlier that the numerical evaluation of a double integral is considerably more time consuming on the computer than the evaluation of the single integral. For a finite wing with a much larger number of surface elements as compared to the semi-infinite wing, the evaluation of double integrals in Eqs. (45), (47) and (48) can lead to prohibitive computational time for each iteration. This provides strong motivation to investigate ways and means to reduce the computational time.

A study of the mathematical formulation of the iterative procedure reveals that the double integrals arise

because of the curved vortex filaments constituting the surface vorticity distribution. This in turn results from the fact that no approximations are made to the geometry of the curved surface elements. It should also be noted that the α-type vorticity distribution inboard of the tip is composed of straight line filaments and the velocity induced by this distribution at any control point is given by Eq. (43) involving only a single integral. Based on these observations, the following approximations are incorporated in the formulation.

The contribution of the β-type surface vorticity distribution to the induced velocity at any control point is given by Eqs. (47) and (48). These are used only for that surface element which contains the control point where the velocities are being computed. The remaining surface elements inboard of the tip are replaced by flat panels formed by joining the corners of the surface elements by straight lines. The induced velocity due to the β-type velocity distribution on the flat panels can be expressed as a single integral even though the vorticity strength itself varies linearly on each of the panels (see Appendix D, Eq. D-1).

The half-body-of-revolution tip is divided into half frustums of cones of axial lengths determined by the adjacent k-stations. The m-stations then divide each of the half frustums of cones into smaller elements. For this geometry

of the surface elements, the induced velocity due to the β-type surface vorticity distribution can be expressed by a single integral (see Appendix D, Eq. D-2). The Biot-Savart law is, of course, used in each of the cases. No appreciable change is noticed in the numerical values as a result of these approximations when the contributions of the β-type vorticity distribution are compared with the results obtained earlier for all curved surface elements with no approximations.

The contribution of the α-type surface vorticity distribution on the surface element inboard of the tip to the induced velocity at any control point is given by Eq. (43). Since the expression involves only a single integral, no apparent saving in the computer time is possible by replacing the elements by flat panels. The approximations can only lead to some loss in accuracy. However, the tip formed by the half body of revolution is divided into frustums of cones as described earlier. The contribution of the α-type surface vorticity distribution on the tip to the induced velocity can be expressed by a single integral (see Appendix D, Eq. D-3) rather than the double integral of Eq. (45). This approximation of the tip has very little effect on the numerical values for the control points inboard of the tip but the computed values showed impairment of the accuracy of the results for the control points lying on the tip. A

considerable improvement in the latter case is realized by replacing the frustum of a cone which contains the control point where the velocities are to be computed by the original body shape and using Eq. (45) for the surface elements on this section only. This compromise still results in an appreciable saving in the computational time with better agreement with the values obtained earlier for all curved surface elements with no approximation.

5.3. Numerical Procedure and Results

The iterative scheme is applied to obtain the potential flow on a nonlifting NACA 0012 wing of aspect ratio 3. The coordinate system and the typical surface elements are shown in Figure 26. The starting surface vorticity distribution in the present case is chosen to be the input distribution, II_M, for the third iteration for the semi-infinite NACA 0012 wing (see Section 4.2). The numerical evaluation of the integrals for the surface element on which the control point lies is exactly the same as described in Section 4.1. All the other integrals are evaluated by using Simpson's rule. The mode and number of subdivisions on each surface element is also retained (see Section 4.2). The total number of k-stations is 20, the number of m-stations is 13, and the number of ℓ-stations is increased to 12 which includes the station at $y = 1.5c$ (see Figure 21) and the station in the X-Z plane - the plane

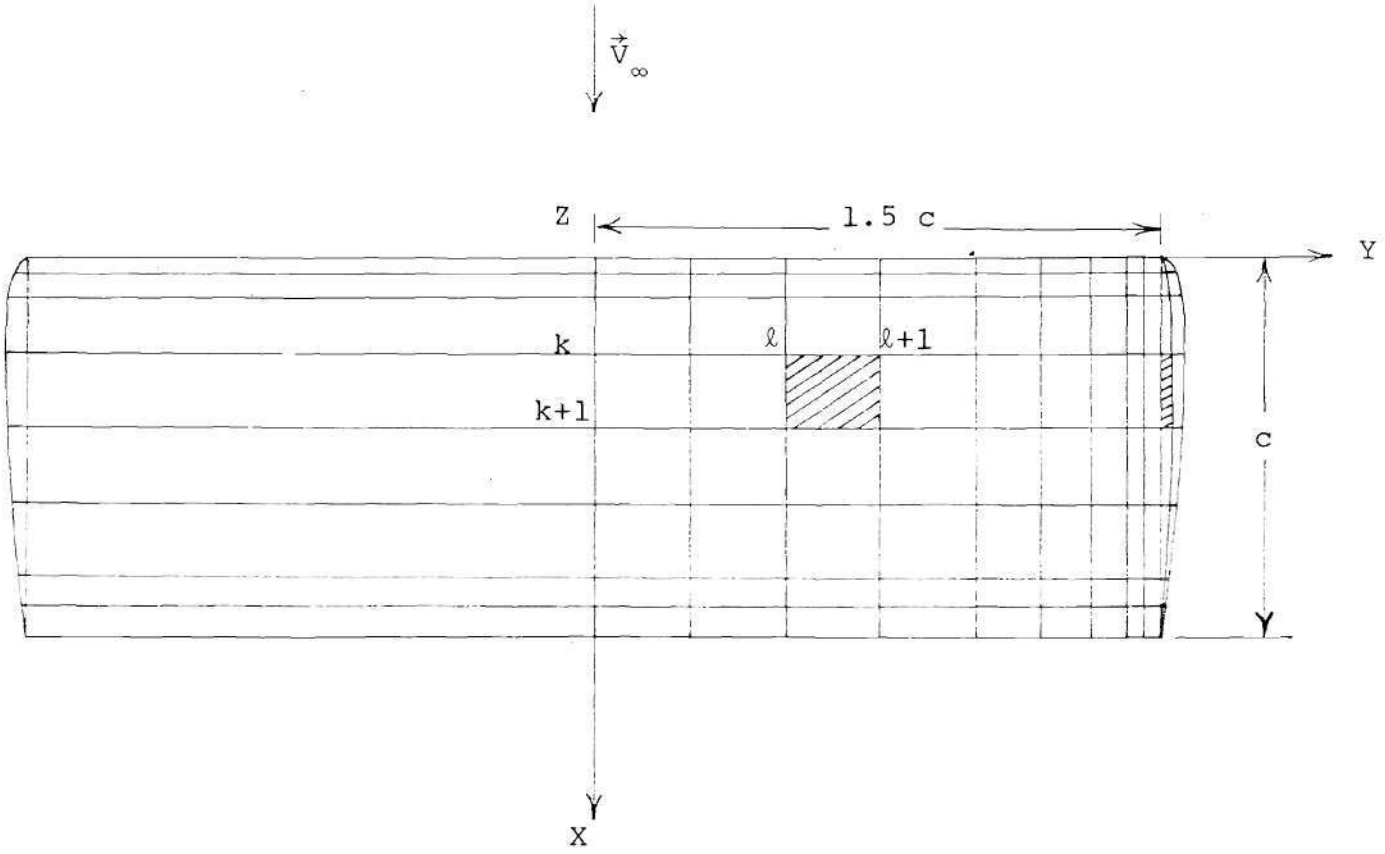

Figure 26. Top View of NACA 0012 Wing; AR = 3

of symmetry. This results in a total of 1292 surface elements on the entire wing. However, owing to symmetry, the control points need be designated in only one of the quadrants.

Starting from the input surface vorticity distribution, II_M, the results of the next iteration, III, and of the successive iteration are tabulated in Appendix E for a few representative locations. It is observed that the difference of the results III and the input II_M is less than half a percent based on a free stream value of unity for a major portion of the wing between the chordwise locations at 5% and 75% chordlength. On the remaining portion, the difference is of the order of 1% except near the intersection of the leading edge and the tip where the maximum difference approaches 3%. Even better agreement is obtained between the values of the fourth iteration, IV, with its input distribution, III_M, which is the mean of the III and the II_M. The differences are less than half a percent on the entire body and much less than this on a major portion of the wing. It can be concluded that the finiteness of the wing requires only a minor readjustment of the initial surface vorticity distribution which corresponds to that of a semi-infinite wing of the same cross-section. In Table 10, the chordwise distribution of the pressure coefficient is presented and the corresponding plots are

Table 10. Chordwise Pressure Coefficient, C_p, Distribution on the Surface of the Nonlifting NACA 0012 Wing, AR = 3

x/c \ y/c	0.0	0.5	1.0	1.4	1.47	1.5 (ψ=0°)	ψ=30°	ψ=60°	ψ=90°
.0	1.0	.9999	.9999	.996	.9777	.8296	.8296	.8296	.8296
.0055	.3215	.3337	.3369	.3420	.3367	.2481	.1395	.0957	.0707
.0125	-.0053	.0141	.019	.0306	.0355	.0047	-.0672	-.0846	-.082
.025	-.2219	-.2097	-.1993	-.1792	-.1616	-.1566	-.1897	-.1882	-.1786
.055	-.3613	-.3592	-.3510	-.3156	-.2808	-.2496	-.2463	-.2302	-.2161
.105	-.4092	-.4041	-.3939	-.3424	-.3007	-.2748	-.2640	-.2460	-.2320
.17	-.3979	-.3913	-.3795	-.3194	-.2841	-.2522	-.2366	-.2186	-.2042
.25	-.3616	-.3546	-.3417	-.2802	-.2547	-.2230	-.2119	-.1967	-.1818
.4	-.2766	-.2702	-.2574	-.2052	-.1952	-.1599	-.1587	-.1476	-.1300
.6	-.1622	-.1579	-.1484	-.1153	-.1103	-.0892	-.0998	-.0920	-.0745
.775	-.0563	-.0577	-.0523	-.0400	-.0360	-.0343	-.0540	-.0460	-.0306
.875	.0172	.0150	.0180	.0153	.0131	.0021	-.0250	-.0150	.0001
.9575	.1299	.1144	.1161	.1002	.0821	.0514	.0174	.0310	.0450
1.00855	1.0	.9999	.9998	.9956	.9868	.9471	.9471	.9471	.9471

given in Figure 27.

A comparison of the computational time for the present case and for the semi-infinite wing case indicates the usefulness of the appropriate approximations of the surface elements. Even with more than twice the number of surface elements on the finite wing, the computational time for one complete iteration is approximately 50 minutes on the CDC Cyber 70/74 NOS 1.1-419/420 as against nearly 85 minutes required for the semi-infinite wing. The attendant impairment of accuracy is negligible for all practical purposes.

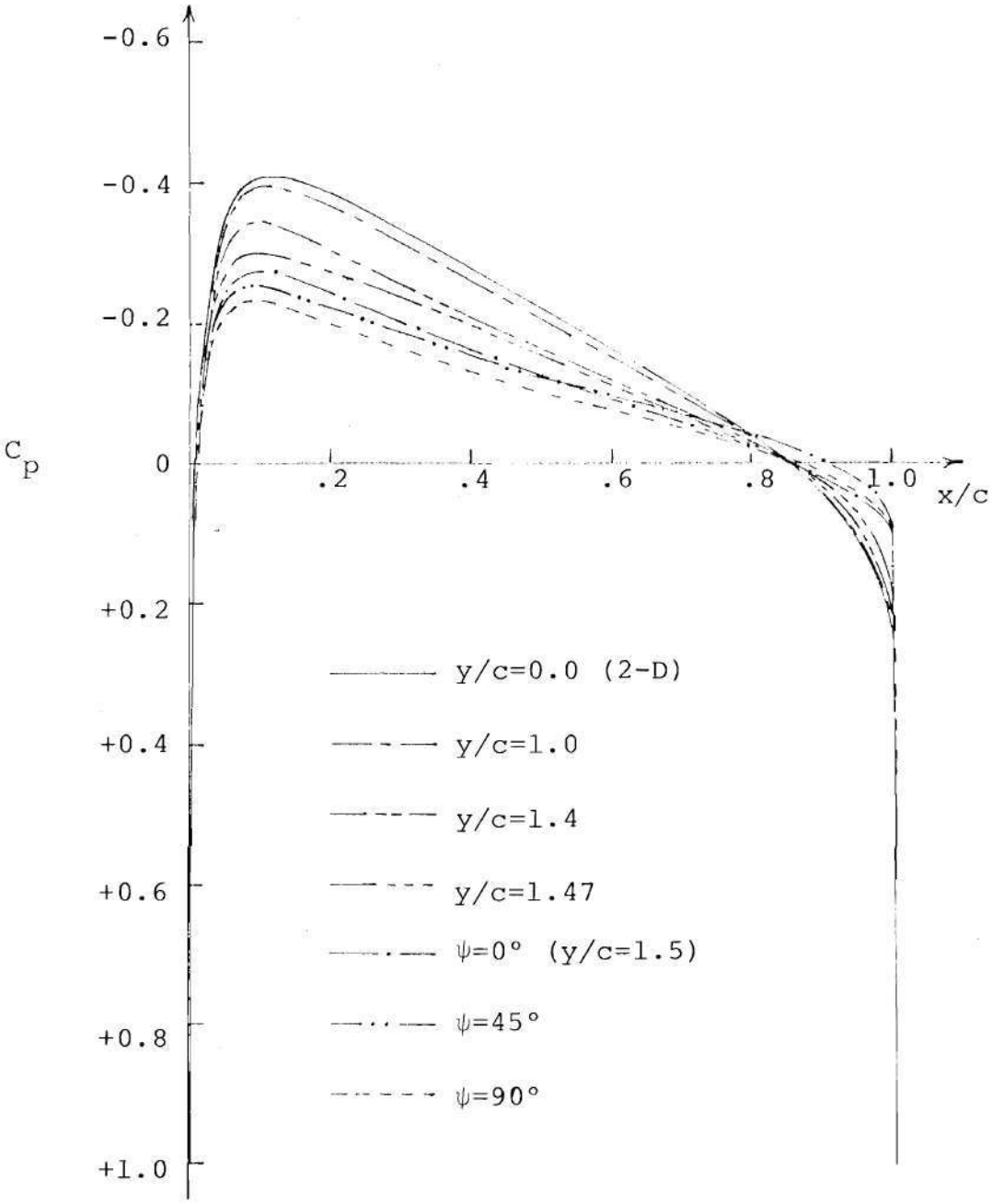

Figure 27. Chordwise Distribution of the Pressure Coefficient, C_p, on Nonlifting NACA 0012 Wing of AR=3

CHAPTER VI

CONCLUSIONS AND RECOMMENDATIONS

The more widely used numerical methods to solve potential flow problems involve basically a surface source distribution with an added vorticity distribution to account for circulation and lift. However, in the opinion of the author, the formulation of an incompressible, inviscid flow problem using only surface vorticity distribution appears to be more natural as the vorticity represents the physical phenomenon more closely than either sources or doublets. The use of vorticity offers another important advantage that the surface velocity is directly obtained as the solution without any further computation. In the present work, therefore, a surface vorticity distribution has been utilized to study several two- and three-dimensional flow problems for a steady, uniform free-stream.

The two-dimensional problems were formulated as an integral equation. This was approximated with a set of linear, algebraic equations by satisfying the no-normal-flow boundary condition on the surface elements and by using the Elementary Vortex Distribution (EVD) technique.

The use of the EVD led to a coefficient matrix with dominant diagonal and off-diagonal elements for the system of equations. The equations could, therefore, be easily solved by the Gauss-Jordan reduction method using maximum pivot strategy. Also, the EVD technique results in a piecewise linear but continuous solution on the surface. For a circular cylinder with 72 surface elements, the computed values were within one percent of the exact analytical solution. Even better agreement was obtained for larger number of surface elements. The surface velocity distributions were obtained for NACA basic thickness form airfoils (6%, 12%, 18% and 24% thick) for nonlifting and lifting cases. Approximately 60 surface elements provided a reasonably accurate velocity distribution.

An iterative procedure was formulated and developed to compute the three-dimensional flow in the tip region of a circular cylinder with a hemispherical tip. Initially, a vortex sheet whose chordwise strength distribution is the same as that of the two-dimensional cylinder was "wrapped" around the tip. In three iterations, the vortex sheet strength in the tip region was readjusted to a three-dimensional distribution which merged smoothly with the two-dimensional distribution further inboard from the tip. The results of the first iteration are different

from the solution obtained after the third iteration by amounts which are less than five percent based on unit free stream. The difference between the results of the second and the third iteration is less than two percent. It is observed that the results of the successive iterations, starting from the initial approximation, exhibit a damped oscillatory pattern of convergence. This phenomenon is also noticed when the basic iterative procedure is applied to a semi-infinite NACA 0012 wing with half-body-of-revolution tip. Based on these observations the basic procedure was modified to achieve accelerated convergence.

Using the modified scheme for a semi-infinite wing, the results of the second iteration were within one percent of its input distribution on a major portion of the wing (between the chordwise locations at 5% and 75% chord-length). The results of a third iteration were in even better agreement with their input surface vorticity distribution. The modified method was extended to a nonlifting NACA 0012 wing of aspect ratio three. Only one iteration was needed to obtain the solution with an initial approximation which was the solution of the semi-infinite wing. The differences were only marginal between the final results and the input distribution. The results of the finite wing and semi-infinite wing show that the effect of the tip is largely confined to a small fraction ($\sim$.2) of the

the problem is to start the iterative procedure with a surface vorticity distribution on the wing which corresponds to the nonlifting solution with an additional vorticity distribution superimposed to account for circulation and lift. Moreover, a suitable model for the trailing vorticity sheet has to be assumed as an initial approximation and the kinematic boundary condition will have to be satisfied on this trailing vorticity sheet. The successive iterations should readjust the vorticity strength distribution on the wing and the strength and the location of the trailing vortex system to yield the final solution. The iterative procedure developed in the course of present investigation can also be used to compute the detailed flow on a helicopter blade which may be treated as a wing in a linearly varying free stream. A nonlifting blade will require only minor changes in the execution of the iterative procedure whereas the case of a lifting blade is more involved because of the presence of a vortex wake.

The application of the iterative procedure to compute a detailed and accurate three-dimensional flow on the tip region of a wing requires a large amount of computational time if no approximations are made to the geometry of the curved surface elements. However, certain suitable approximations discussed in Section 5.2 reduced the computational time required for the semi-infinite wing

chord inboard from the tip and the flow is essentially two-dimensional inboard of approximately one chord length from the tip.

The most important advantage of the iterative procedure is that a detailed three-dimensional surface velocity and pressure distribution can be computed without having to solve an extremely large matrix. Such matrices when obtained from the approximation of the integral equation of the first kind for surface vorticity distribution models are not usually well behaved. Also, the surface vorticity distribution is equivalent to the surface velocity distribution which can be used to compute the pressure distribution readily. The detailed pressure distribution finds application in the boundary-layer computations and the surface vorticity distribution provides the boundary condition in solving the Navier-Stokes equations by the stream function-vorticity transport equation model.

The logical extension of the present work is an application of the iterative procedure to a three-dimensional lifting wing. This case is quite important because the solution is very likely to provide more insight into the problems related with the wing tip vortex. This is, however, more complicated than a nonlifting case since the vorticity distribution and geometry of a trailing vortex system are unknown. One of the possible ways to approach

by approximately 70% of the 85 minutes needed for each iteration when no approximations are made. A comparison of the results for these cases showed an insignificant loss of accuracy due to the approximations. Therefore, the use of these approximations is recommended especially if the surface elements have large radii of curvature. It should also be pointed out that further reduction in the computational time can be accomplished by introducing approximations and/or modifications to either the mathematical formulation or the numerical techniques. The results given here for the cases involving no approximations provide a basis to check the validity of any approximation or modification. An extensive study of the relative magnitudes of the contributions to the induced velocity at a control point from the surface elements might help in identifying the elements which contribute insignificantly. It may be possible to entirely omit them from the calculations and hence reduce the computational time or alternatively, to express the contribution of such elements as a simple, analytical expression by assuming a uniform, constant strength distribution which is an average of the actual distribution for each of the elements.

APPENDIX A

USE OF SYMMETRY FOR TWO-DIMENSIONAL FLOWS

Consider the system of Eqs. (26) for four surface elements on the body. The set of equations is

$$A_{11}\gamma_1 + A_{12}\gamma_2 + A_{13}\gamma_3 + A_{14}\gamma_4 = b_1,$$

$$A_{21}\gamma_1 + A_{22}\gamma_2 + A_{23}\gamma_3 + A_{24}\gamma_4 = b_2,$$

$$A_{31}\gamma_1 + A_{32}\gamma_2 + A_{33}\gamma_3 + A_{34}\gamma_4 = b_3,$$

$$A_{41}\gamma_1 + A_{42}\gamma_2 + A_{43}\gamma_3 + A_{44}\gamma_4 = b_4 .$$

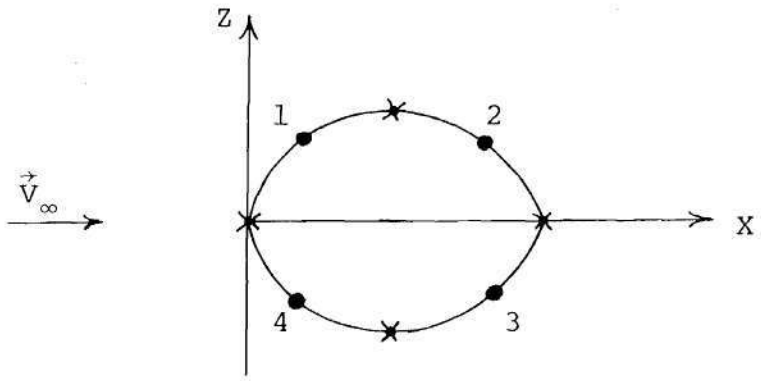

Using top and bottom symmetry, i.e.,

$$\gamma_1 = -\gamma_4,$$

$$\gamma_2 = -\gamma_3,$$

the surface distribution can be obtained by solving the following system of equations

$$(A_{11}-A_{14})\gamma_1 + (A_{12}-A_{13})\gamma_2 = b_1,$$

$$(A_{21}-A_{24})\gamma_1 + (A_{22}-A_{23})\gamma_2 = b_2 .$$

APPENDIX B

SURFACE VORTICITY DISTRIBUTION ON SEMI-INFINITE CIRCULAR CYLINDER WITH A HEMISPHERICAL TIP

α-Type, ψ=90°

x/c	2-D	0^{th}	I	II	III	IV
.0	.0	.4184	.3034	.3358	.3270	.3294
.025	.6322	.7792	.6710	.6721	.6761	.6706
.05	.8814	.8126	.8308	.8220	.8300	.8224
.1	1.2072	.9964	1.052	1.0328	1.0434	1.0358
.15	1.4324	1.1304	1.2104	1.1856	1.1960	1.1908
.2	1.6029	1.2330	1.3314	1.3012	1.3126	1.3084
.25	1.7343	1.3130	1.4306	1.3904	1.4032	1.3992
.3	1.8349	1.3748	1.5040	1.4592	1.4730	1.4688
.35	1.9095	1.4212	1.5588	1.5102	1.5248	1.5208
.4	1.9611	1.4540	1.5966	1.5456	1.5608	1.5568
.45	1.9914	1.4744	1.6188	1.5664	1.5820	1.5780
.5	2.0014	1.4794	1.6254	1.5724	1.5882	1.5842

α-Type, ψ=30°

x/c	2-D	0^{th}	I	II	III	IV
.0	.0	.2092	.1516	.1679	.1635	.1647
.025	.6322	.6289	.6328	.6274	.6345	.6270
.05	.8814	.7912	.8188	.8062	.8164	.8068
.1	1.2072	1.0112	1.0642	1.0452	1.0564	1.0474
.15	1.4324	1.1638	1.2344	1.2132	1.2228	1.2166
.2	1.6029	1.2772	1.3624	1.3406	1.3478	1.3448
.25	1.7343	1.3642	1.4664	1.4392	1.4496	1.4442
.3	1.8349	1.4308	1.5426	1.5134	1.5244	1.5188
.35	1.9095	1.4802	1.5994	1.5684	1.5798	1.5742
.4	1.9611	1.5146	1.6384	1.6064	1.6182	1.6126
.45	1.9914	1.5356	1.6614	1.6288	1.6406	1.6350
.5	2.0014	1.5403	1.6669	1.6340	1.6458	1.6404

β-Type, ψ=30°

x/c	2-D	0^{th}	I	II	III
.0	.0	.3624	.2627	.2908	.2832
.025	.0	.2478	.1795	.2002	.1925
.05	.0	.2086	.1496	.1681	.1619
.1	.0	.1584	.1140	.1278	.1240
.15	.0	.1242	.0900	.1006	.0984
.2	.0	.0981	.0717	.0800	.0786
.25	.0	.0766	.0565	.0630	.0622
.3	.0	.0579	.0433	.0484	.0478
.35	.0	.0411	.0314	.0352	.0349
.4	.0	.0256	.0205	.0230	.0228
.45	.0	.0111	.0105	.0114	.0113
.5	.0	.0	.0	.0	.0

α-Type, $\psi=0°$

x/c	2-D	0^{th}	I	II	III	IV
.0	.0	.0	.0	.0	.0	.0
.025	.6322	.5099	.5480	.5304	.5426	.5318
.05	.8814	.7136	.7642	.7422	.7572	.7610
.1	1.2072	.9930	1.0514	1.0278	1.0418	1.0304
.15	1.4324	1.1884	1.2412	1.2292	1.2400	1.2322
.2	1.6029	1.3342	1.4014	1.3792	1.3888	1.3826
.25	1.7343	1.4462	1.5170	1.4940	1.5034	1.4976
.3	1.8349	1.5318	1.6088	1.5818	1.5944	1.5856
.35	1.9095	1.5954	1.6748	1.6466	1.6598	1.6506
.4	1.9611	1.6396	1.7204	1.6916	1.7052	1.6956
.45	1.9914	1.6662	1.7472	1.7178	1.7316	1.7220
.5	2.0014	1.6746	1.7556	1.7256	1.7395	1.7299

β-Type, $\psi=0°$

x/c	2-D	0^{th}	I	II	III
.0	.0	.4184	.0334	.3358	.3270
.025	.0	.3973	.2899	.3198	.3112
.05	.0	.3676	.2738	.3014	.2950
.1	.0	.3334	.2438	.2698	.2626
.15	.0	.2910	.2136	.2362	.2300
.2	.0	.2484	.1832	.2026	.1974
.25	.0	.2058	.1528	.1690	.1646
.3	.0	.1631	.1224	.1354	.1318
.35	.0	.1204	.0918	.1016	.0990
.4	.0	.0776	.0612	.0676	.0660
.45	.0	.0349	.0306	.0339	.0330
.5	.0	.0	.0	.0	.0

α-Type, y/c=-0.2

x/c	2-D	0^{th}	I	II	III	IV
.0	.0	.0	.0	.0	.0	.0
.025	.6322	.5467	.5710	.5572	.5685	.5578
.05	.8814	.7652	.7970	.7800	.7934	.7808
.1	1.2072	1.064	1.097	1.0802	1.0922	1.0814
.15	1.4324	1.2730	1.3056	1.2920	1.2998	1.2934
.2	1.6029	1.4288	1.4624	1.4500	1.4558	1.4514
.25	1.7343	1.5484	1.5830	1.5708	1.5760	1.5724
.3	1.8349	1.6398	1.6752	1.6630	1.6676	1.6646
.35	1.9095	1.7078	1.7436	1.7314	1.7356	1.7330
.4	1.9611	1.7550	1.7970	1.7784	1.7826	1.7802
.45	1.9974	1.7830	1.8188	1.8062	1.8102	1.8080
.5	2.0014	1.7924	1.8282	1.8156	1.8198	1.8177

β-Type, y/c=-0.2

x/c	2-D	0^{th}	I	II	III
.0	.0	.214	.1463	.1664	.1622
.025	.0	.2031	.1392	.1582	.1542
.05	.0	.1922	.318	.1499	.1461
.1	.0	.1705	.1174	.1334	.1301
.15	.0	.1487	.1028	.1167	.1139
.2	.0	.1271	.0881	.1001	.0977
.25	.0	.1054	.0725	.0834	.0814
.3	.0	.0838	.0588	.0668	.0652
.35	.0	.0622	.0441	.0508	.0489
.4	.0	.0406	.0294	.0334	.0326
.45	.0	.0193	.0147	.0167	.0163
.5	.0	.0	.0	.0	.0

α-Type, y/c=-0.5

x/c	2-D	0^{th}	I	II	III	IV
.0	.0	.0	.0	.0	.0	.0
.025	.6322	.5744	.5902	.5784	.5896	.5784
.05	.8814	.8038	.8238	.8096	.8230	.8096
.1	1.2072	1.1178	1.1340	1.1216	1.1328	1.1216
.15	1.4324	1.3372	1.3498	1.3416	1.3484	1.3416
.2	1.6029	1.5008	1.5120	1.5056	1.5104	1.5056
.25	1.7343	1.6262	1.6368	1.6312	1.6352	1.6312
.3	1.8349	1.7220	1.7322	1.7270	1.7304	1.7270
.35	1.9095	1.7928	1.8030	1.7980	1.8010	1.7980
.4	1.9611	1.8420	1.8518	1.8470	1.8498	1.8470
.45	1.9914	1.8708	1.8806	1.8758	1.8786	1.8758
.5	2.0014	1.8801	1.8899	1.8851	1.8879	1.8851

β-Type, y/c=-0.5

x/c	2-D	0^{th}	I	II	III
.0	.0	.1001	.0854	.0814	.0796
.025	.0	.0951	.0700	.0774	.0756
.05	.0	.0900	.0062	.0734	.0716
.1	.0	.0800	.0590	.0652	.0638
.15	.0	.0698	.0516	.0571	.0558
.2	.0	.0596	.0442	.0489	.0478
.24	.0	.0495	.0369	.0408	.0400
.3	.0	.0395	.0295	.0326	.0319
.34	.0	.0294	.0221	.0245	.0239
.4	.0	.0194	.0147	.0163	.0159
.45	.0	.0094	.00734	.0082	.0080
.5	.0	.0	.0	.0	.0

APPENDIX C

SURFACE VORTICITY DISTRIBUTION ON THE SEMI-INFINITE WING WITH HALF-BODY-OF-REVOLUTION TIP, WING AIRFOIL SECTION NACA 0012

α-Type, $\psi=90°$

x/c	2-D	0^{th}	I	I_M	II	III	II_M	III_A
.0	.0	.5612	.3660	.4635	.4069	.4197	.4352	.4133
.0055	.8237	.9796	.9522	.9659	.9424	.9420	.9541	.9422
.0125	1.0026	1.0482	1.0434	1.0458	1.0260	1.0245	1.0359	1.0252
.025	1.1054	1.0752	1.0968	1.0860	1.0751	1.0723	1.0805	1.0737
.055	1.1667	1.0827	1.1246	1.1036	1.1004	1.0961	1.1020	1.0983
.105	1.1871	1.0798	1.1281	1.1038	1.1038	1.0984	1.1038	1.1012
.17	1.1823	1.0729	1.1215	1.0972	1.0982	1.0927	1.0977	1.0955
.25	1.1669	1.0628	1.1096	1.0862	1.0878	1.0824	1.0870	1.0851
.4	1.1299	1.0480	1.0838	1.0659	1.0654	1.0612	1.0656	1.0633
.6	1.0780	1.0390	1.0480	1.0435	1.0376	1.0360	1.0405	1.0368
.775	1.0280	1.0454	1.0101	1.0278	1.0136	1.0162	1.0207	1.0149
.875	.9914	1.0640	-.974	1.0190	.9957	1.0030	1.0074	.9993
.9575	.9328	1.1224	.8986	1.0105	.9690	.9841	.9898	.9766
1.00855	.0	.2142	.2640	.2391	.2230	.2240	.2360	.2368

α-Type, ψ=30°

x/c	2-D	0^{th}	I	I_M	II	III	II_M	III_A
.0	.0	.2806	.1829	.2318	.2035	.2098	.2176	.2067
.0055	.8237	.8994	.8830	.8912	.8698	.8690	.8805	.8694
.0125	1.0026	1.0065	1.0134	1.0100	.9940	.9921	1.0020	.9930
.025	1.1054	1.0582	1.0863	1.0722	1.0687	1.0609	1.0680	1.0623
.055	1.1667	1.0834	1.1288	1.1061	1.1049	1.1008	1.1055	1.1029
.105	1.1871	1.0874	1.1385	1.1130	1.1150	1.1101	1.1140	1.1125
.17	1.1823	1.0828	1.1336	1.1082	1.1112	1.1061	1.1097	1.1087
.25	1.1669	1.0722	1.1223	1.0973	1.1013	1.0963	1.0993	1.0988
.4	1.1299	1.0543	1.0963	1.0753	1.0786	1.0746	1.0769	1.0766
.6	1.0780	1.0398	1.0574	1.0486	1.0472	1.0456	1.0479	1.0464
.775	1.0280	1.0405	1.0151	1.0278	1.0181	1.0207	1.0230	1.0194
.875	.9914	1.0540	.9762	1.0151	.9968	1.0038	1.0059	1.0002
.9575	.9328	1.1018	.8961	.9990	.9645	.9791	.9818	.9718
1.00855	.0	.1071	.1320	.1196	.1164	.1115	.1180	.1134

β-Type, ψ=30°

x/c	2-D	0^{th}	I	I_M	I	III	II_M	III_A
.0	.0	.4860	.3169	.4014	.3524	.3650	.3769	.3577
.0055	.0	.3235	.2393	.2814	.2575	.2621	.2695	.2598
.0125	.0	.2729	.2062	.2395	.2216	.2256	.2306	.2236
.025	.0	.2246	.1729	.1987	.1861	.1896	.1924	.1879
.055	.0	.1644	.1282	.1463	.1384	.1414	.1423	.1398
.105	.0	.1113	.0851	.0982	.0923	.0945	.0953	.0934
.17	.0	.0692	.0566	.0629	.0612	.0626	.0620	.0619
.25	.0	.0333	.0286	.0310	.0310	.0320	.0310	.0315
.4	.0	-.0146	-.0117	-.0132	-.0128	-.0132	-.0130	-.0130
.6	.0	-.0632	-.0611	-.0622	-.0660	-.0683	-.0641	-.0671
.775	.0	-.1043	-.1049	-.1046	-.1127	-.1164	-.1086	-.1146
.875	.0	-.1340	-.1389	-.1364	-.1473	-.1510	-.1419	-.1492
.9575	.0	-.1750	-.1815	-.1782	-.1882	-.1910	-.1832	-.1896
1.00855	.0	-.1855	-.2286	-.2071	-.2017	-.1932	-.2044	-.1964

α-Type, y/c=0.0

x/c	2-D	0^{th}	I	I_M	II	III	II_M	III_A
.0	.0	.0	.0	.0	.0	.0	.0	.0
.0055	.8237	.7773	.7978	.7875	.7773	.7746	.7824	.7759
.0125	1.0026	.9344	.9625	.9485	.9387	.9357	.9436	.9372
.025	1.1054	1.0215	1.0614	1.0414	1.0366	1.0333	1.0390	1.0350
.055	1.1667	1.0726	1.1240	1.0983	1.0999	1.0961	1.0991	1.0980
.105	1.1871	1.0864	1.1420	1.1142	1.1194	1.1149	1.1168	1.1173
.17	1.1823	1.0845	1.1387	1.1116	1.1174	1.1128	1.1145	1.1151
.25	1.1669	1.0752	1.1264	1.1008	1.1064	1.1018	1.1036	1.1041
.4	1.1299	1.0535	1.0960	1.0747	1.0788	1.0750	1.0767	1.0769
.6	1.0780	1.0307	1.0519	1.0413	1.0414	1.0401	1.0414	1.0408
.775	1.0280	1.0212	1.0058	1.0135	1.0079	1.0104	1.0107	1.0091
.875	.9914	1.0237	.9641	.9939	.9832	.9899	.9886	.9865
.9575	.9328	1.0534	.8827	.9681	.9482	.9616	.9581	.9549
1.00855	.0	.0	.0	.0	.0	.0	.0	.0

β-Type, y/c=0.0

x/c	2-D	0^{th}	I	I_M	II	III	II_M	III_A
.0	.0	.5611	.3659	.4635	.4069	.4197	.4352	.4133
.0055	.0	.4874	.3212	.4043	.3595	.3719	.3819	.3657
.0125	.0	.4246	.2792	.3519	.3149	.3270	.3334	.3210
.025	.0	.3524	.2323	.2924	.2643	.2756	.2783	.2700
.055	.0	.2555	.1680	.2118	.1932	.2024	.2025	.1978
.105	.0	.1693	.1082	.1388	.1262	.1325	.1325	.1293
.17	.0	.1020	.0670	.0845	.0785	.0825	.0815	.0805
.25	.0	.0462	.0310	.0386	.0368	.0388	.0377	.0378
.4	.0	-.0252	-.0161	-.0206	-.0181	-.0188	-.0194	-.0184
.6	.0	-.0924	-.0646	-.0785	-.0746	-.0778	-.0765	-.0762
.775	.0	-.1452	-.1030	-.1241	-.1189	-.1238	-.1215	-.1214
.875	.0	-.1819	-.1303	-.1561	-.1487	-.1543	-.1524	-.1515
.9575	.0	-.2306	-.1660	-.1982	-.1828	-.1891	-.1905	-.1860
1.00855	.0	-.2142	-.2640	-.2391	-.2329	-.2231	-.2360	-.2268

α-Type, y/c=-0.03

x/c	2-D	0^{th}	I	I_M	II	III	II_M	III_A
.0	.0	.0	.0	.0	.0	.0	.0	.0
.0055	.8237	.8098	.8112	.8105	.8007	.8017	.8056	.8012
.0125	1.0026	.9716	.9845	.9780	.9708	.9712	.9744	.9710
.025	1.1054	1.055	1.0846	1.0698	1.0683	1.0678	1.0691	1.0681
.055	1.1667	1.0926	1.1443	1.1184	1.1256	1.1234	1.1220	1.1245
.105	1.1871	1.0946	1.1571	1.1259	1.1375	1.1339	1.1317	1.1357
.17	1.1823	1.0857	1.1498	1.1177	1.1304	1.1261	1.1241	1.1283
.25	1.1669	1.072	1.1350	1.1035	1.1161	1.1117	1.1098	1.1139
.4	1.1299	1.0463	1.1027	1.0745	1.0859	1.0820	1.0802	1.0840
.6	1.0780	1.0178	1.0580	1.0379	1.0469	1.0447	1.0424	1.0458
.775	1.0280	.9987	1.0142	1.0065	1.0130	1.0132	1.0098	1.0131
.875	.9914	.9870	.9792	.9831	.9892	.9906	.9861	.9899
.9575	.9328	.9733	.9250	.9492	.9557	.9558	.9524	.9558
1.00855	.0	.0	.0	.0	.0	.0	.0	.0

β-Type, y/c=-0.03

x/c	2-D	0^{th}	I	I_M	II	III	II_M	III_A
.0	.0	.2458	.0810	.1634	.1312	.1494	.1473	.1403
.0055	.0	.2415	.0824	.1619	.1300	.1473	.1460	.1386
.0125	.0	.2345	.0829	.1587	.1274	.1436	.1431	.1355
.025	.0	.2198	.0813	.1505	.1212	.1356	.1358	.1284
.055	.0	.1834	.0727	.1280	.1042	.1156	.1161	.1099
.105	.0	.1336	.0558	.0947	.0780	.0858	.0864	.0819
.17	.0	.0858	.0368	.0613	.0513	.0562	.0563	.0538
.25	.0	.0420	.0179	.0300	.0256	.0280	.0278	.0268
.4	.0	-.0175	-.0081	-.0128	-.0099	-.0106	-.0114	-.0103
.6	.0	-.0739	-.0313	-.0526	-.0433	-.0470	-.0479	-.0451
.775	.0	-.1134	-.0426	-.0780	-.0636	-.0696	-.0708	-.0666
.875	.0	-.1331	-.0366	-.0879	-.0703	-.0784	-.0791	-.0743
.9575	.0	-.1397	-.0322	-.0859	-.0672	-.0790	-.0766	-.0731
1.00855	.0	-.1123	-.1234	-.1179	-.1175	-.1152	-.1177	-.1163

α-Type, y/c=-0.1

x/c	2-D	0^{th}	I	I_M	II	III	II_M	III_A
.0	.0	.0	.0	.0	.0	.0	.0	.0
.0055	.8237	.8215	.8098	.8156	.8076	.8096	.8116	.8086
.0125	1.0026	.9917	.9850	.9883	.9813	.9834	.9848	.9824
.025	1.1054	1.0855	1.0890	1.0872	1.0833	1.0848	1.0853	1.0840
.055	1.1667	1.1331	1.1551	1.1441	1.1457	1.1456	1.1449	1.1456
.105	1.1871	1.1345	1.1716	1.1531	1.1588	1.1568	1.1559	1.1578
.17	1.1823	1.1196	1.1644	1.1420	1.1497	1.1464	1.1458	1.1480
.25	1.1669	1.0997	1.1483	1.1240	1.1328	1.1289	1.1284	1.1310
.4	1.1299	1.0664	1.1137	1.0901	1.0987	1.0948	1.0944	1.0968
.6	1.0780	1.0321	1.0673	1.0497	1.0463	1.0534	1.0530	1.0548
.775	1.0280	1.0089	1.0231	1.0160	1.0194	1.0182	1.0177	1.0188
.875	.9914	.9916	.9877	.9897	.9917	.9914	.9907	.9915
.9575	.9328	.961]	.9313	.9463	.9480	.9482	.9472	.9481
1.00855	.0	.0	.0	.0	.0	.0	.0	.0

β-Type, y/c=-0.1

x/c	2-D	0^{th}	I	I_M	II	III	II_M	III_A
.0	.0	.1116	.0191	.0653	.0549	.0645	.0601	.0597
.0055	.0	.1113	.0196	.0655	.0548	.0644	.0601	.0596
.0125	.0	.1108	.0201	.0654	.0544	.0639	.0599	.0591
.025	.0	.1091	.0208	.0650	.0534	.0626	.0592	.0580
.055	.0	.1022	.0214	.0618	.0500	.9583	.0559	.0541
.105	.0	.0853	.0198	.0525	.0420	.0486	.0472	.0453
.17	.0	.0611	.0148	.0380	.0303	.0349	.0341	.0326
.25	.0	.0336	.0078	.0210	.0167	.0192	.0187	.0180
.4	.0	-.0089	-.0036	-.0062	-.0046	-.0051	-.0054	-.0048
.6	.0	-.0506	-.0131	-.0319	-.0252	-.0288	-.0285	-.0270
.775	.0	-.0752	-.0145	-.0448	-.0364	-.0420	-.0406	-.0391
.875	.0	-.0812	-.0144	-.0463	-.0388	-.0450	-.0425	-.0418
.9575	.0	-.0762	-.0066	-.0414	-.0367	-.0416	-.0390	-.0392
1.00855	.0	-.0663	-.0685	-.0674	-.0674	-.0667	-.0674	-.0671

APPENDIX D

INDUCED VELOCITY DUE TO VORTICITY DISTRIBUTION ON APPROXIMATE SURFACE ELEMENTS

The component of the induced velocity in a direction defined by (c_1,c_2,c_3) at the i-th control point, (x_i,y_i,z_i), due to β-type surface vorticity distribution on a flat panel located inboard of the tip can be expressed as a single integral. The vorticity strength varies linearly on the panel. The Cartesian coordinates of the panel are (x_k,y_ℓ,z_k), $(x_k,y_{\ell+1},z_k)$, (x_{k+1},y_ℓ,z_{k+1}), and $(x_{k+1},y_{\ell+1},z_{k+1})$. Then

$$V_{U_\beta,L_\beta} = \sum_{k=1}^{K} \sum_{\ell=1}^{L} \Delta V_{k\ell}, \qquad (D-1)$$

where

$$\Delta V_{k\ell} = \frac{1}{4\pi}\int_{y_\ell}^{y_{\ell+1}} (I_1+I_2)\left[\{(z_i-d)-mx_i\}c_2+(mc_1-c_3)(y_i-y)\right]dy$$

with

$$m = \frac{z_{k+1}-z_k}{x_{k+1}-x_k},$$

$$d = \frac{z_k x_{k+1} - z_{k+1} x_k}{x_{k+1} - x_k} ,$$

$$I_1 = - \frac{2\gamma_1}{4ac-b^2}\left[\frac{bx_{k+1}+2a}{\sqrt{(a+bx_{k+1}+cx_{k+1}^2)}} - \frac{bx_k+2a}{\sqrt{(a+bx_k+cx_k^2)}}\right] ,$$

$$I_2 = \frac{2\gamma_2}{4ac-b^2}\left[\frac{2cx_{k+1}+b}{\sqrt{(a+bx_{k+1}+cx_{k+1}^2)}} - \frac{2cx_k+b}{\sqrt{(a+bx_k+cx_k^2)}}\right] ,$$

$$a = x_i^2+(y_i-y)^2+(z_i-d)^2 ,$$

$$b = -2\{m(z_i-d)+x_i\},$$

$$c = 1+m^2,$$

$$\gamma_1 = (\gamma_{k+1}-\gamma_k)/(x_{k+1}-x_k),$$

$$\gamma_2 = (\gamma_k x_{k+1}-\gamma_{k+1}x_k)/(x_{k+1}-x_k)$$

$$\gamma_k = \gamma_3 y+\gamma_4 ,$$

$$\gamma_{k+1} = \gamma_5 y+\gamma_6 ,$$

$$\gamma_3 = (\gamma_{k+\ell+1} - \gamma_{k,\ell})/(y_{\ell+1} - y_\ell) ,$$

$$\gamma_4 = (\gamma_{k,\ell} y_{\ell+1} - \gamma_{k,\ell+1} y_\ell)/(y_{\ell+1} - y_\ell) ,$$

$$\gamma_5 = (\gamma_{k+1,\ell+1} - \gamma_{k+1,\ell})/(y_{\ell+1} - y_\ell) ,$$

$$\gamma_6 = (\gamma_{k+1,\ell} y_{\ell+1} - \gamma_{k+1,\ell+1} y_\ell)/(y_{\ell+1} - y_\ell) .$$

The component of induced velocity at the i-th control point due to the β-type surface vorticity distribution on the k-m surface element on a half frustum of a cone on the tip can be expressed as a one-dimensional integral

$$V_{T_\beta} = \sum_{k=1}^{K} \sum_{m=1}^{M} \Delta V_{km} \qquad (D\text{-}2)$$

where

$$\Delta V_{km} = -\frac{1}{4\pi} \int_{\psi_m}^{\psi_{m+1}} K[m\gamma_1 I_1 + (d\gamma_1 + m\gamma_2) I_2 + d\gamma_2 I_3] d\varepsilon$$

with

$$m = (\rho_{k+1} - \rho_k)/(x_{k+1} - x_k) ,$$

$$d = (\rho_k x_{k+1} - \rho_{k+1} x_k)/(x_{k+1} - x_k) \ ,$$

$$K = m(z_i \sin\varepsilon - y_i \cos\varepsilon)c_1 + (x_k m \cos\varepsilon - z_i + d \cos\varepsilon)c_2$$

$$+ (y_i - d \sin\varepsilon - x_i m \sin\varepsilon)c_3 ,$$

$$\rho_k = z(x_k)\Big|_{\psi=0}$$

$$\rho_{k+1} = z(x_{k+1})\Big|_{\psi=0}$$

$$I_1 = \frac{2ab+(2b^2-4ac)x_{k+1}}{qc\sqrt{(a+bx_{k+1}+cx_{k+1}^2)}} - \frac{2ab+(2b^2-4ac)x_k}{qc\sqrt{(a+bx_k+cx_k^2)}}$$

$$+ \frac{1}{c^{3/2}} \ln\left[\frac{b+2cx_{k+1}+2\sqrt{c(a+bx_{k+1}+cx_{k+1}^2)}}{b+2cx_k+2\sqrt{c(a+bx_k+cx_k^2)}}\right] ,$$

$$I_2 = -\frac{2}{q}\left[\frac{2a+bx_{k+1}}{\sqrt{(a+bx_{k+1}+cx_{k+1}^2)}} - \frac{2a+bx_k}{\sqrt{(a+bx_k+cx_k^2)}}\right] ,$$

$$I_3 = \frac{2}{q}\left[\frac{b+2cx_{k+1}}{\sqrt{(a+bx_{k+1}+cx_{k+1}^2)}} - \frac{b+2cx_k}{\sqrt{(a+bx_k+cx_k^2)}}\right] ,$$

$$q = 4ac-b^2 \ .$$

$$a = x_i^2+y_i^2+z_i^2+d^2-2d(y_i \sin\varepsilon+z_i \cos\varepsilon) \ ,$$

$$b = 2\{md-x_i-m(y_i \sin\varepsilon+z_i \cos\varepsilon)\},$$

$$c = 1+m^2 ,$$

$$\gamma_1 = \gamma_{11} \sin\phi+\gamma_{12} ,$$

$$\gamma_2 = \gamma_{21} \sin\phi+\gamma_{22} ,$$

$$\gamma_{11} = (\gamma_5\rho_{k+1}-\gamma_3\rho_k)/(x_{k+1}-x_k) ,$$

$$\gamma_{12} = (\gamma_6-\gamma_4)/(x_{k+1}-x_k),$$

$$\gamma_{21} = (\gamma_3\rho_k x_{k+1}-\gamma_5\rho_{k+1}x_k)/(x_{k+1}-x_k) ,$$

$$\gamma_{22} = (\gamma_4 x_{k+1}-\gamma_6 x_k)/(x_{k+1}-x_k) ,$$

$$\gamma_3 = (\gamma_{k,m+1}-\gamma_{k,m})/(\rho_k \sin\psi_{m+1}-\rho_k \sin\psi_m),$$

$$\gamma_4 = (\gamma_{k,m} \sin\psi_{m+1}-\gamma_{k,m+1} \sin\psi_m)/(\sin\psi_{m+1} - \sin\psi_m),$$

$$\gamma_5 = (\gamma_{k+1,m+1}-\gamma_{k+1,m})/(\rho_{k+1} \sin\psi_{m+1}-\rho_{k+1} \sin\psi_m) ,$$

$$\gamma_6 = (\gamma_{k+1,m} \sin\psi_{m+1}-\gamma_{k+1,m+1} \sin\psi_m)/(\sin\psi_{m+1}-\sin\psi_m) .$$

The component of the induced velocity at the i-th control point due to the α-type surface vorticity distribution on k-m surface element on the half frustum of cone on the tip is given by

$$V_{T_\alpha} = \sum_{k=1}^{K} \sum_{m=1}^{M} \Delta V_{km} \qquad (D-3)$$

where

$$\Delta V_{km} = \frac{\sqrt{(1+m^2)}}{4\pi} \int_{\psi_m}^{\psi_{m+1}} (I_1+I_2+I_3+I_4)\, d\varepsilon ,$$

with m, d, ρ_k, ρ_{k+1}, and q defined in (D-2) and

$$I_1 = \frac{2d_1}{q}\left[\frac{b+2cx_{k+1}}{\sqrt{(a+bx_{k+1}+cx_{k+1}^2)}} - \frac{b+2cx_k}{\sqrt{(a+bx_k+cx_{k+1}^2)}}\right] ,$$

$$I_2 = -\frac{2d_2}{q}\left[\frac{2a+bx_{k+1}}{\sqrt{(a+bx_{k+1}+cx_{k+1}^2)}} - \frac{2a+bx_k}{\sqrt{(a+bx_k+cx_k^2)}}\right] ,$$

$$I_3 = d_3\left[\frac{2ab+(2b^2-4ac)x_{k+1}}{cq\sqrt{(a+bx_{k+1}+cx_{k+1}^2)}} - \frac{2ab+(2b^2-4ac)x_k}{cq\sqrt{(a+bx_k+cx_k^2)}}\right.$$

$$\left. + \frac{1}{c^{3/2}} \ln\left\{\frac{b+2cx_{k+1}+2\sqrt{c(a+bx_{k+1}+cx_{k+1}^2)}}{b+2cx_k+2\sqrt{c(a+bx_k+cx_k^2)}}\right\}\right] ,$$

$$I_4 = d_4\Big[\frac{a(8ac-3b^2)/c^2+b(10ac-3b^2)x_{k+1}/c^2+qx_{k+1}^2/c}{q\sqrt{(a+bx_{k+1}+cx_{k+1}^2)}}$$

$$- \frac{a(8ac-3b^2)/c^2+b(10ac-3b^2)x_k/c^2+qx_k{}^2/c}{q\sqrt{(a+bx_k+cx_k{}^2)}}$$

$$- \frac{3}{2}\frac{b}{c^{5/2}}\ln\Big\{\frac{b+2cx_{k+1}+2\sqrt{c}(a+bx_{k+1}+cx_{k+1}^2)}{b+2cx_k+2\sqrt{c}(a+bx_k+cx_k{}^2)}\Big\}\Big] ,$$

$$d_1 = dA\gamma_2 ,$$

$$d_2 = dB\gamma_2+(m\gamma_2+d\gamma_1)A ,$$

$$d_3 = mA\gamma_1+(m\gamma_2+d\gamma_1)B ,$$

$$d_4 = mB\gamma_1 ,$$

$$A = c_1(z_i\cos\phi + y_i\sin\varepsilon - d)-x_i(c_2\sin\varepsilon+c_3\cos\varepsilon) ,$$

$$B = c_2\sin\varepsilon+c_3\cos\varepsilon-mc_1 .$$

The expressions for γ_1 and γ_2 are given in Eq. (D-2) except that in the numerical evaluation, the appropriate α-type vorticity strength is to be used in Eq. (D-3).

APPENDIX E

SURFACE VORTICITY DISTRIBUTION ON THE FINITE WING OF ASPECT RATIO 3, WING AIRFOIL SECTION NACA 0012

α-Type, ψ=90°

x/c	2-D	II_M	III	III_M	IV
.0	.0	.4352	.4030	.4191	.4128
.0055	.8237	.9541	.9650	.9596	.9640
.0125	1.0026	1.0359	1.0420	1.0389	1.0402
.025	1.1054	1.0805	1.0876	1.0840	1.0856
.055	1.1667	1.1020	1.1050	1.1035	1.1028
.105	1.1871	1.1038	1.1126	1.1082	1.1100
.17	1.1823	1.0977	1.0994	1.0986	1.0974
.25	1.1669	1.0870	1.0887	1.0879	1.0871
.4	1.1299	1.0657	1.0644	1.0650	1.0630
.6	1.0780	1.0405	1.0374	1.0390	1.0366
.775	1.0280	1.0206	1.0154	1.0180	1.0152
.875	.9914	1.0073	1.0050	1.0035	1.0000
.9575	.9328	.9898	.9803	.9831	.9772
1.00855	.0	.2360	.2340	.2350	.2300

α-Type, ψ=45°

x/c	2-D	II_M	III	III_M	IV
.0	.0	.0377	.2850	.2963	.2919
.0055	.8237	.9119	.9211	.9165	.9199
.0125	1.0026	1.0188	1.0253	1.0221	1.0235
.025	1.1054	1.0755	1.0826	1.0791	1.0807
.055	1.1667	1.1054	1.1089	1.1072	1.1069
.105	1.1871	1.1104	1.1200	1.1152	1.1176
.17	1.1823	1.1052	1.1082	1.1067	1.1062
.25	1.1669	1.0955	1.0982	1.0968	1.0965
.4	1.1299	1.0744	1.0746	1.0745	1.0734
.6	1.0780	1.0472	1.0460	1.0466	1.0452
.775	1.0280	1.0249	1.0208	1.0228	1.0206
.875	.9914	1.0086	1.0028	1.0057	1.0030
.9575	.9328	.9868	.9758	.9813	.9763
1.00855	.0	.1669	.1600	.1662	.1626

β-Type, ψ=45°

x/c	2-D	II_M	III	III_M	IV
.0	.0	.3077	.2850	.2964	.2919
.0055	.0	.2021	.201	.2016	.2018
.0125	.0	.1707	.1736	.1722	.1742
.025	.0	.1415	.1452	.1433	.1457
.055	.0	.1045	.1076	.1060	.1079
.105	.0	.0703	.0690	.0697	.0689
.17	.0	.0463	.0474	.0468	.0473
.25	.0	.0236	.0243	.0240	.0242
.4	.0	-.0091	-.0100	-.0096	-.0104
.6	.0	-.0483	-.0533	-.0508	-.0540
.775	.0	-.0836	-.0996	-.087	-.0915
.875	.0	-.1104	-.1180	-.1142	-.1189
.9575	.0	-.1446	-.1508	-.1477	-.1515
1.00855	.0	-.1669	-.1654	-.1662	-.1626

α-Type, y/c=1.5

x/c	2-D	II_M	III	III_M	IV
.0	.0	.0	.0	.0	.0
.0055	.8237	.7824	.7854	.7839	.7836
.0125	1.0026	.9436	.9450	.9443	.9430
.025	1.1054	1.0390	1.0419	1.0405	1.0399
.055	1.1667	1.0990	1.1016	1.1004	1.0996
.105	1.1871	1.1170	1.1237	1.1202	1.1216
.17	1.1823	1.1145	1.1178	1.1161	1.1161
.25	1.1669	1.1036	1.1067	1.1051	1.1052
.4	1.1299	1.0767	1.0779	1.0773	1.0768
.6	1.0780	1.0414	1.0414	1.0414	1.0408
.775	1.0280	1.0107	1.0097	1.0102	1.0096
.875	.9914	.9886	.9869	.9877	.9873
.9575	.9328	.9581	.9551	.9566	.9561
1.00855	.0	.0	.0	.0	.0

β-Type, y/c=1.5

x/c	2-D	II_M	III	III_M	IV
.0	.0	.4352	.4030	.4191	.4128
.0055	.0	.3819	.3687	.3753	.3712
.0125	.0	.3334	.3236	.3285	.3257
.025	.0	.2783	.2726	.2755	.2743
.055	.0	.2025	.2001	.2013	.2014
.105	.0	.1325	.1334	.1329	.1295
.17	.0	.0815	.0912	.0864	.0811
.25	.0	.0377	.0377	.0377	.0377
.4	.0	-.0194	-.0191	-.0192	-.0194
.6	.0	-.0765	-.0772	-.0769	-.0777
.775	.0	-.1215	-.1214	-.1215	-.1211
.875	.0	-.1524	-.1511	-.1517	-.1518
.9575	.0	-.1905	-.1851	-.1878	-.1855
1.00855	.0	-.2359	-.2340	-.2350	-.2300

α-Type, y/c=1.4

x/c	2-D	II_M	III	III_M	IV
.0	.0	.0	.0	.0	.0
.0055	.8237	.8116	.8091	.8104	.8090
.0125	1.0026	.9848	.9832	.9840	.9828
.025	1.1054	1.0853	1.0848	1.0850	1.0843
.055	1.1667	1.1449	1.1465	1.1457	1.1457
.105	1.1871	1.1559	1.1588	1.1574	1.1577
.17	1.1823	1.1458	1.1494	1.1476	1.1482
.25	1.1669	1.1284	1.1325	1.1305	1.1313
.4	1.1299	1.0944	1.0990	1.0967	1.0978
.6	1.0780	1.0530	1.0567	1.0548	1.0557
.775	1.0278	1.0177	1.0197	1.0187	1.0190
.875	.9914	.9907	.9918	.9913	.9914
.9575	.9328	.9427	.9481	.9476	.9478
1.00855	.0	.0	.0	.0	.0

β-Type, y/c=1.4

x/c	2-D	II_M	III	III_M	IV
.0	.0	.0601	.0620	.0611	.0629
.0055	.0	.0601	.0587	.0594	.0596
.0125	.0	.0599	.0583	.0591	.0592
.025	.0	.0592	.0574	.0583	.0583
.055	.0	.0559	.0537	.0548	.0545
.105	.0	.0472	.0446	.0459	.0452
.17	.0	.0341	.0323	.0332	.0326
.25	.0	.0187	.0177	.0182	.0178
.4	.0	-.0054	-.0051	-.0052	-.0052
.6	.0	-.0285	-.0270	-.0278	-.0274
.775	.0	-.0406	-.0386	-.0396	-.0392
.875	.0	-.0425	-.0410	-.0418	-.0416
.9575	.0	-.0390	-.0383	-.0387	-.0387
1.00855	.0	-.0674	-.0662	-.0668	-.0662

α-Type, y/c=1.0

x/c	2-D	II_M	III	III_M	IV
.0	.0	.0	.0	.0	.0
.0055	.8237	.8173	.8140	.8157	.8143
.0125	1.0026	.9930	.9902	.9916	.9904
.025	1.1054	1.0966	1.0948	1.0957	1.0951
.055	1.1667	1.1623	1.1621	1.1622	1.1623
.105	1.1871	1.1804	1.1805	1.1804	1.1806
.17	1.1823	1.1746	1.1744	1.1745	1.1745
.25	1.1669	1.1585	1.1582	1.1583	1.1583
.4	1.1299	1.1215	1.1213	1.1214	1.1214
.6	1.0780	1.0717	1.0717	1.0714	1.0716
.775	1.0278	1.0261	1.0255	1.0258	1.0258
.875	.9914	.9912	.9906	.9909	.9909
.9575	.9328	.9402	.9398	.9400	.9401
1.00855	.0	.0	.0	.0	.0

β-Type, y/c=1.0

x/c	2-D	II_M	III	III_M	IV
.0	.0	.0082	.0084	.0084	.0086
.0055	.0	.0082	.0077	.0080	.0079
.025	.0	.0080	.0077	.0078	.0078
.055	.0	.0076	.0073	.0074	.0074
.105	.0	.0067	.0065	.0066	.0066
.17	.0	.0054	.0052	.0053	.0053
.25	.0	.0035	.0034	.0035	.0034
.4	.0	-.0003	-.0003	-.0003	-.0003
.6	.0	-.0047	-.0045	-.0046	-.0046
.775	.0	-.0072	-.0069	-.0070	-.0070
.875	.0	-.0078	-.0074	-.0076	-.0076
.9575	.0	-.0080	-.0076	-.0078	-.0078
1.00855	.0	-.0158	-.0154	-.0156	-.0154

REFERENCES

1. Morse, P. N. and Feshbach, H., "Methods of Theoretical Physics", McGraw-Hill, New York, 1953.

2. Moon, P. and Spencer, D. E., "Field Theory for Engineers", Van Nostrand, Princeton, 1961.

3. Milne-Thomson, "Theoretical Aerodynamics", Dover Publications, Inc., New York, 1973.

4. Karamecheti, K., "Principles of Ideal-Fluid Aerodynamics", John-Wiley & Sons, Inc., New York, 1966.

5. Theodorsen, T., "Theory of Wing Sections of Arbitrary Shape", NACA Report No. 411, 1932.

6. Thwaites, B. (ed.), "Incompressible Aerodynamics, Fluid Motion Memoirs", Oxford University Press, 1960.

7. Von Kármán, T., "Calculation of Pressure Distribution on Airship Hulls", NACA TM 574, 1930.

8. Lamb, H., "Hydrodynamics", Dover Publications, Inc., New York, 1945.

9. Lotz, I., "Calculation of Potential Flow Past Airship Bodies in Yaw", NACA TM 675, 1932.

10. Vandrey, F., "A Method for Calculating the Pressure Distribution of a Body of Revolution Moving in a Circular Path Through a Perfect Incompressible Fluid", Aeronautical Research Council, R&M No. 3139, 1960.

11. Giesing, J. P., "Potential Flow about Two-dimensional Airfoils", Douglas Aircraft Co. Report No. LB-31946, Dec. 65.

12. Hess, J. L. and Smith, A. M. O., "Calculation of Potential Flow about Arbitrary Bodies", Progress in Aeronautical Sciences, Vol. 8, 1966.

13. Hess, J. L., "Higher Order Numerical Solution of the Integral Equation for the Two-dimensional Neumann Problem," Computer Methods in Applied Mechanics and Engineering, Vol. 2, 1973, pp. 1-15.

14. Hess, J. L., "The Problem of Three-dimensional Lifting Potential Flow and its Solution by Means of Surface Singularity Distribution," Computer Methods in Applied Mechanics and Engineering, Vol. 4, 1974, pp. 283-319.

15. Hess, J. L., "The Use of Higher Order Surface Singularity Distributions to Obtain Improved Potential Flow Solutions for Two-dimensional Lifting Airfoils," Computer Methods in Applied Mechanics and Engineering, Vol. 5, 1975, pp. 11-35.

16. Hess, J. L., "Review of Integral Equation Techniques for Solving Potential Flow Problems with Emphasis on the Surface Source Method," Computer Methods in Applied Mechanics and Engineering, Vol. 5, 1975, pp. 145-196.

17. Hess, J. L., "Improved Solution for Potential Flow about Arbitrary Axisymmetric Bodies by the Use of a Higher Order Surface Source Method," Computer Methods in Applied Mechanics and Engineering, Vol. 5, 1975, pp. 297-308.

18. Geissler, W., "Calculation of Potential Flow about Axially Symmetric Fuselages, Annular Profiles and Engine Inlets," NASA TT F-15, 213, Dec. 1973.

19. Pien, P. C., "Calculation of Nonlifting Potential Flow about Arbitrary Three-dimensional Bodies Based on Doublet Distribution," Naval Ship Research and Development Center, Report No. SPD-601-01, Jan. 1975.

20. Summa, J. N., "Potential Flow about Three-dimensional Streamlined Lifting Configurations with Application to Wings and Rotors," AFOSR-TR-74-1914, Sept. 1974.

21. Prager, W., "Die Druckverteilung an Körpern in ebener Potentialströmung," Physik. Zeitschr. XXIV, 865, 1928.

22. Martensen, E., "Berechnung der Druckverteilung an Gitterprofilen in ebener Potentialströmung mit einer Fredholmschen Integralgleichung," Arch. Rat. Mech. and Analysis, 3, No. 3, 1959, p. 235.

23. Jacob, K., and Riegels, F. W., "Berechnung der Druckverteilung endlich dicker Profile ohne und mit Klappen und Vorflügeln," Zeitschr. für Flugwissenschaften, Vol. II, No. 9, 1963, pp. 357-367.

24. Mavriplis, F., "Aerodynamic Research on High Lift Systems," Canadian Aeronautics and Space Journal, 17, 1971, pp. 175-183.

25. Mavriplis, F., "Comparison of Surface-vorticity Method with Surface-source Method, etc.," Canadian Aeronautics and Space Journal, 19, 1973, pp. 411-143.

26. Klein, A. and Mathew, J., "Incompressible Potential Flow Solution for Axisymmetric Body-duct Configurations," Z. Flugwiss. 20, 1972, pp. 221-228.

27. Kress, R., "Treatment of Prager Problem of Potential Theory by the Integral Equation Method," Physics of Fluids, Supplement II, 1969, pp. 120-125.

28. Lopez, M. L., et al., "A Theoretical Method for Calculating the Aerodynamic Characteristics of Arbitrary Jet-flapped Wings: Vol. I," Douglas Aircraft Co. Report No. MDC J5519-01, May 1973.

29. Rektorys, K. (ed.), "Survey of Applicable Mathematics," MIT Press, 1969.

30. Carnahan, B., Luther, H. A., and Wilkes, J. O., "Applied Numerical Methods," John Wiley & Sons, Inc., New York, 1969.

31. Jacobs, E. N., Ward, K. E., and Pinkerton, R. M., "The Characteristics of 78 Related Airfoil Sections from Tests in the Variable-density Wind Tunnel," NACA Report No. 460, 1933, pp. 299-354.

32. Abbott, I. H., et al., "Summary of Airfoil Data," NACA Report No. 824, 1945, pp. 259-387.

VITA

Pradeep Raj was born on December 15, 1949. He had his early education in Muzaffar Nagar, India. He received the Bachelor of Science degree from Meerut University in 1967. He was awarded the Chencellor's Medal for securing the highest percentage of marks.

Mr. Raj joined the Indian Institute of Science, Bangalore, India and in 1970, he obtained the degree of Bachelor of Engineering with Distinction in Electrical Technology. He stood first in the Bachelor's program in Engineering and he was awarded the Hay Medal by the Council of the Institute. He continued his education at the Indian Institute of Science and in 1972, he received the degree of Master of Engineering with Distinction in Aeronautics. He entered the Georgia Institute of Technology in the Fall of 1972.

Mr. Raj is a student member of the AIAA and the American Helicopter Society.